University of Thessaly
Department of Civil Engineering

Numerical simulation of pool hydrocarbon fires and their effect on adjacent tanks

Christina Goula, Civil Engineer
Chrysoula Malkotsi, Civil Engineer

Master Thesis

Submitted to
The Department of Civil Engineering
In Fulfillment of the Requirements
Of Master in Science in
''Analysis and design of energy infrastructure constructions''

Supervisor: Daphne Pantousa, Adjunct Lecturer

University of Thessaly
Department of Civil Engineering

Numerical simulation of pool hydrocarbon fires and their effect on adjacent tanks

Christina Goula, Civil Engineer
Chrysoula Malkotsi, Civil Engineer

Master Thesis

Submitted to
The Department of Civil Engineering
In Fulfillment of the Requirements
Of Master in Science in
''Analysis and design of energy infrastructure constructions''

Examination Committee:
Daphne Pantousa, Adjunct Lecturer in Department of Civil Enginneering, Uth (Supervisor)
Olympia Panagouli, Assistant Professor in Department of Civil Engineering, UTh (Advisor committee)
Konstantinos Tzaros, Adjunct Lecturer in Department of Civil Engineering, UTh (Advisor committee)

Volos 2017

Contents

Acknowledgements

This master journey is a team work by two beloved colleagues who shared the dreams for our career. Completing this master journey is a result of constant work by both of us and of the best possible collaboration between us.

No matter of our effort, this research couldn't be accomplished, if it wasn't our advisors support. We are deeply grateful to our advisors Dr Daphne Pantousa and Dr Candidate Kalliopi Zografopoulou for our tremendous guidance, encouragement and successful collaboration during the course of the research.

Many thanks to our dear friends and colleagues; Anna Maria Kollatou and Mimi Mpalamoti for their help and support during this master. Their care and love accompanied us through this journey.

Our last and special debt of gratitude must go to our families who teach us never to stop trying; to Anastasios, Athanasia and Marinaya and to Christos and Stergios. Their support and encouragement helped us to continue when it seemed impossible to do so.

ABSTRACT

Tank fire incidents take place mainly in petroleum refineries, oil terminals or storage tanks and they can prove to be catastrophic. During the last years, engineering societies (American petroleum institute, National Fire Protection Association etc) have published strict engineering guidelines and standards for the construction, material selection, design and safe management of storage tanks. Nevertheless, tank fire incidents are increasing in the last decades. The problem addressed in this thesis is the thermal response of steel fixed roof oil-storage cylindrical tanks that are heated during pool fires. The first objective is to identify the parameters that describe the burning tanks and the geometric characteristics of flames are calculated. Numerical models are developed which include both burning tanks and the heated tank. The problem is solved numerically using the Finite Element method. The general purpose Finite Element code MSC Marc, which is optimized for non-linear problems, is used for the simulation. The three-dimensional models are developed through four-node shell elements. The behavior of the heated tank is examined for multiple pool fire scenarios. First, the case of one unique burning tank is examined. In rest scenarios, the fire spreads to adjacent tanks. Thus, in those scenarios the examined tank is heated by multiple sources (burning tanks). Parametric numerical analyses are conducted to study the influence of a combination of various parameters: diameter of the burning tank, type of stored fuel (gasoline or ethanol), incidence of wind, separation distance between tanks and the number of burning tanks involved. Furthermore, the study aims to propose an index for the evaluation of risk for fuel's autoignition in the heated tank It is also examined if the safety distances that are recommended in current regulations (NFPA30:2012) are safe or not. The material properties of steel at elevated temperatures are according to EN 1993-1-2.

It is found that the temperature distribution on the tank wall of the adjacent tank is not uniform. The temperature rise takes place on the side of the tank wall which is on the face of the source tank while the opposite side is not affected by the pool fire. This pattern becomes more complicated as more burning tanks are added. In both fuel types - Ethanol and Gasoline - the rate of reduction of the maximum temperature, as the separation distance increases, is more affected by the presence of wind than of the diameter of the burning tank. Under wind conditions, in smaller diameters of the source tank the rate of temperature reduction with the increase of the separation distance is not affected by the fuel type. In bigger burning tank diameters it has an effect. Under no wind conditions, the rate of temperature reduction with the separation distance is more influenced by the fuel type.

According to the recommendations of NFPA30:2012, almost 62.5% of the case studies are on the unsafe side. It is concluded that the wind is the most critical parameter that should be considered for the determination of separation distance between tanks.

Concerning the risk index that is defined in this thesis, the results of analyses indicate that under wind conditions, for both fuel types, at large diameters, the fire risk rate declines in a linear way. In small diameters for both fuel types the fire risk rate shows a rapid reduction in closer separation distances. When the two tanks become more separated, the fire risk becomes zero. Finally, the risk of autoignition in the heated tank increases as the number of burning tanks rises and, moreover, the risk in case of Ethanol is bigger in Gasoline models under both wind conditions.

CHAPTER 1. INTRODUCTION

The main hazards associated with tanks containing flammable fluids are the explosions and fire attacks. Explosions are the major cause of structural damage in most of the fire events identified until now. On the other hand the tank failure due to fire load seems to be of similar importance. Storage tanks contain large volume of flammable and hazardous liquids and a fire accident may result in socio-economical losses, injuries, deaths, stock devaluation or company bankruptcy and environmental disasters. During the last years engineering societies such as the American petroleum institute (API), the American institute of chemical engineers (AIChE), the American society of mechanical engineers (ASME), and the National Fire Protection Association (NFPA) have published strict engineering guidelines and standards for the construction, material selection, design and safe management of storage tanks. Although most companies are following the instructions, oil tank fire accidents are still happening.

Recently, a massive fire and explosions incident of oil tanks in a storage facility near Kiev (Figure 1-1) killed five firefighters and various Ukrainian officials gave contradicting reports indicating the environmental situation in Kiev after the blaze. On December 11, 2005 a catastrophic tank fire took place at the Buncefield Oil Storage Depot in the north of London (Figure 1-2). International attention was given in the specific fire event since it was the largest fire in Europe and significant alert was placed on the serious risks that may arise.

In the case of a fire engulfed tank, that contains flammable liquids such as oil, it can be easily foreseen that the tank will collapse due to material degradation at elevated temperatures. The temperature rise in these cases is high enough and come up to 1200°C which is the melting point of steel. The fire engulfed tank is actually the heat generator for adjacent tanks. The heat is transferred mainly through radiation and becomes the thermal load for neighbor tanks. The adjacent tank's temperature distribution is non-uniform in both circumferential and axial direction and depends on the position of the fire engulfed tank. Thus, there exists an important temperature difference between the hotter and the colder part of the heated tank that may lead to the structural failure of the tank, caused by the reduction of mechanical properties of steel in conjunction or even to the fire spread (domino effect) (Pantousa 2015).

Figure 1-1 Kiev oil tank fire event (Pantousa 2015)

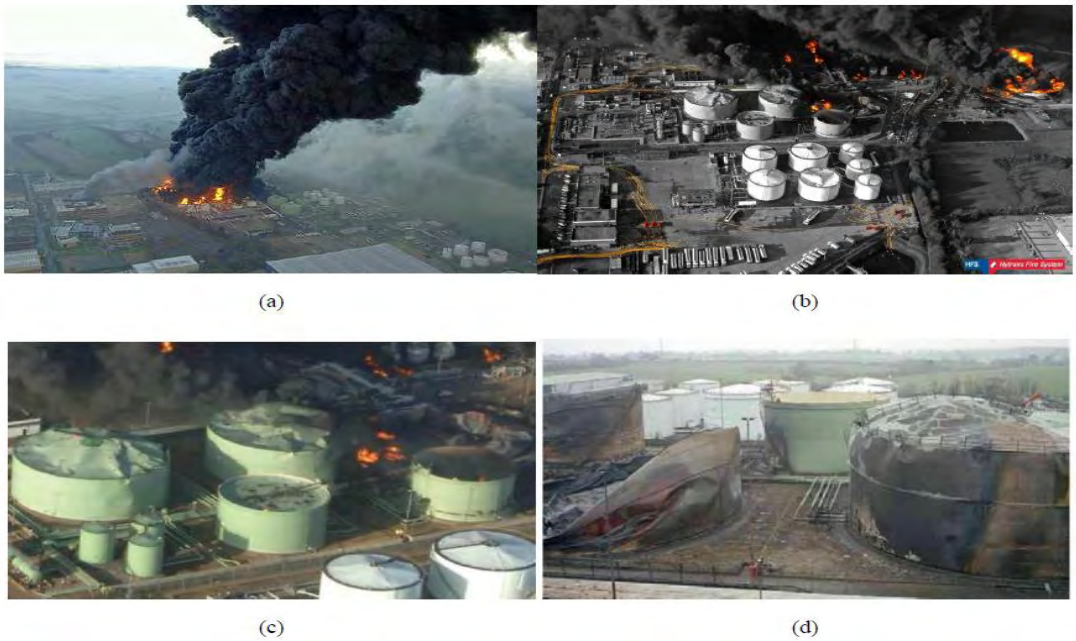

Figure 1-2 Buncefield Oil Storage Depot fire event (Pantousa 2015)

In order to minimize the risk, several organizations (e.g. APO, NFPA, EPA etc) propose guidelines regarding the tank layout in the oil depot. The suggested layout takes into account the accessibility of fire-fighting vehicles and the safe distances between the process plant and residential infrastructures. The minimum distance between the tanks is calculated through the heat flux between the fire engulfed tank and the adjacent tank and obviously this varies as the distance between them changes. The distance at which the heat flux becomes equal to 4.732 kW/m2 is considered to be the safe inter-tank distance since no material is expected to ignite with a heat flux lower than this value (Sengupta et al. 2010). Nevertheless, questions arise if these limits are assuring the structural integrity of the heated adjacent tanks. In another research a critical temperature of 540°C is deemed to be a threshold for the safety of steel tanks (Liu 2011, Beyler 2004b) in determining safe separations. Recent research activity in this area (Santos and Landesmann 2014, Fontenelle 2012) demonstrated that the temperature variation on the target tank can be up to 800°C depending on the type of stored fuel (gasoline or ethanol), the structural tank side wall material (steel or concrete) and the incidence of wind. Specifically, in the study of Santos and Landesmann (2014) it is indicated that the minimum safety distances are changing rapidly with the wind and that the present NFPA30:2012 design recommendations need to be modified, in order to achieve a satisfactory failure prediction for different storage fuels (e.g. ethanol).

The previous indicate that the minimum safety distances do not take into account all the involved factors that may affect the behavior of the heated factors that mainly affect the behavior of the heated tanks during the burning stage of the fire-engulfed tank. Further research should be conducted in order to study the behavior of the heated tanks.

This thesis addresses the problem of the thermal response of steel fixed-roof oil storage tanks that are heated during pool fires. The first objective is to identify the parameters that describe the burning tanks and the geometric characteristics of flames are calculated. Numerical models are developed which include both burning tanks and the heated tank. The problem is solved numerically using the Finite Element method. The behaviour of the heated tank is examined for multiple pool fire scenarios. First, the case of one unique burning tank is examined. In rest scenarios, the fire spreads to adjacent tanks. Thus, in those scenarios the examined tank is

heated by multiple sources (burning tanks). Parametric analyses are conducted to study the influence of various parameters which are the diameter of the burning tank, the type of stored fuel (gasoline or ethanol), the incidence of wind, the separation distance between tanks and the number of burning tanks involved. Furthermore, the study aims to propose an index for the evaluation of risk for fuel's autoignition in the heated tank. Finally, it is examined if the safety distances that are recommended in current regulations (NFPA30:2012) are safe or not.

CHAPTER 2. STATE OF THE ART - LITERATURE REVIEW

This Chapter presents a state of the art report on the main scientific areas of this thesis, which are the pool fire modelling and the heat transfer mechanisms. Moreover, the review covers the most relevant scientific studies relative to the pool fire modelling and the thermal response of heated tanks that are included in the literature. Finally, current standards relatively to the safety design in tank farms, are presented.

2.1 Pool fire modeling

2.1.1 Pool fire

A pool fire is defined as a turbulent diffusion of fire burning above a horizontal pool of vaporizing hydrocarbon fuel. Pool fires are buoyantly controlled gas burners. The fuel can be liquid gas or solid. The shape of the pool may be of random geometry although common shapes are circular, elliptical and rectangular. Pool fires are defined by the total heat release rate, the flame spread rate and the power radiated to the surroundings. The risk of a fire incident can be increased or minimized due to ambient conditions such as the absence or presence of an enclosure, wind, currents or ventilation.

Based on experimental observations the fire envelope can be divided in two layers. The luminous one emits radiation at a maximum level. The upper layer that is almost obscured by smoke reduces the emission of radiation. The fuel combustion process and the size of fire determine the amount of smoke generated, that can be up to 20% of the fuel mass.

The obscuration effect is most pronounced for fires that are tens or hundreds of meters in diameter because of the decreased efficiency of combustion at these scales (McGrattan et al. 2000). In Figure 2-1 is illustrated a large liquid fuel fire.

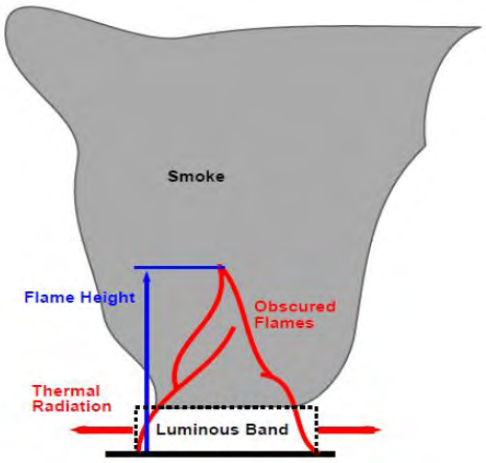

Figure 2-1 Large liquid fuel fire scheme (McGrattan et al. 2000)

There is a wide range of mathematical expressions which are used to predict the attitude of hydrocarbon pool fires that differ from field models (also known as Computational Fluid Dynamics, or CFD, models) to empirical models (or semi-empirical models). Field models are

more complicated, solve Navier-Stokes equations of fluid flow and use sub-models that estimate the fire's chemical and physical mechanism.

Field models provide a rigorous framework for solving combustion problems and for the moment they are essentially research tools. Although they can predict a wide range of fire scenarios, they demand a great deal of time and effort (human and computational).

Empirical models describe the pool fire geometry and they are based on dimensionless modeling and experimental data predictions. They are divided into two types: point source models and solid flame models (Figure 2-2).These kind of models can predict more accurate the heat flux from a pool fire to external objects than the field models do. They also provide reliable results without demanding excess time effort. Their predictions provide adequate compatibility with the experimental data since trey are used within their range of applicability.

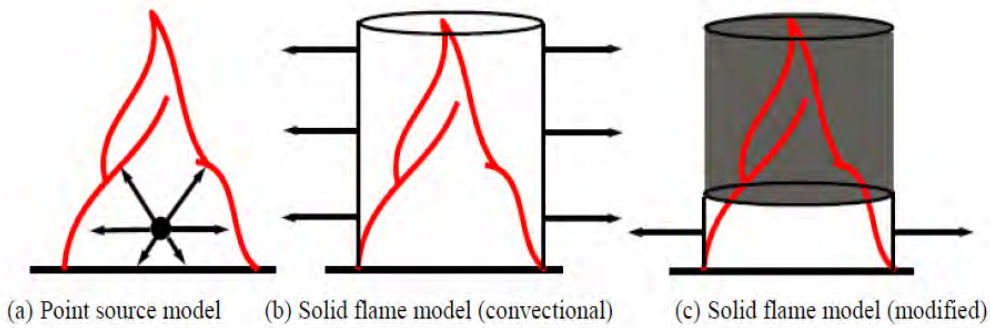

Figure 2-2 Schematic diagrams of empirical models: (a) point source, (b) solid flame and, (c) modified solid flame

Point source models are the simplest type of empirical models and can be used to estimate the radiant heat flux around a fire. These models use only few parameters for their predictions. However, according to Cowley and Johnson (1992) for more reliable estimations should be used for target tanks that are placed beyond five times the pool diameter (D) from the flame.

Solid flame models are based on appropriate experiments to derive a flame shape such as a cylinder or an ellipse, dependent on factors such as fuel type and wind speed. Further calculations are used to estimate the emissive power of the flame that is acquired from a wide range of experimental data. The main parameters describe solid flame models are flame's geometry (size and shape), mass burning rate and average flame emissive power.

Incident heat flux at the target is obtained by calculating its view factor with the surface emissive power of the flame and the atmospheric transmissivity of the intervening air:

$$q = \tau \cdot F \cdot E \qquad (2.1)$$

where,
q = incident heat flux at the receiver (kW/m^2)
τ = atmospheric transmissivity
F = view factor between the flame and the receiver
E= surface emissive power of flame (kW/m^2)

2.1.2 Fire characteristics

Solid flame models are described by mass burning rate, flame geometry and radiation heat flux. The flame geometry is described by the flame shape, the diameter, the length, the tilt and the drag. The calculation of radiation heat flux is based on flame surface emissive power, lower zone length, unobscured ratio, atmospheric transmissivity and radiation view factor. All the previous parameters are described in the following.

2.1.2.1 Mass burning rate

Mass burning rate is the mass of the liquid fuel consumed by the flame per unit time, per unit area of the pool. For a particular fuel, the mass burning rate has been found to vary with pool diameter. Babrauskas (1983) relates the actual burning rate to the maximum burning rate for a fuel.

$$\dot{m}_b = \dot{m}_{max} \cdot (1 - e^{(-k\beta)\cdot D}) \quad (2.2)$$

$\dot{m}_{max}$ = maximum burning rate of a liquid fuel ($kg.m^{-2}s^{-1}$)
D = the tank diameter (m)
k_β = the empirical constant (m^{-1})

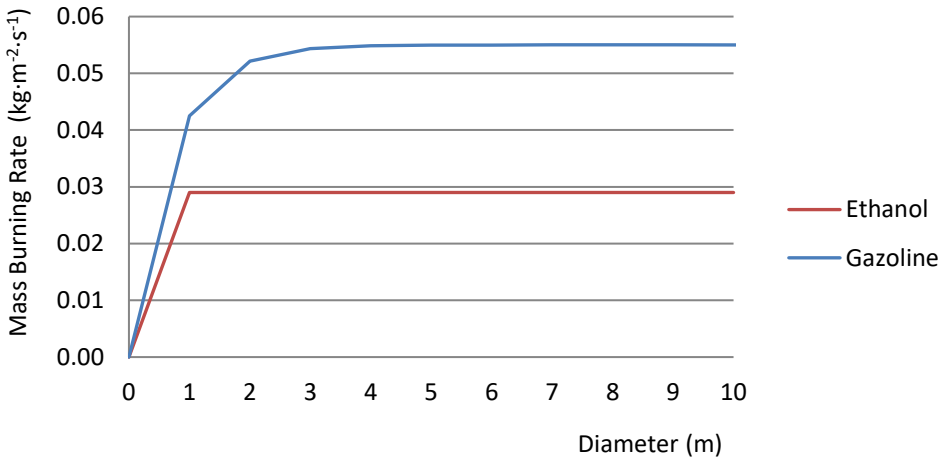

Figure 2-3 A comparison of the mass burning rate of gasoline and diesel for different pool diameters

Figure 2-3 presents the dependence of Mass Burning Rate on the pool diameter, for both gasoline and diesel. It is observed that as the diameter gets larger, mass burning rate asymptotes maximum burning rate. Thus, there is a limit magnitude where any further increase in pool diameter does not produce an increase in emitted radiation. The pool diameter at which this occurs is fuel dependent. Thus there is a diameter where the radiative feedback to the pool surface reaches the maximum (Rew & Hulbert, 1999). For gasoline fires, the mass burning rate approaches the maximum mass burning rate at approximately 3m diameter and even earlier, at approximately 2m diameter, for ethanol fires.

The maximum mass burning rate for various liquid fuels and their k_β values are empirically determined and summarized in the following Table 2-1.

Fuel	**Maximum Mass Burning Rate**	**Empirical Constant**	**Heat of Combustion**	**Surface Emissive Power**	**Empirical Constant**	**Carbon to Hydrogen Ratio**	**Un-obscuration Ratio U_r ($m^2 \cdot m^{-2}$)**		
	$\dot{m}_{max}$ ($kg.m^{-2}s^{-1}$)	k_β (m^{-1})	ΔHc (kJ/kg)	SEPmax ($kW \cdot m^{-2}$)	Km (m^{-1})	C/H	D<10m	10m<D<20m	D<20m
Acetone	0.038	2.238	25.800	130	100	0.50	0.02	0.02	0.02
Benzine	0.085	2.700	40.100	130	100	1.00	0.02	0.02	0.02
Butane	0.110	0.852	45.700	225	0.937	0.40	0.23	0.12	0.08
Crude Oil	0.051	1.301	42.600	130	100	0.54	0.05	0.05	0.05
Diesel	0.054	1.301	44.400	130	100	0.53	0.02	0.02	0.02
Ethanol	0.029	100.000	29.700	130	100	0.33	1.00	1.00	1.00
Fuel Oil	0.034	1.67	39.700	130	100	0.61	0.02	0.02	0.02
Gasoline/ Petrol	0.055	1.480	43.700	130	100	0.43	0.02	0.02	0.02
Heptane	0.081	1.394	44.600	200	100	0.438	0.23	0.12	0.08
Hexane	0.075	1.394	44.700	200	100	0.429	0.23	0.12	0.08
Hydrogen/ Liquified	0.161	6.741		70	7.415	0.00	1.00	1.00	1.00
GP4	0.056	1.962	43.500	130	100	0.46	0.02	0.02	0.02
GP5/ Kerosene	0.063	1.269	43.000	130	100	0.45	0.02	0.02	0.02
LNG	0.141	0.136		265	0.149	0.25	0.77	0.69	0.55
LPG	0.181	0.500		250	0.55	0.375	0.55	0.23	0.16
Methanol	0.020	100.000	20.000	70	100	0.25	1.00	1.00	1.00
Naphtha/ Pentane	0.095	100.000		200	100	0.417	0.23	0.12	0.08
Octane	0.081	1.394		200	100	0.444	0.23	0.12	0.08
Toluene	0.066	3.370		130	100	0.875	0.02	0.02	0.02
Xylene	0.090	1.400	40.800	130	100	0.80	0.02	0.02	0.02

Table 2-1 Fuel properties (SFPE Handbook of Fire Protection Engineering 3rd Edition 2002

The maximum burning rate can also be estimated from the expression given by Burgess & Hertzberg (1974).

$$\dot{m}_{max} = \frac{0.001 \cdot \Delta Hc}{\Delta Hv*} \quad (2.3)$$

where,
ΔH_c = net heat of combustion of the fuel at its boiling point (kJ/kg)
ΔH_v* = modified heat of vaporization of the fuel (kJ/kg), given by the following expression:

$$\Delta Hv* = \Delta Hv + C_p \cdot (T_b - T_\circ) \quad (2.4)$$

where,
ΔH_v = heat of vaporization of the fuel at its boiling point (kJ/kg)
C_p = heat capacity of the liquid (kJ/kgK)

T_b = liquid boiling temperature (K)
T_o = initial temperature of the liquid (K)

Mudan & Croce (1988) suggested an alternative method for estimating the mass burning rate, using the linear regression rate (Equations 2.5 and 2.6).

$$\dot{y} = 1.27 \cdot 10^{-6} \cdot \frac{\Delta Hc}{\Delta Hv*} \quad (2.5)$$

$$\dot{y} = \dot{m}_b/\rho_L \quad (2.6)$$

where,
$\dot{y}$ = linear regression rate of fuel (m/s)
ρ_L = density of fuel at boiling point (kg/m^3)

2.1.2.2 Flame geometry

2.1.2.2.1 Flame shape

Cowly and Johnson (1991) approximated the shapes of the flame in the majority of the pool fire solid flame models using regular geometric shapes. The most commonly used shapes for solid flame models are vertical cylinder or cone (absence of wind blow), tilted or sheared circular or elliptical cylinder (presence of wind blow). (Figure 2-4)

Rew and Helberd (1996) claimed that sheared elliptical cylinder describes the real flame length more accurately and can be used to give predictions of radiation not only for targets that are places laterally but also for those that are placed downwind of the flame.

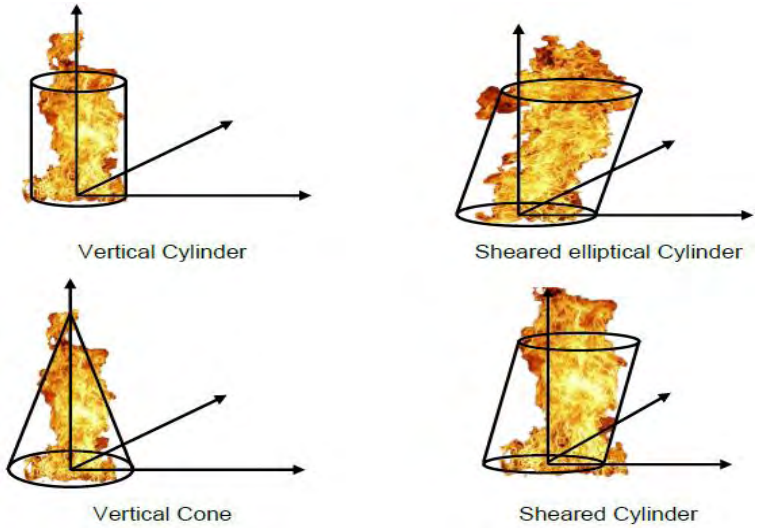

Figure 2-4 Regular flame shapes commonly used in pool fire modelling

2.1.2.2.2 Flame length

According to Cowley and Johnson (1991) the flame length is the length from the flame base along the flame direction to the higher point of visible flame. In this point should be mentioned that some models require flame height as an input. Figure 2-5 identifies that flame length is not the same with the flame height. Flame height is the vertical projection of flame

length. Only in case of wind absence where the flame shape is not sheared by wind, flame height is exactly the same with the flame length.

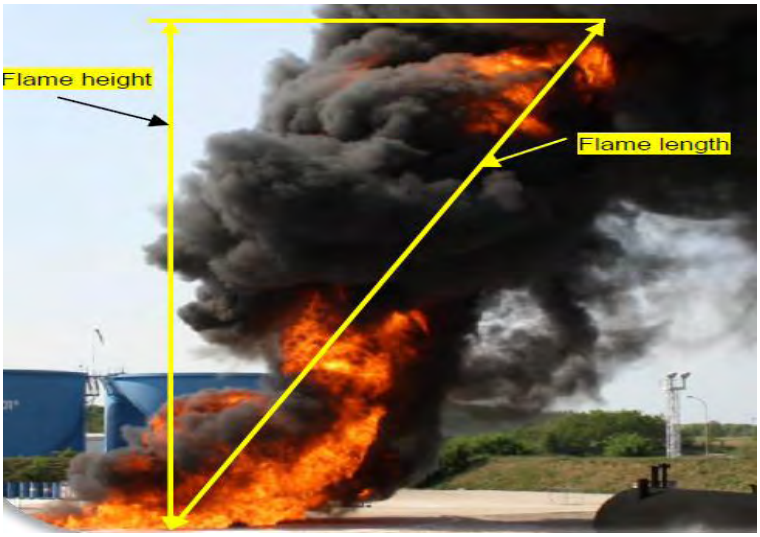

Figure 2-5 Flame length and flame height of gasoline fire (Mansour 2012)

The most commonly used expressions to predict the flame length is produced by Thomas (1963) and it is based on the dimensionless mass burning rate (Equations 2.7 and 2.8).

$$\frac{L}{D} = 42 \cdot [\dot{m}*]^{0.61} \quad (2.7)$$

$$\dot{m}* = \frac{\dot{m}_b}{\rho_a \cdot (g \cdot D)^{1/2}} \quad (2.8)$$

where,
L = flame length (m)
$\dot{m}^*$ = dimensionless mass burning rate of the fuel
ρ_a = density of air at ambient conditions (kg/m^3)
g = acceleration due to gravity (m/s^2)

Pritchard & Binding (1992) produced a two layer solid flame model with a realistic flame shape. This model uses an alternative expression for flame length (equation 2.9).

$$\frac{L}{D} = 10.615 \cdot (\dot{m}*)^{0.305} \cdot (U_9^*)^{-0.03} \quad (2.9)$$

where,
U_9*= dimensionless windspeed at a height of 9 m (set to 1, if less than 1) is given by the following equation

$$U_9^* = \frac{U_9}{(g \cdot \dot{m}_b \cdot D/\rho_a)^{1/3}} \quad (2.10)$$

and
U_9 = windspeed measured at a height of 9 m (m/s)

2.1.2.2.3 Flame tilt

Flame tilt acts as a consequence of the wind blow. The wind affects the shape of the flame as many studies carried out, such as by Moorhouse (1982), Pritchard & Binding (1992), Rew and Helberd (1999). Generally the wind causes the flame to stretch downwind (Figure 2-6).

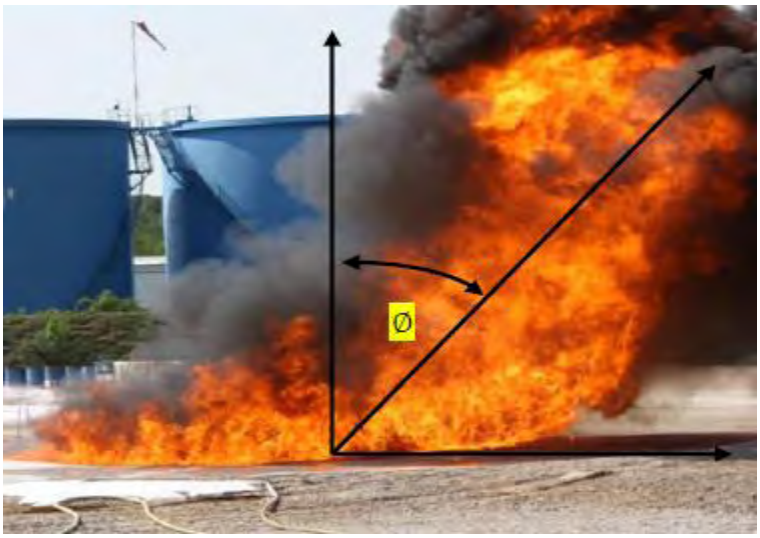

Figure 2-6 Flame tilt of gasoline fire (Mansour 2012)

According the American Gas Asssociation (AGA) (1974) the expression of calculation of flame tilt is the following:

For $U_{1.6}$*≤1.0:

$$cos\,\theta = 1 \quad (2.11)$$

For $U_{1.6}$*>1.0:

$$cos\,\theta = \frac{1}{\sqrt{U^*_{1.6}}} \quad (2.12)$$

where,
θ=tilt of flame from vertical (degrees)
$U_{1.6}$*= dimensionless wind speed at a height of 1.6 m (set to 1, if less than 1)

This equation has been criticized by a lot of researchers due to its failure of predicting flame tilt at low wind speeds.

Wellker & Sliepcevich (1966) recommend the following type for tilt prediction, and Johnson and Pritcard and Binding (1992) completed it:

$$\frac{tan\theta}{cos\theta} = c \cdot Fr^a \cdot Re^b \quad (2.13)$$

where,
Fr = Froude number of pool fire calculated by the following expression:

$$Fr = \frac{U^2}{g \cdot D} \quad (2.14)$$

and, U is the wind speed (m/s)

2.2 Heat transfer theory

In order to model pool fire in a tank farm, is necessary to take into account the heat transfer mechanism between the burning tank and the environment. Heat transfer is the exchange of thermal energy in a system due to temperature difference. There are three types of heat transfer: conduction, convection and radiation.

2.2.1 Conduction

Conduction is the process of molecular heat transfer by microparticles (molecules, atoms, ions, etc.) in a medium with a non-uniform temperature distribution. Conduction is the most significant means of heat transfer within a solid or between solid objects in thermal contact. There are two types of conduction: Steady state and Transient. The basic principle of Steady State Conduction is Fourier's 1st law where the amount of heat entering a section is equal to amount of heat coming out. One the other hand Transient Conduction implies variation with time.

2.2.2 Convection

The second heat transfer process is convection, or heat transfer due to a flowing fluid. The fluid can be a gas or a liquid. In convection heat is transferred at the interface between a fluid and a solid surface. Convection can be forced or natural. In forced convection fluid motion is generated by any external source contrary to natural convection, where the heat transfer is occurred by density differences in the fluid, due to temperature gradients.

2.2.3 Radiation

Unlike conduction and convection, radiation is a method of heat transfer that does not rely upon any contact between the heat source and the heated object. No mass is exchanged and no intervening medium is required. Radiation is the process of heat transfer from one body to another by electromagnetic waves. Radiation can be absorbed, transmitted or reflected at a surface.

When a tank fire incident occur the main mechanism in heat exchange is radiation. The external surface of the burning tank radiates out to the environment, thus the adjacent tank receives radiation on its surface. Conduction is the mechanism of heat transfer through the tank wall, from the hotter parts of wall to the colder ones. The heat from the inner surfaces of the tank wall is transferred to the storage fuel and the air inside by convection. With the same mechanism heat is been exchanged from the outer surface of the tank wall to the ambient air.

2.2.4 Equations and boundary conditions

Depending on the number of primary directions, the temperature varies along within the medium during the heat transfer; the problem can be classified as one, two or three dimensional.

The one-dimensional heat conduction is expressed by Fourier's law of heat conduction, given by the following equation:

$$\dot{Q} = -k \cdot \frac{dT}{dx} \tag{2.15}$$

where k is the thermal conductivity of the material, which is a measure of the ability of a material to conduct heat, and dT/dx is the temperature gradient. The minus sign indicates that the temperature flows from hot to cold region. Thermal conductivity of the material varies with the temperature.

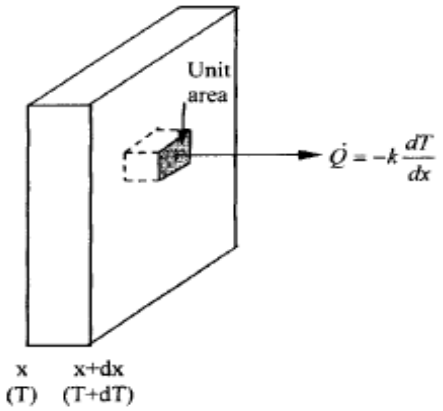

Figure 2-7 One-dimensional heat transfer by conduction

In structures, heat transfer through a medium is more often three-dimensional. That is, the temperature varies along all three primary directions within the medium during the heat transfer process. In rectangular coordinates, the heat conduction vector can be expressed in terms of its components as:

$$\vec{\dot{Q}}_n = \dot{Q}_x \cdot \vec{i}_x + \dot{Q}_y \cdot \vec{i}_y + \dot{Q}_z \cdot \vec{i}_z \tag{2.16}$$

where $\vec{i}_x$, $\vec{i}_y$, $\vec{i}_z$ are the vectors and $\dot{Q}_x$, $\dot{Q}_y$ and $\dot{Q}_z$ are the magnitude of heat transfer rates in x-,y-,z-direction, which can be expressed by Fourier's law as

$$\dot{Q}_x = -k_x \cdot \frac{dT}{dx}, \quad \dot{Q}_y = -k_y \cdot \frac{dT}{dy} \quad \textit{and} \quad \dot{Q}_z = -k_z \cdot \frac{dT}{dz} \tag{2.17}$$

where k_x, k_y, k_z are the thermal conductivities of the material in each one of the three spatial directions.

The application of the energy conservation principle differs whether we have to express steady state heat transfer or transient one. During a steady-heat-flow process, the heat flows through a material volume steadily, experiencing no change with time at a fixed position and can be expressed by the following partial differential correlation:

$$k_x \cdot \frac{\partial^2 T}{\partial x^2} + k_y \cdot \frac{\partial^2 T}{\partial y^2} + k_z \cdot \frac{\partial^2 T}{\partial z^2} = 0 \tag{2.18}$$

In case of transient analysis the heat flow varies with time, the temperature through a material volume isn't constant. The partial differential equation can be given as:

$$k_x \cdot \frac{\partial^2 T}{\partial x^2} + k_y \cdot \frac{\partial^2 T}{\partial y^2} + k_z \cdot \frac{\partial^2 T}{\partial z^2} = \rho \cdot C \cdot \frac{\vartheta T}{\vartheta t} \tag{2.19}$$

where ρ is the density of the material and *C* is its specific heat. Like thermal conductivity coefficient, the specific heat is normally dependent on the temperature of the material.

Specifying boundary conditions is essential for removing derivatives, in order to obtain a solution to the previous equation.

2.2.4.1 Fixed (or specified) temperature boundary conditions

In specific points of the material, the temperature is assumed known:

$$T = T_o \tag{2.20}$$

One of the easiest ways to specify the thermal conditions to a point is to specify the temperature on its surface.

2.2.4.2 Fixed flux boundary conditions

In the case when we know the temperature, the heat flux in a direction normal to a boundary surface is assumed known and can be expressed as:

$$-k_n \cdot \frac{\vartheta T}{\vartheta n} = \dot{q_o} \tag{2.21}$$

where k_n is the thermal conductivity measured in the direction normal to the boundary surface and $\dot{q_o}$ is the known heat flux.

2.2.4.3 Adiabatic boundary conditions

For systems with no significant heat exchange with surroundings the previous equation can be written as:

$$-k_n \cdot \frac{\vartheta T}{\vartheta n} = 0 \tag{2.22}$$

Such a system is said to be adiabatic. The absence of any heat transfer can be due to perfect thermal insulation or the fact that the system and surroundings are at the same temperature.

The symmetry conditions resemble the insulation or zero heat flux boundary condition, where no heat exchange occurs along the symmetry axis or surface.

2.2.4.4 Convection boundary conditions or boundary conditions at solid – Fluid boundaries

One condition of solid boundaries being in contact with moving fluids, is expressed as:

$$-k_n \cdot \frac{\vartheta T}{\vartheta n} = h_f \cdot \left(T_f - T_s\right) = h_f \cdot \Delta T \tag{2.23}$$

where h_f is the heat transfer coefficient and ϑT is the temperature difference between the fluid and the solid boundary surface. In this case T_f is the fluid ambient temperature (assumed as

known) and T_s is the temperature of the solid surface, which is not a priori known, but is calculated as a result of the solution process. Convection is probably the most common boundary condition encountered in practice since most heat transfer surfaces are exposed to an environment at a specified temperature.

2.2.4.5 Combined convection and radiation boundary conditions

In most cases in structural engineering convective and radiation heat exchange occurs at the same time, therefore:

$$-k_n \cdot \frac{\vartheta T}{\vartheta n} = a \cdot (T\_f - T\_s)^{\beta} + \Phi \cdot \varepsilon_r \cdot \sigma \cdot (T_f^4 - T_s^4) \quad (2.24)$$

where *a* and β are coefficients that depend on the side of the structural elements (fire side or ambient temperature air side), Φ is the configuration or view factor, ε_r is the emissivity and σ is the Stefan-Boltzmann constant. The first part is the convective term whereas the second one is the radiative term.

Emissivity is being evaluated as

$$\varepsilon r = \varepsilon f \cdot \varepsilon s \quad (2.25)$$

where ε_f is the emissivity of fire (usually taken equal to 1.0) and ε_s is the emissivity of the structural material.

2.3 Design regulations and standards

There are various regulations and standards to design and construct fuel storage tanks. Regulations and standards define subjects such as material properties, tank's layout and minimum distance between them, safety tasks, etc. The most commonly used standards for tanks and vessels are the following:

2.3.1 American standards

Flammable and Combustible Liquids Code NFPA 30 (1996), the National Fire Protection Association (NFPA)

Welded Steel Tanks for Oil Storage APl 650 (2007), the American Petroleum Institute (API).

2.3.2 British standards

BS EN 14015:2004 Specification for the design and manufacture of site built, vertical, cylindrical, flat-bottomed, above ground, welded, steel tanks for the storage of liquids at ambient temperature and above (BS EN14015:2004 2004).

2.3.3 European standards

EN 1993-1-6 Eurocode 3: Design of steel structures, Part 1-6: General rules -Strength and stability of shell structures (EN1993 1-6 2007).

EN 1993-1-2 Eurocode 3: Design of steel structures, Part 1-2: General rules -Structural fire design (EN1993 1-2 2007).

EN 1993-4-2 Eurocode 3- Design of steel structures, Part 4-2: Tanks (EN1993 4-2, 2007).

prEN 14015-1: Specification for the Design and Manufacture of Site Built Vertical Cylindrical Flat-Bottomed Above Ground Welded Metallic Tanks for the Storage of Liquids at Ambient Temperature and Above - Part 1: Steel Tanks EN 14015, draft issued for public comment in 2000 (prEN 14015-1 2000).

2.3.4 Company standards

Some of the major companies involved with the use of or the design and construction of storage tanks produced their own Standards such as the Shell standards, and some of these have become influential within the industry and have attained the status of unofficial Standards.

2.4 Literature review

An accurate simulation of pool fire has to rely on valid knowledge of pool fire physical properties. Scientists in order to determine fire characteristics were based on experimental investigations from laboratory to field scale fires of different fuels. Babrauskas (1983), Burgess & Hertzberg (1974), , Mudan & Croce (1988), Cowly and Johnson (1991), Rew and Helberd (1996), Pritchard & Binding (1992), Moorhouse (1992), the American Gas Asssociation (AGA) 91974) , Wellker & Sliepcevich (1966), Ditali et al (1992), Considine (1984), Cook et al (1990), Wayne (1984) and Casal (2008) suggested mathematical expressions to describe and model the flame properties as mentioned in fire modeling in details. Although some approaches were incomplete, their offer in fire safety design is major. Great care is required when choosing an expression to describe a pool fire, taking into account the type of the fuel and the existing conditions.

The simulation of pool fire in current study, is based on the work of P.J. Rew and W.G. Hulbert (1996) for the HSE in UK. They examined two pool fire models; POOLFIRE5 created by HSE and POOL by WS Atkins. POOLFIRE5 includes state-of-the-art modeling for much of the physics, but cannot easily be applied and POOL, whose physics is less sophisticated but can be used in most cases. they made recommendations to improve those two models, based on their research on the recent developments in pool fire modeling. Furthermore, they developed a new model POOLFIRE6, which is a code able to predict radiation at any point. The geometric characteristics of the flame in this thesis are the same with the ones that have been used in POOLFIRE6.

K.A. Mansour (2012) in his thesis also provides a review of the literature on radiant heat modeling. He presents three types of fire models on details, SPS model, which is a single point model, IRAD model, which is a solid flame model, and FDS model which is a field model (CFD). These models are compared with the LASTFIRE model, an experimental project carried out by Loughborough University. All the analyses were conducted for two types of fuel: gasoline and ethanol. IRAD model found to be the most accurate; proved to be in better

agreement with the experimental results. Not forget to mention that IRAD model, is derived from FIRE2 model, that was developed by Pritchard and Binding (1992). Mansour estimated the total radiant heat flux received by target tank for separation distances 0.5D, 1D & 1.5D and concluded that as the separation increases the total heat flux reduces dramatically. He also reviewed over the minimum separation distance between the tanks suggested by the available engineering codes in order to estimate the time needed for the PVRV of the adjacent tank to open; a serious hazardous condition that can lead to the escalation.

A.Sengupta (2010) on the other hand, deals with the location of tanks in a tank farm. He compares varied separation spacing between the tanks with the safety distance proposed by regulations. For his research uses three models, the point source model, Shokri-Beyler's method and Mudan's method to simulate the burning tank, under no wind conditions, as well as in the presence of wind, for gasoline and LNG. The accurate distance between the tanks, is when the calculated heat flux becomes equal to 4.732 kW/m^2. This value is proposed (Daniel, Crowl and Louvar (2002), Lees (1995)) considered to be the safe-inter-tank distance.

Great work has been done by Y.Liu (2012) concerning the thermal distribution patterns developed in an oil tank under the heating from an adjacent tank fire. Heat transfer analysis was conducted to explore the temperature distribution developed in the tank when the fire reaches a steady state. Parameters and assumptions used in the adopted pool fire model were carefully examined. The results showed that a rather non-uniform distribution of temperature is developed in the tank especially around the tank circumference. A simple model was then proposed to describe the temperature distribution based on the numerical heat transfer analysis. The accuracy of the proposed temperature distribution model for predicting the structure behavior was evaluated by comparing its predictions with those using directly the temperature distribution obtained from the numerical heat transfer analysis. Various fire scenarios and tank conditions on the temperature distribution in the tank have been studied, such as the effect of liquid filling height, of vertical fire location and flame height, of horizontal fire location (distance) and of fire diameter. From the above scenarios was found that if the separation between tanks is fixed, the larger the fire diameter is, the higher the temperature is developed in the tank and the wider the tank is heated. If the separation distance follows the requirement of NFPA30 (1996), in which the separation is a linear function of the diameter of both the tank and the fire, the highest temperature is not produced by the largest diameter fire scenario but the heated region still increase in size with an increase in the fire diameter.

F.S. Santos and A. Landesmann (2014) based on the available literature and ABAQUS finite element program developed a pool fire semi-empirical model to simulate the burning tank, in order to determine the temperature variation on the target tank. The obtained results were validated with CFD analysis results performed by Fontenelle (2012). In sequential they argued whether or not the current NFPA 30:2012 design recommendations over the safety distance between the tanks needs to be modified. Their analysis considered the impact of various parameters such as the fuel type (gasoline or ethanol), the structural material (steel or concrete), the presence or absence of wind and several distances. It may be concluded that the only accurate failure prediction of NFPA 30:2012, concerning the steel tank was under no fire conditions, with gasoline as storage fuel.

Tank layouts and spacing at the refineries, petrochemical sites and terminals are built to meet the codes and standards. The Table 2.2 below presents the main minimum separation distances recommended by international codes and standards that are proposed by literature:

Engineering Code	**Minimum Separation Distance**	**Definition**

NFPA 30/1996	1/6 sum of adjacent tank diameters but no less than ~1m	Used : for tanks with diameter D<45m, with fixed roofs
NFPA 30/2012	The separation distance where Internal Temprature < Autoignition Temperature	Autoignition Temperature: Gazoline: 298,9°C Ethanol: 392,0°C
European Model Code of Safe Practice, Part II	The minimum separation distance between fixed-roof storage tanks is half the diameter of the larger tank.	
Institute of Petroleum Model Code Safe Practice	The minimum required spacing distance between fixed-roof tanks is half the diameter of the larger tank, but not less than 10m and no more than 15m.	
Lee: Loss Prevention in Process Industry	4,732 kW/m^2	The limit of threshold of pain- limit for workers of the plant continue doing essential tasks (second limit)

Table 2-2 Safety distances between tanks specified by codes and standards

In NFPA 30:1996 the safety distance between the tanks is a linear function of the diameter of the tanks including. For tanks with diameter D=10m, the safety distance is equal to 3,33 m when there are only two tanks and is increased to 10m when there are 6 tanks.

In NFPA 30:2012 the safety distance is defined by autoignition temperature. Autoignition temperature is the minimum temperature required to ignite the fuel contained in the adjacent tank without a spark or flame being present. Failure of the target tank is expected to occur when the internal sidewall temperature of the target tank gets equal to or bigger than the autoignition temperature.

According to European Model Code of Safe Practice the distance is determined by the diameter of the larger tank. If the diameter of the bigger tank is D=10m, the safety distance is equal to 5m, and equal to 10m if the bigger tank's diameter is D=20m.

The safety distance between the tanks specified by Institute of Petroleum Model Code Safe Practice varies from 10 m to 15m.

Last but not least in Loss Prevention in Process Industry the minimum distance between the tanks is calculated through the heat flux between the fire engulfed tank and the adjacent tank and obviously this varies as the distance between them changes. The distance at which the heat flux becomes equal to 4.732 kW/m^2 is considered to be the safe inter-tank distance since.

CHAPTER 3. MATERIAS PROPERTIES OF STEEL AT ELEVATED TEMPERATURES

The properties of steel at elevated temperatures are very important for the analysis of structures subjected to fire. Taking into account the conclusions of studies that have been conducted in the past from various researchers, it is obvious that it is of great importance to simulate numerically the dependence of material properties to temperature, in order to study the response of structures in fire conditions. The dependence of all mechanical-thermal properties of materials to temperature contributes to a more complex numerical analysis. The following section describes the mechanical and thermal properties of steel, which are adopted in the present study, complied with the mathematical models as are proposed in EN 1993-1-2.

For heating rates between 2 and 50 K/min, the strength and deformation properties of steel at elevated temperatures are obtained by the stress-strain curve of Figure 3.1. At high temperatures, the stress-strain diagram of structural steel is modified compared to that at room temperature as shown in Figure 3.2. The elastic part continuous to an elliptic branch, until the suggested strain limit of $\varepsilon_{y,\theta}$=2%. In the end of the curve a yield plateau is observed until is reached the strain value $\varepsilon_{t,\theta}$=15%. The variation of the stress-strain relationship, for structural steel S275, as the temperature increases is presented in Figure 3.2. The strength of steel begins to decrease at temperatures above 400°C. The decline is rapidly and at the temperature of 800°C the yield stress is being reduced 89%. In the present study, it is assumed that steel melts at the temperature of 1200°C where its strength is becoming zero.

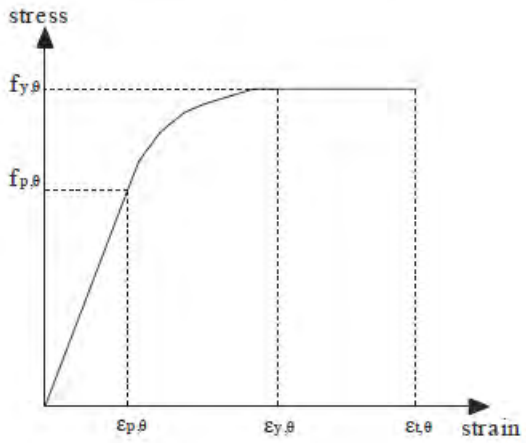

$f_{y,\theta}$ effective yield strength;
$f_{p,\theta}$ proportional limit;
$E_{a,\theta}$ slope of the linear elastic range;
$\varepsilon_{p,\theta}$ strain at the proportional limit;
$\varepsilon_{y,\theta}$ yield strain;
$\varepsilon_{t,\theta}$ limiting strain for yield strength;
$\varepsilon_{u,\theta}$ ultimate strain.

Figure 3-1 Stress-strain relationships of structural steel at elevated temperatures.

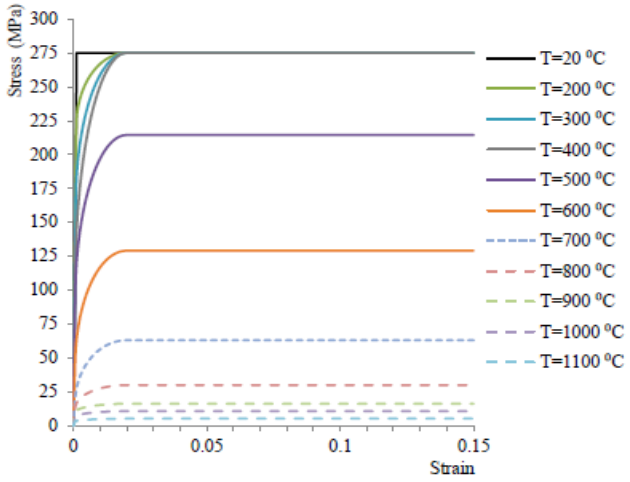

Figure 3-2 Stress-strain relationships of structural steel S275 at elevated temperatures.

At elevated temperatures, effective yield strength, proportionality limit and slope of linear elastic range are reduced according to factors specified on Figure 3.1 EN 1993-1-2 for structural steel.

The temperature dependent thermal properties of steel that determine the response of the structures under fire conditions are thermal elongation, thermal conductivity and specific heat. The relative thermal elongation of steel increases as the temperature rises. As it shown in Figure 3.3 thermal elongation increases linearly until 750°C, where a platue appears until 860°C. Afterwards the thermal elongation continuous to increases linearly until 1200°C.

The behavior of thermal conductivity k under fire loading is illustrated in Figure 3.4 Thermal conductivity reduces as the temperature increases until it reaches the value of 27.3 W/mk at 800°C and then till the end becomes stable.

The specific heat is barely increased at elevated temperatures until 600°C. In the range between 600°C and 735°C the specific heat increases immediately until the value of 5000 J/kg (Figure 3.5). This occurs due to the phase transition of steel at this temperature. Between the 735°C and 900°C the specific heat declines rapidly until it stays stable the value of 650 J/kg.

The unit mass of stele may be considered to be independent of the steel temperature and be taken:

$$\rho_a = 7850 kg/m^3$$

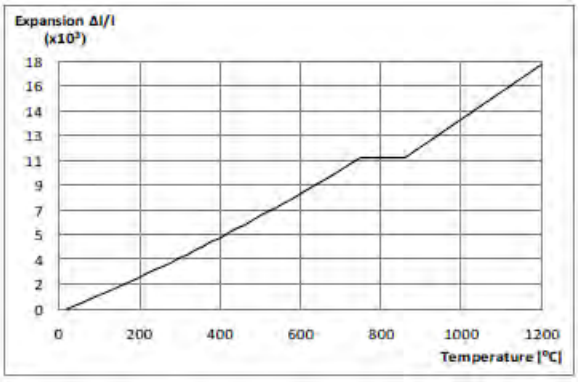

Figure 3-3 Thermal expansion of steel.

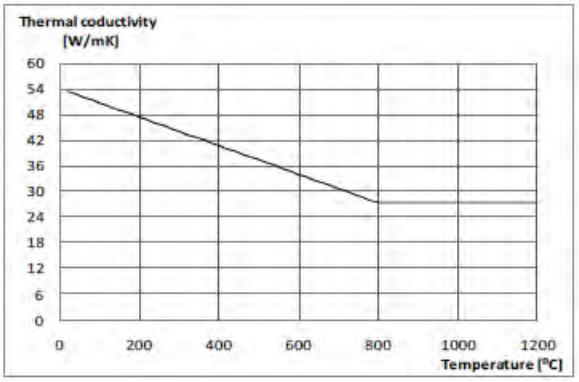

Figure 3-4 Thermal conductivity of steel.

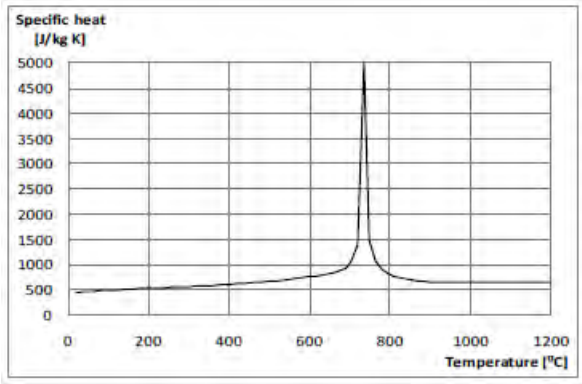

Figure 3-5 Specific heat of steel.

CHAPTER 4. DESCRIPTION OF THE PROBLEM - THE CASE STUDIES

This chapter defines the problem that is being addressed within the present work. The fixed roof tanks examined and the type of thermal load used are presented extensively. Furthermore, the basic assumptions adopted during the study of the problem are analyzed.

4.1 Description of the problem

A common threat in a tank farm is when a fire incident takes place. The burning tank, that contains flammable liquids, is expected to collapse due to material deformation at elevated temperatures. The burning tank can be seen as the heat generator for the adjacent tanks. The heat is transferred through radiation to the nearby tanks, and turns into thermal loading to them. The thermal loading causes temperature development on the neighbor tanks that can lead either to their failure or even to fire expansion.

This thesis focuses on the pool fire modeling of the burning tank and on the parameters that affect the temperature distribution on the adjacent tank. The parameters being examined are the diameter of the burning tank, which is actually the diameter of the pool fire, the combustible content (ethanol or gasoline), the presence or absence of wind conditions and the distance between the tanks.

In this thesis, the flame is simulated through a cylinder or sheared elliptical cylinder, as it is described in Figure 4-1, depending if the wind is considered or not.

.

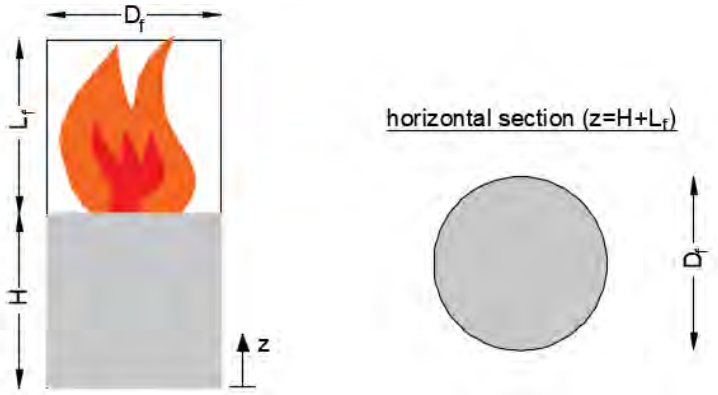

Figure 4-1a. Geometric characteristics of flame in case where the wind is not considered

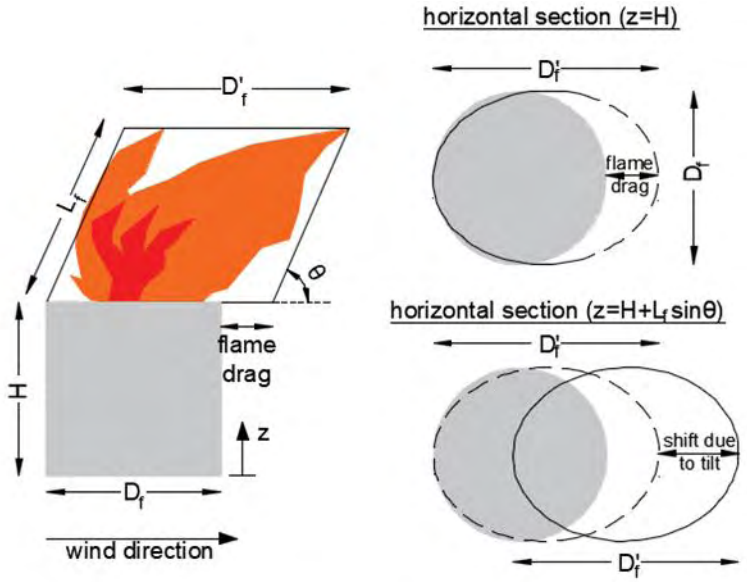

Figure 4-1b. Geometric characteristics of flame in case where the wind is considered

The equations used for the calculation of flame's geometry are summarized in the following.

The mass burning rate is calculated using the expression suggested by Babrauskas (1983)

$$\dot{m}_b = \dot{m}_{max} \cdot (1 - e^{(-k\beta)\cdot D}) \quad (4.1)$$

where:
L = flame length (m)
ṁ* = dimensionless mass burning rate of the fuel
ρ_a = density of air at ambient conditions (kg/m^3)
g = acceleration due to gravity (m/s^2)

The values of $\dot{m}_{max}$ *and* $k\beta$ are dependent on the fuel type and are taken from the Table 2.1.

The estimation of the flame length is based on Thomas (1963) proposal,:

$$\frac{L}{D} = 42 \cdot [\dot{m}*]^{0.61} \quad (4.2)$$

where,

$$\dot{m}* = \frac{\dot{m}_b}{\rho_a \cdot (g \cdot D)^{1/2}} \quad (4.3)$$

L = flame length (m)
ṁ* = dimensionless mass burning rate of the fuel
ρ_a = density of air at ambient conditions (kg/m^3)
g = acceleration due to gravity (m/s^2)

Flame tilt in this study is dependent on Froude number, as proposed at least square fit method.

$$\frac{tan\theta}{cos\theta} = 3.13\ Fr^{0.431} \quad (4.4)$$

$$Fr = \frac{U^2}{g \cdot D} \quad (4.5)$$

where,
Fr = Froude number of pool fire
U = wind speed (m/s)

Flame drag, according to Moorhouse (1982), is calculated as follows:

$$\frac{D'}{D} = 1.5 \cdot (Fr_{10})^{0.069} \quad (4.6)$$

Based on Mudan's (1984) qualitative experimental data of pool fires, the luminous zone for gasoline is taken as 20% of the flame surface area. One the other hand in the ethanol fire, according to Santos (2014) the rate of visible parts is 80%.

The flame average emissive power is predicted using the unobscured ration (U_R) as:

$$Eav = E \cdot U_R + Es \cdot (1 - U_R) \quad (4.7)$$

where
E= emissive power of flame
Es= emissive power of smoke, (taken as 20kW/m^2).

Therefore in agreement with Landesman and Santos (2014) the following values for ethanol and gasoline are obtained: E_{av},ethanol= 164,93 kW/m^2 and E_{av},gazoline=42,74 kW/m^2.

Transmissivity, according to Casal (2008) is calculated as function of the distance (*d*) between the flame and the target according to the following equation:

$$\tau = \begin{cases} 0.976 \cdot d^{-0.06}, d < 5\ m \\ 1.029 \cdot d^{-0.06}, 5 \leq d \leq 55\ m \\ 1.159 \cdot d^{-0.12}, d > 55\ m \end{cases} \quad (4.8)$$

The flame radiation temperature is given by the following expression:

$$Tfe = \sqrt[4]{\frac{e_f \cdot \sigma \cdot T_a^4 + E_{av} \cdot \tau}{\varepsilon_f \cdot \sigma}} \quad (4.9)$$

where,
T_{fe} = radiation temperature of the flame (K)
e_f= emissivity (equal to 1)
σ = Stefan – Boltzmann constant (equal to 6.124X10^{-8} kW/m^2)
T_a = ambient temperature (equal to 293K)

4.2 The case studies

The layout of storage tanks that is considered in this thesis, is illustrated in Figure 4.2. Four different scenarios are studied depending on the number of burning tanks. The "target tank" in all cases has the same geometric characteristics and is considered to be empty. Basic goal is to study the fire-behavior of this tank.

In scenario 1, the case of one unique burning tank is examined. Parametric case studies are examined with respect to parameters that may affect the behavior of target tank. The different case studies for Scenario A are presented in Table 1. The parameters that are considered are the type of the geometry of burning tank, the fuel that is stored (Ethanol or gasoline), the presence of wind and the separation distance between the burning and the target tank. The wind direction is indicated in Figure 4.2 3. The short name of each case study is also included in Table 4.2. This name consists of five parts. The first is the diameter of the burning tank, the second is the separation distance, the third is the type of burning fuel (E for ethanol and G for gasoline), the fourth indicates if the wind is considered (W for the case of wind and NW for the wind free case) and the fifth part is the name of the scenario.

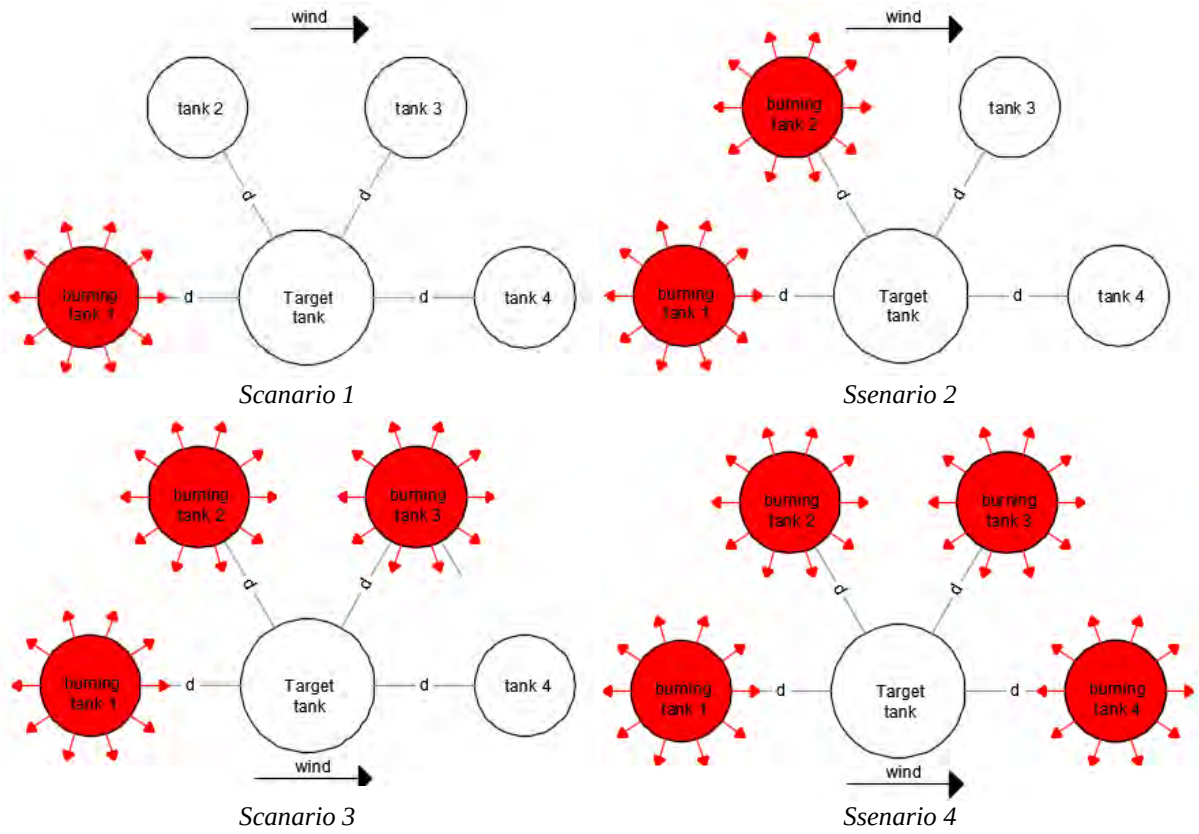

Figure 4. Layout of tanks and the fire scenarios

Scenario 2 corresponds to the case where the fire spreads from tank 1 to the adjacent one (tank 2). The further propagation of fire to more adjacent tanks (tanks 3 and 4) is incorporated in Scenarios 3 and 4. In scenarios with multiple tank fires it is assumed that the fire spreads simultaneously to adjacent tanks. In these scenarios the parameters that are considered are the wind conditions and the type of fuel and the case studies are presented in Table 2.

Both tanks are typical cylindrical thin walled tanks and have a uniform thickness of 10 mm. The burning tank is 10 m high and two values for its diameter is considered, 10m & 15m. The target tank is 20m high and has a steady diameter in all models, equal to 20m. The source tank is opened roof for convenience in calculations while the adjacent tank is assumed fixed roof, conical in shape and with 10^{o} slope. It would be more appropriate to use internal trusses for support that improve the stiffness of the roof instead of fixed roof tank. The internals trusses are more sophisticated in modeling, that´s why they give more accurate results. However they would not give any profit to this study.

Two fuel types are examined; ethanol and gasoline. The tanks are considered to be fully contained with the flammable liquid, thus the level of the fuel rises 10 m high, for the burning tank, and 20 m high for the target tank. The diameter of the burning tank and the type of the fuel as mentioned before affect the size of the pool fire.

The incident of the wind during a fire event is also taken into account, which affects the shape of the flame envelope. Two scenarios are examined, a wind free situation with null wind speed, u=0m/s and windy one with a wind speed magnitude of u=5m/s. The shape of the flame is considered to be a vertical elliptical cylinder under no wind conditions, while is assumed to be a sheared elliptical cylinder when the wind blows.

Finally three different separation distances are examined. The target tank is placed 15, 20 and 25m away from the source tank.

		BURNING TANK DIMENSIONS		FLAME CHARACTERISTICS										TARGET TANK DIMENSIONS	
A/A	NAME	D	H heigth	BURNING FUEL	D2 1st diameter of ellipse	D'	D2 2nd diameter of ellipse	L Flame length	W Wind speed	Θ flame tilt	τ	Tf	d distance	D	H heigth
		(m)	(m)		(m)	(m)	(m)	(m)	(m/s)	(degrees)	(m)	(°C)	(m)	(m)	(m)
1	10_15_E_W_1	10	10	ETHANOL	10	13.65	9.05	10.68	5	48.82	1.121	1071.30	15	20	
2	10_20_E_W_1	10	10	ETHANOL	10	13.65	9.05	10.68	5	48.82	1.121	1071.30	20	20	20
3	10_25_E_W_1	10	10	ETHANOL	10	13.65	9.05	10.68	5	48.82	1.121	1071.30	25	20	20
4	15_15_E_W_1	15	10	ETHANOL	15	19.91	13.57	14.16	5	45.58	1.121	1071.30	15	20	20
5	15_20_E_W_1	15	10	ETHANOL	15	19.91	13.57	14.16	5	45.58	1.121	1071.30	20	20	20
6	15_25_E_W_1	15	10	ETHANOL	15	19.91	13.57	14.16	5	45.58	1.121	1071.30	25	20	20
7	10_15_G_W_1	10	10	GAZOLINE	10	13.65	9.05	15.78	5	48.82	1.121	687.54	15	20	20
8	10_20_G_W_1	10	10	GAZOLINE	10	13.65	9.05	15.78	5	48.82	1.121	687.54	20	20	20
9	10_25_G_W_1	10	10	GAZOLINE	10	13.65	9.05	15.78	5	48.82	1.121	687.54	25	20	20
10	15_15_G_W_1	15	10	GAZOLINE	15	19.91	13.57	20.92	5	45.58	1.121	687.54	15	20	20
11	15_20_G_W_1	15	10	GAZOLINE	15	19.91	13.57	20.92	5	45.58	1.121	687.54	20	20	20
12	15_25_G_W_1	15	10	GAZOLINE	15	19.91	13.57	20.92	5	45.58	1.121	687.54	25	20	20
13	10_15_E_NW_1	10	10	ETHANOL	10	10	9.05	10.68	0	0.00	1.121	1071.30	15	20	20
14	10_20_E_NW_1	10	10	ETHANOL	10	10	9.05	10.68	0	0.00	1.121	1071.30	20	20	20
15	10_25_E_NW_1	10	10	ETHANOL	10	10	9.05	10.68	0	0.00	1.121	1071.30	25	20	20
16	15_15_E_NW_1	15	10	ETHANOL	15	15	13.57	14.16	0	0.00	1.121	1071.30	15	20	20
17	15_20_E_NW_1	15	10	ETHANOL	15	15	13.57	14.16	0	0.00	1.121	1071.30	20	20	20
18	15_25_E_NW_1	15	10	ETHANOL	15	15	13.57	14.16	0	0.00	1.121	1071.30	25	20	20
19	10_15_G_NW_1	10	10	GAZOLINE	10	10	9.05	15.78	0	0.00	1.121	687.54	15	20	20
20	10_20_G_NW_1	10	10	GAZOLINE	10	10	9.05	15.78	0	0.00	1.121	687.54	20	20	20
21	10_25_G_NW_1	10	10	GAZOLINE	10	10	9.05	15.78	0	0.00	1.121	687.54	25	20	20
22	15_15_G_NW_1	15	10	GAZOLINE	15	15	13.57	20.92	0	0.00	1.121	687.54	15	20	20
23	15_20_G_NW_1	15	10	GAZOLINE	15	15	13.57	20.92	0	0.00	1.121	687.54	20	20	20
24	15_25_G_NW_1	15	10	GAZOLINE	15	15	13.57	20.92	0	0.00	1.121	687.54	25	20	20

Table 4-1 Names, properties and variables of the first 24 models

				BURNING TANK DIMENSIONS		FLAME CHARACTERISTICS									TARGET TANK DIMENSIONS	
A/A	**NAME**	**NUMBER OF BURNING TANKS**	**FACTS**	**D**	**H**	**BURNING FUEL**	**D2 1st diameter of ellipse**	**D'**	**D2 2nd diameter of ellipse**	**L flame length**	**w wind speed**	**θ tilt of flame**	**τ**	**Tf**	**d distance**	**D**	**H**
				(m)	(m)		(m)	(m)	(m)	(m)	(m/s)	(degrees)	(m)	(°C)	(m)	(m)	(m)
25	15_15_E_W_2	2	model4	15	10	ETHANOL	15	19.91	13.57	14.16	5	45.58	1.121	1071.30	15	20	20
26	15_15_E_W_3	3	model4	15	10	ETHANOL	15	19.91	13.57	14.16	5	45.58	1.121	1071.30	15	20	20
27	15_15_E_W_4	4	model4	15	10	ETHANOL	15	19.91	13.57	14.16	5	45.58	1.121	1071.30	15	20	20
28	15_15_G_W_2	2	model10	15	10	GAZOLINE	15	19.91	13.57	20.92	5	45.58	1.121	687.54	15	20	20
29	15_15_G_W_3	3	model10	15	10	GAZOLINE	15	19.91	13.57	20.92	5	45.58	1.121	687.54	15	20	20
30	15_15_G_W_4	4	model10	15	10	GAZOLINE	15	19.91	13.57	20.92	5	45.58	1.121	687.54	15	20	20
31	15_15_E_NW_2	2	model16	15	10	ETHANOL	15	15	13.57	14.16	0	0.00	1.121	1071.30	15	20	20
32	15_15_E_NW_3	3	model16	15	10	ETHANOL	15	15	13.57	14.16	0	0.00	1.121	1071.30	15	20	20
33	15_15_E_NW_4	4	model16	15	10	ETHANOL	15	15	13.57	14.16	0	0.00	1.121	1071.30	15	20	20
34	15_15_G_NW_2	2	model22	15	10	GAZOLINE	15	15	13.57	20.92	0	0.00	1.121	687.54	15	20	20
35	15_15_G_NW_3	3	model22	15	10	GAZOLINE	15	15	13.57	20.92	0	0.00	1.121	687.54	15	20	20
36	15_15_G_NW_4	4	model22	15	10	GAZOLINE	15	15	13.57	20.92	0	0.00	1.121	687.54	15	20	20

Table 4-2 Names, properties and variables of the next 12 model

CHAPTER 5. NUMERICAL SIMULATION

5.1 Finite elements analysis

The finite element method (FEM) is a numerical method for solving problems of engineering and mathematical physics. Typical problem areas of interest include structural analysis, heat transfer, fluid flow, mass transport, and electromagnetic potential. Traditionally, engineering analysis of mechanical systems has been done by deriving differential equations related to the variables involved. However, solving the resulting mathematical models is often impossible, especially when the resulting models are non-linear partial differential equations. This method can solve not only linear analysis problems that assumes linear elastic behavior and infinitesimally small displacements and strains but also nonlinear analysis problems, such as buckling, or dynamic problems.

Although FEM is capable of predicting a wide range of problems there is a distinct disadvantage associated with this method; requires a great deal of computational effort, especially when deals with more sophisticated models. The technological progress and computational development in the last decades eliminate this disadvantage. In accordance to what has already been mentioned FEM is most preferred by scientists in research and industry in order to give reliable results in any kind of problem, no matter how complicated it is.

The basic concept behind Finite Elemental Method is to divide complex shapes using a large number of regular / simple shapes (like a rectangle, triangle, etc.). These shapes are then combined to correctly model the original part. These smaller, simpler shapes are called finite elements because each shape occupies a finite sub-space within the original, complex shape. The simple equations that model these finite elements are then assembled into a larger system of equations that models the entire problem. FEM then uses alternative methods from the calculus of variations to approximate a solution by minimizing an associated error function. The problem then is expressed through the linear equations and is solved numerically.(1.Bathe 2. Hughes)

In order to eliminate the numerical error in simulation, the properties of the elements must be chosen accurately and the mess applied must be dense. Some of the factors that affect test results are accurate inputs of geometry, physics, properties of the material and loads. Is required not only a better knowledge of the nature of the problem but also having experience on similar analysis, in order to be accurate. If the experience is not possible, a mesh sensitivity study must be performed in order to estimate the point of convergence in the accurate solution.

5.2 Numerical simulation

The problem is solved numerically using the Finite Element (FE) method. The numerical model is developed using the nonlinear finite element code MSC-Marc (2011). The three-dimensional model that is developed for the simulation of the behavior of the thin-walled steel tank uses the element of type 85 of the library of MSC-Marc (2011) for the thermal problem. This is a four-node heat transfer shell element with temperatures as nodal degrees of freedom. Bilinear interpolation is used for the temperatures in the plane of the shell and either a linear or a quadratic temperature distribution is assumed in the shell thickness direction. A four-point Gaussian integration is chosen for the element in the plane of the shell and an eleven-point

Simpson's rule is used in the thickness direction. All the material prpoperties are according to EN 1993-1-2. The emissivity of fire and steel are taken equal to 1 and 0.8 respectively.

The roof of the target tank is simulated using a conical shell with slope equal to 10°. Actually, in practice the type of roof that is used depends mainly on the diameter of the cylindrical tank and as the diameter increases it is more realistic to choose internal trusses to support the roof. Nevertheless, in this study the roof is simulated through conical shell in order to simplify the calculations.

The meshing at both circumferential and vertical coordinated should be carefully chosen. The discretization should be non-uniform in order to decrease the total number of the finite elements that are used in the simulation in order to avoid excessive computational cost and to capture accurately the temperature gradiation on the surface of the tank. Mesh sensitivity study is conducted to determine the mesh of the cylindrical tank and is presented in the following section.

5.3 Mesh sensitivity test

Since there is no analytical solution for comparison, first a mesh sensitivity study is performed. A more dense mesh is adopted near the base, at the liquid surface and which is consider being the upper bound of the cylindrical shell as it is illustrated in Figure 5.1.

Regarding the circumferential direction, the reference mesh size is considered equal to 2° while in the vertical coordinate the loose mesh is 0.5m and the refined mesh is 0.1m. This mesh scheme is considered to be the reference state. The reference temperature response is compared to the values that result from analysis with different meshing schemes, equal to 1^{o} and 3^{o}. The results for ethanol are presented on the Figure 5.2-5.6 and for gasoline on the Figures 5.7-5.11. The diagrams show the temperature distribution along the circumferential plane at height 0, 5, 10, 15 & 20m.

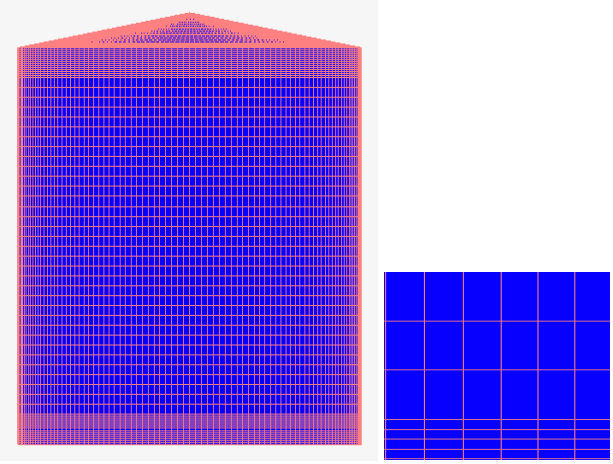

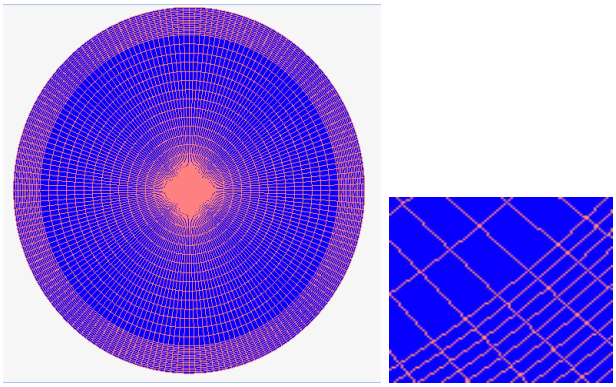

Figure 5-1 Mesh discretization of the target tank

5.3.1 Ethanol

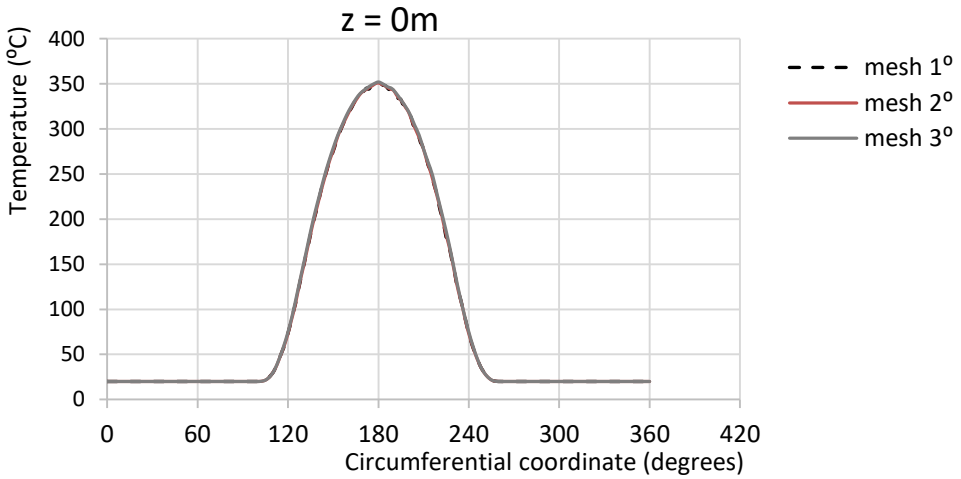

Figure 5-2 Temperature distribution along the circumferential plane at height 0m (base of the tank)

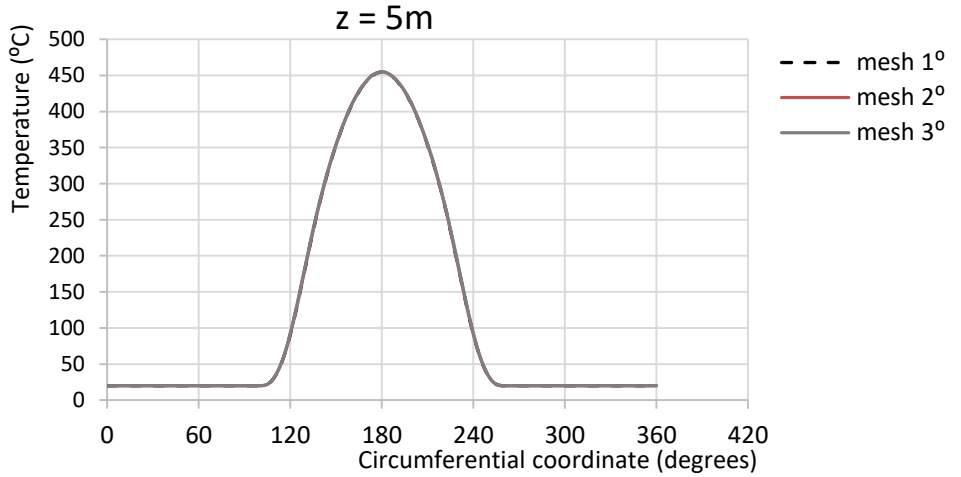

Figure 5-3 Temperature distribution along the circumferential plane at height 5m

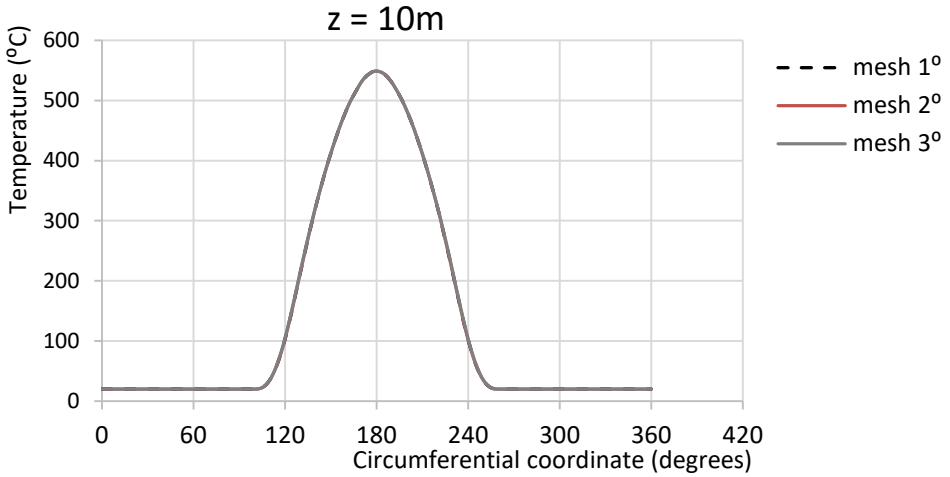

Figure 5-4 Temperature distribution along the circumferential plane at height 10m

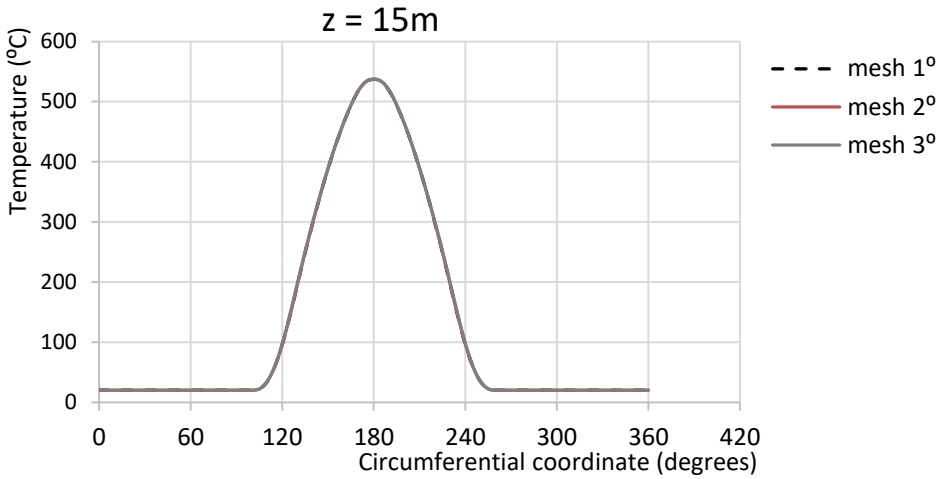

Figure 5-5 Temperature distribution along the circumferential plane at height 15m

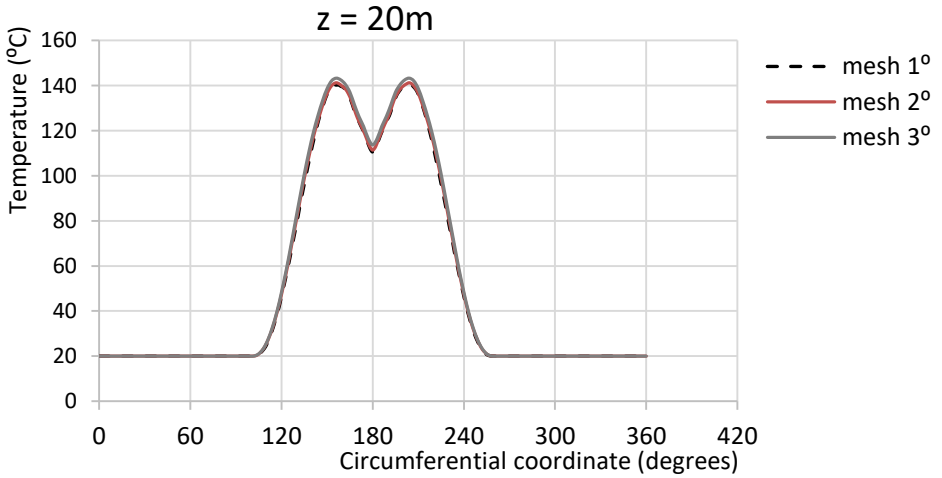

Figure 5-6 Temperature distribution along the circumferential plane at height 20m

5.3.2 Gasoline

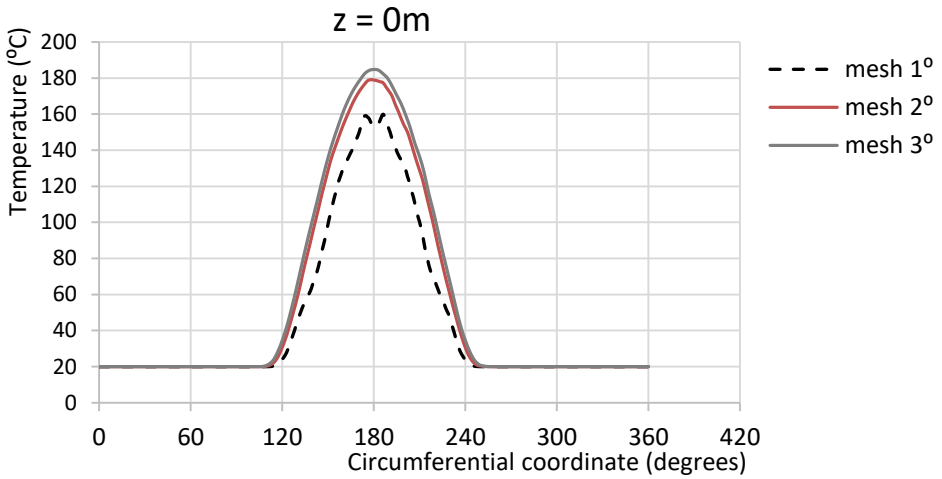

Figure 5-7 Temperature distribution along the circumferential plane at height 0m (base of the tank)

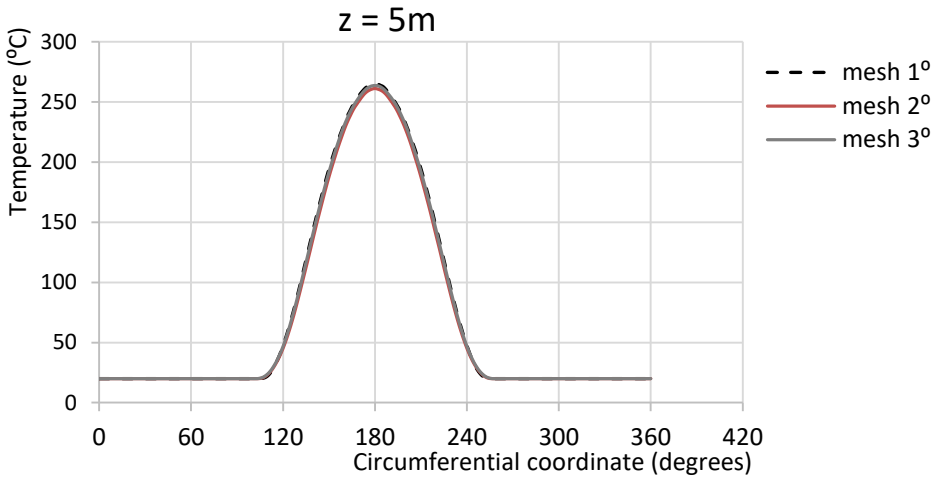

Figure 5-8 Temperature distribution along the circumferential plane at height 5m

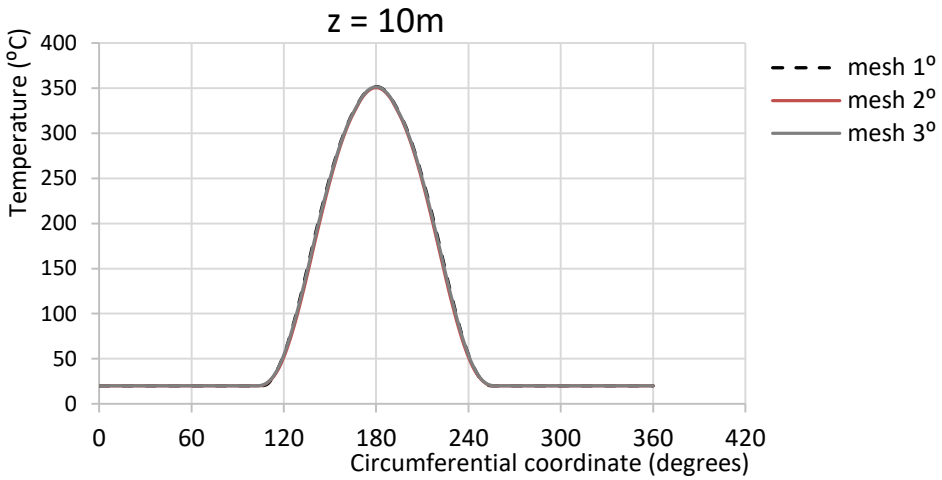

Figure 5-9 Temperature distribution along the circumferential plane at height 10m

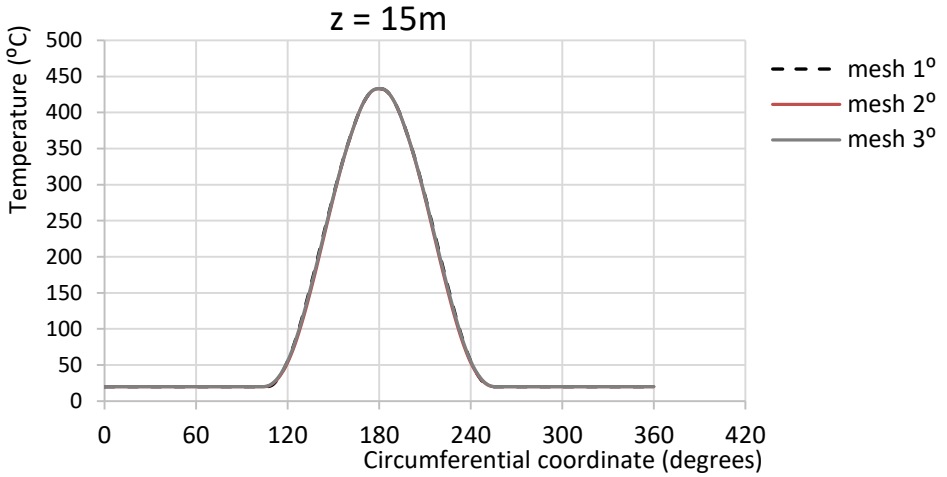

Figure 5-10 Temperature distribution along the circumferential plane at height 15m

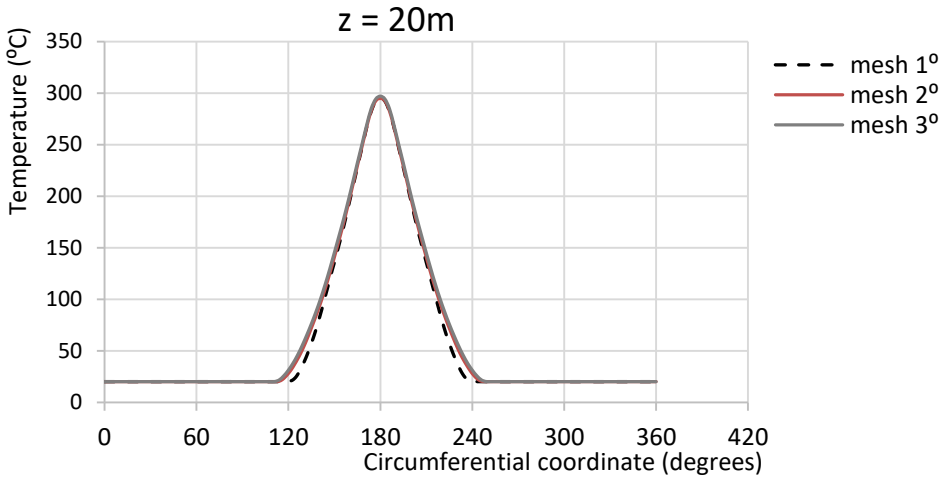

Figure 5-11 Temperature distribution along the circumferential plane at height 20m

The temperature distribution for ethanol is exactly the same for all the three meshes, at any height that is examined. For gasoline the temperature distribution at heights 5m, 10m, 15m and 20m coincides on for the three meshes. At height 0m the temperature distribution for mesh 1° & 2° is almost the same while the temperature distribution for the mesh 3° differs slightly in shape and size. In last case the temperature is 20 degrees lower than the other two meshes.

According to the above, it can be concluded that the results of the temperature response of 1° and 2° meshing schemes converge to the reference case. Thus the meshing scheme of the reference case is adopted in this study.

5.4 Numerical analysis

5.4.1 Heat transfer

MSC Marc contains a solid body heat transfer capability for one-, two-, and three-dimensional, steady-state and transient analyses. This capability allows to obtain temperature distributions in a structure for linear and nonlinear heat transfer problems. The nonlinearities in the problem may include temperature-dependent properties, latent heat (phase change) effect, heat convection in the flow direction, and nonlinear boundary conditions (convection and

radiation).The temperature distributions can, in turn, be used to generate thermal loads in a stress analysis.

MSC Marc can be used to solve the full range of two- and three-dimensional transient and steady-state heat conduction and heat convection problems. Also provides heat transfer elements that are compatible with stress elements. Consequently, the same mesh can be used for both the heat transfer and stress analyses. Transient heat transfer is an initial boundary value problem, so proper initial and boundary conditions must be prescribed to the problem in order to obtain a realistic solution. MSC Marc accepts nonuniform nodal temperature distribution as the initial condition, and can handle temperature/time-dependent boundary conditions. The thermal conductivity can be isotropic, orthotropic, or anisotropic. Both the thermal conductivity and the specific heat in the problem can be dependent on temperature; however, for conventional heat transfer, the mass density remains constant at all times. Latent heat effects (solid-to solid, solid-to-liquid phase changes) can be included in the analysis. A time-stepping procedure is available for transient heat transfer analysis. Temperature histories can be stored on a post file and used directly as thermal loads in subsequent stress analysis. User subroutines are available for complex boundary conditions such as nonlinear heat flux, directional heat flux, convection, and radiation.

As it is already mentioned, transient heat transfer analysis is imposed on the models. During a transient heat transfer analysis, for every time step, the program estimates the temperature reached at the end of the step. From the estimated temperature, the emissivity (temperature dependent) is computed. The temperatures at the end of the step are computed by solving the finite element equations.

The problem is solved using non-linear transient thermal/structural numerical analysis and large displacements are considered in the formulation.

The environmental temperature is set equal to 20ºC. The temperature of the flame is defined through fixed nodal temperature option and remains constant during the analysis.

An open cavity is defined for the treatment of heat transfer problem from burning tanks to the target tank through radiation. There are six approaches to solve radiation problems in MSC Marc with different levels of sophistication. They include:

- View factor calculation by direct adaptive integral method.
- View factor calculation by Monte Carlo method.
- View factor calculation by Pixel Based Modified Hemi-cube method.
- Radiation to Space using the FILMS model definition option.
- Radiation to Space using any of the CONTACT or THERMAL CONTACT options.
- Radiation into the body using the QVECT option.

There are several aspects in performing a radiation view factor calculation including:

- Defining the edges or faces involved in the view factor calculation and determining if the region (cavity) is open or closed.
- Calculation of the view factors.
- If the region is open defining the environment temperature. This temperature may be constant or varying with time.

- Definition of the surface emissivity and absorptivity, including temperature dependence and frequency dependence (spectral behavior). By default, the absorptivity is equal to the emissivity.
- Redefinition of the view factors due to large deformation or other phenomena.
- Redefinition of the view factors due to either local or global adaptive meshing.
- Radiation between surfaces results in increasing the size of the operator (stiffness) matrix, which results in greater memory requirements and increased computational times.

In the radiation calculations in Marc, there are several assumptions made:

- Each surface is a diffuse emitter and reflector; i.e., the thermal behavior is independent of the orientation of the radiation.
- Each surface is black; i.e., is a perfect absorber for all incident radiation.
- The surfaces are isothermal.

The third assumption requires either that an "adaptive" procedure is used to insure accuracy or that the finite elements are sufficiently small for each surface to be assumed to be isothermal.

Using modern mesh generation techniques, there is a tendency to over-refine the finite element mesh, so the need for these adaptive techniques may be less significant.

In theory, the view factors form a symmetric matrix, the size of which is dependent on the number of radiating surfaces. If one has a closed cavity the summation of all view factors emitting from a surface should be equal to one. If desired, the numerically evaluated view factors can be scaled such that the sum is one.

The radiative flow of heat from surface 1 to surface 2 is given by:

$$q_{12} = \sigma \cdot F_{12} \cdot (T_1^4 - T_2^4) \tag{5.1}$$

in which, F_{12} is the view factor and is calculated as:

$$F_{12} = \frac{1}{A_1} \cdot \int_{A_1} \int_{A_2} \frac{\cos\varphi_1 \cdot \cos\varphi_2}{\pi \cdot r^2} dA_2\, dA_1 \tag{5.2}$$

MSC Marc internally computes the view factor between every side of the cavity and all other sides. The matrix with the view factors can be stored into a file, and read in again during a subsequent analysis, thus avoiding a new computation. In this thesis, the calculation of view factors is based on the Pixel Based Modified hemi-cube method.

5.5 Validation study

Full scale fire tests on storage tanks are not available on the literature. To validate the numerical techniques used for the thermal problem, the numerical model is first validated using a fire test of a steel beam found in Compendium UK (xxx).

During the experimental program, numerous fire test on bare steel beams were conducted. The test assembly was mounted in the furnace roof on roller supports in the walls, to provide an effective span of approximately 4.5m and an exposed length of 4m. The opening in the furnace roof was completely closed by a concrete slab cast on the top of the upper flange of the beam. The beams, which are heated in three sides, were instrumented with thermocouples, to obtain detailed temperature profile during the test.

The furnace temperature is controlled to vary with time in accordance with the ISO fire curve:

$$T - T_O = 345 \cdot log_{10}(8 \cdot t + 1) \ (^\circ C) \quad (5.3)$$

where,
t=time on test (min)
T= furnace temperature (^{o}C) at time t
T_o=initial furnace temperature (^{o}C)

Moreover, during the test, the furnace temperature was measured and is provided in the following.

In this study the fire tests 1, 2 and 3 are simulated out. The test include a universal beam (406x178x60kg/m) of steel grade 43A:1979. The dimensions were measured prior the fire test and they are presented ion Table 3.

A three-dimensional numerical model of the steel beam is developed using shell finite elements (Figure 5-12). The numerical model includes the heat transfer though radiation, convection and conduction and the thermal properties of steel according to EN 1993-1-2 were incorporated. The beam was properly discretized, so that the temperature results would be estimated at the exact points the thermocouples were placed. The closed cavity option is utilized for the calculation of view factors (Fig. xx). Actually, through the cavity the furnace is simulated. The emissivity of furnace and steel are set equal to 1 and 0.8 respectively.

The temperature test results are included in sections 5.5.1, 5.5.2 and 5.5.3.

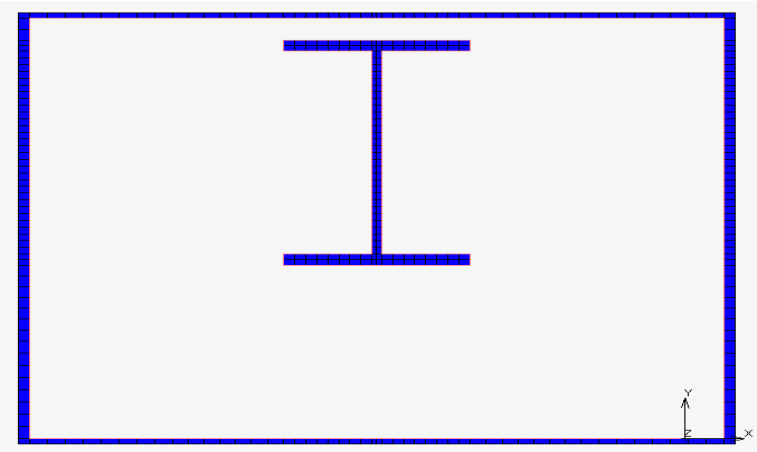

Figure 5-12 Traverse section of the beam as modelled code with MSC Marc (2014) software

5.5.1 Test 1

SECTION SERIAL SIZE AND TYPE mm	DIMENSIONS AND PROPERTIES	MASS PER METRE kg	DEPTH OF SECTION mm	WIDTH OF SECTION mm	THICKNESS		ELASTIC MODULUS		PLASTIC MODULUS		MOMENT OF INERTIA	
					WEB mm	FLANGE mm	AXIS XX cm3	AXIS YY cm3	AXIS XX cm3	AXIS YY cm3	AXIS XX cm4	AXIS YY cm4
254 x 146	NOMINAL	43	259.6	147.3	7.3	12.7	505.3	92.0	568.2	141.2	6558	677
BEAM	ACTUAL	42.7	258.5	148	7.6	12.3					6359.8	

Figure 5-12 Beam dimensions of Test 1

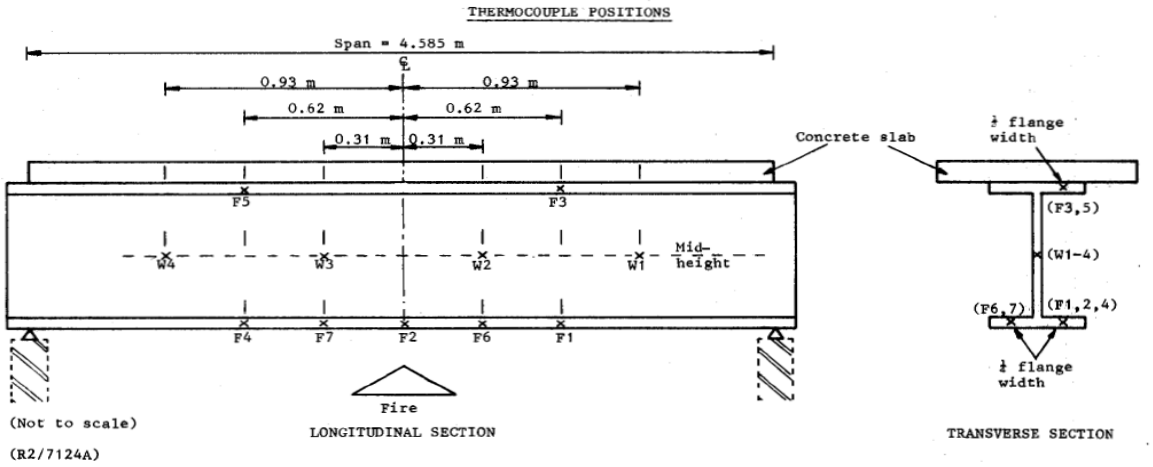

Figure 5-13 Thermocouple positions at longitudinal and transverse section of Test 1

THERMOCOUPLE LOCATION		TEMPERATURE Deg. C AFTER VARIOUS TIMES (MINUTES)							
		3	6	9	12	15	18	21	23
UPPER FLANGE	F3	57	105	161	211	266	322	378	414
	F5	49	99	161	213	268	325	385	432
MEAN		53	102	161	212	267	323	381	423
WEB	W1	109	217	335	431	505	565	609	634
	W2	118	229	352	449	523	582	628	653
	W3	127	250	375	470	541	592	636	661
	W4	114	229	354	445	513	567	615	640
MEAN		117	231	354	449	520	576	622	647
LOWER FLANGE	F1	98	209	329	429	516	583	633	661
	F2	83	190	315	428	518	587	638	665
	F4	113	227	344	440	520	581	630	658
	F6	85	181	299	411	502	573	625	652
	F7	114	221	337	441	526	589	638	663
MEAN		99	206	325	430	516	583	633	660
MEAN FURNACE GAS		433	589	658	705	744	775	793	808
STANDARD CURVE (e)		495	596	656	698	732	759	782	795
DEFLECTION (mm)		1	9	26	37	50	67	100	144

Table 5-1 Temperature input and outpour at thermocouple points of Test 1

5.5.2 Test 2

SECTION SERIAL SIZE AND TYPE mm	DIMENSIONS AND PROPERTIES	MASS PER METRE kg	DEPTH OF SECTION mm	WIDTH OF SECTION mm	THICKNESS		ELASTIC MODULUS		PLASTIC MODULUS		MOMENT OF INERTIA	
					WEB mm	FLANGE mm	AXIS XX cm3	AXIS YY cm3	AXIS XX cm3	AXIS YY cm3	AXIS XX cm4	AXIS YY cm4
254 x 146	NOMINAL	43	259.6	147.3	7.3	12.7	505.3	92.0	568.2	141.2	6558	677
BEAM	ACTUAL	43.4	260	147	*	*					6464.0	

Figure 5-14 Beam dimensions of Test 2

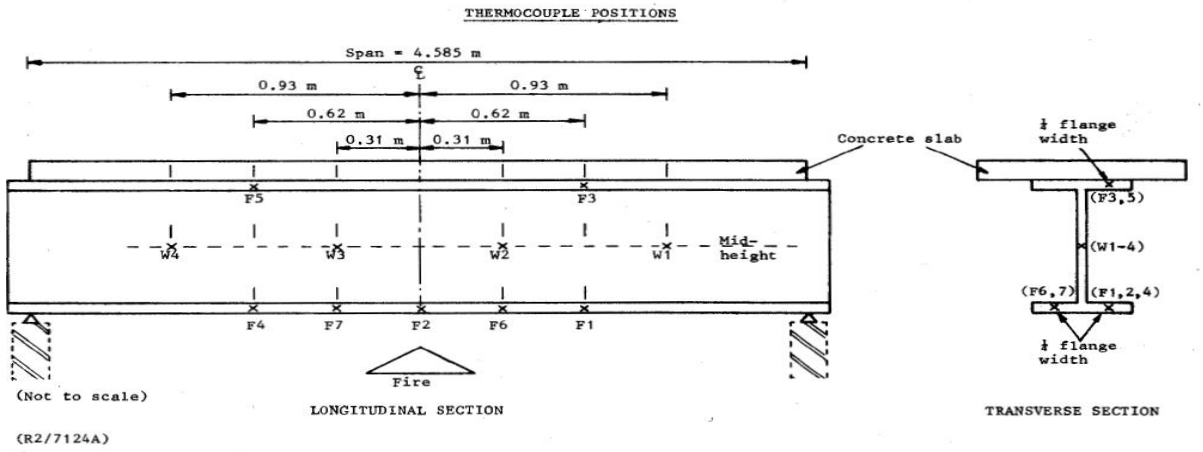

Figure 5-15 Thermocouple positions at longitudinal and transverse section of Test 2

THERMOCOUPLE LOCATION		TEMPERATURE Deg. C AFTER VARIOUS TIMES (MINUTES)							
		3	6	9	12	15	18	21	22
UPPER FLANGE	F3	82	134	192	252	307	358	403	421
	F5	45	97	166	232	287	344	402	426
MEAN		63	115	179	242	297	351	402	423
WEB	W1	110	226	337	430	502	558	597	609
	W2	89	194	309	416	505	569	612	626
	W3	121	250	373	475	542	590	628	641
	W4	118	235	356	456	520	568	605	618
MEAN		109	226	344	444	517	571	610	623
LOWER FLANGE	F1	97	202	320	431	517	580	621	634
	F2	86	194	317	433	522	583	627	639
	F4	75	181	308	426	513	575	619	632
	F6	129	249	362	457	526	577	617	628
	F7	96	205	321	432	520	581	625	638
MEAN		97	206	326	436	520	579	622	634
MEAN FURNACE GAS		496	586	672	721	741	760	777	780
STANDARD CURVE (e)		498	599	659	701	735	762	785	792
DEFLECTION (mm)		4	11	25	37	47	67	116	140

Table 5-2 Temperature input and outpour at thermocouple points of Test 2

5.5.3 Test 3

SECTION SERIAL SIZE AND TYPE mm	DIMENSIONS AND PROPERTIES	MASS PER METRE kg	DEPTH OF SECTION mm	WIDTH OF SECTION mm	THICKNESS WEB mm	THICKNESS FLANGE mm	ELASTIC MODULUS AXIS XX cm3	ELASTIC MODULUS AXIS YY cm3	PLASTIC MODULUS AXIS XX cm3	PLASTIC MODULUS AXIS YY cm3	MOMENT OF INERTIA AXIS XX cm4	MOMENT OF INERTIA AXIS YY cm4
254 x 146	NOMINAL	43	259.6	147.3	7.3	12.7	505.3	92.0	568.2	141.2	6558	677
BEAM	ACTUAL	42.0	260	146	7.34	12.36					6334.5	

Figure 5-16 Beam dimensions of Test 3

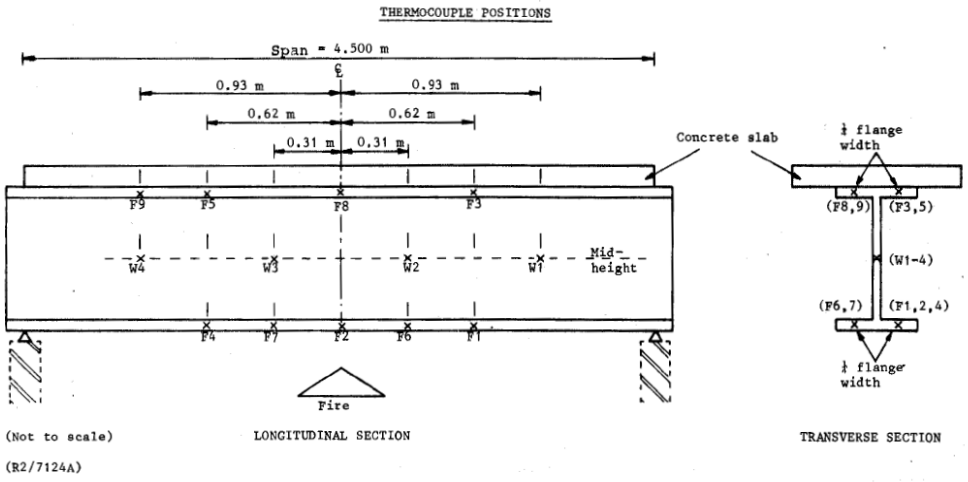

Figure 5-17 Thermocouple positions at longitudinal and transverse section of Test 3

THERMOCOUPLE LOCATION		TEMPERATURE Deg. C AFTER VARIOUS TIMES (MINUTES)									
		3	6	9	12	15	18	21	24	26	27
UPPER FLANGE	F3	86	155	211	273	326	384	431	479	516	535
	F5	122	185	246	305	358	418	464	510	545	563
MEAN		91	149	208	268	325	383	433	481	516	534
WEB	W1	146	276	393	485	552	603	640	671	693	702
	W2	174	303	414	506	572	623	659	690	711	720
	W3	155	284	417	509	576	623	660	689	712	722
	W4	162	286	408	496	563	607	645	674	697	707
MEAN		159	287	408	499	566	614	651	681	703	713
LOWER FLANGE	F1	127	239	364	475	558	619	660	692	711	721
	F2	104	218	355	471	561	624	669	702	722	733
	F4	144	272	401	501	576	633	672	703	723	733
	F6	131	249	371	478	560	619	660	692	713	722
	F7	144	246	370	474	557	616	659	691	713	724
MEAN		130	245	372	480	562	622	664	696	716	727
MEAN FURNACE GAS		515	649	680	730	749	775	793	800	835	832
STANDARD CURVE (e)		499	600	660	702	736	763	786	806	817	823
DEFLECTION (mm)		4	14	27	40	52	66	85	122	150	164

Table 5-3 Temperature input and outpour at thermocouple points of Test 3

5.5.4 Validation of numerical model

The following figures show the comparison of temperature distribution between the results of the fire tests and the outcomes of numerical analyses.

5.5.4.1 Test 1

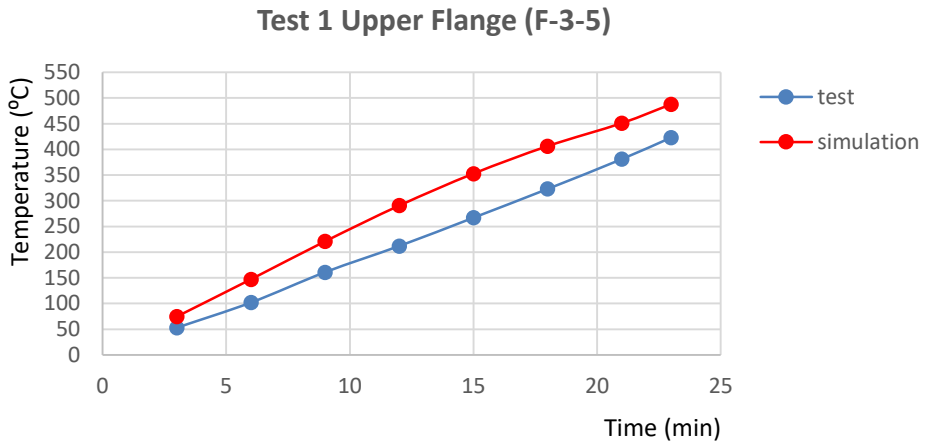

Figure 5-18 Temperature distribution with time at points F-3-5

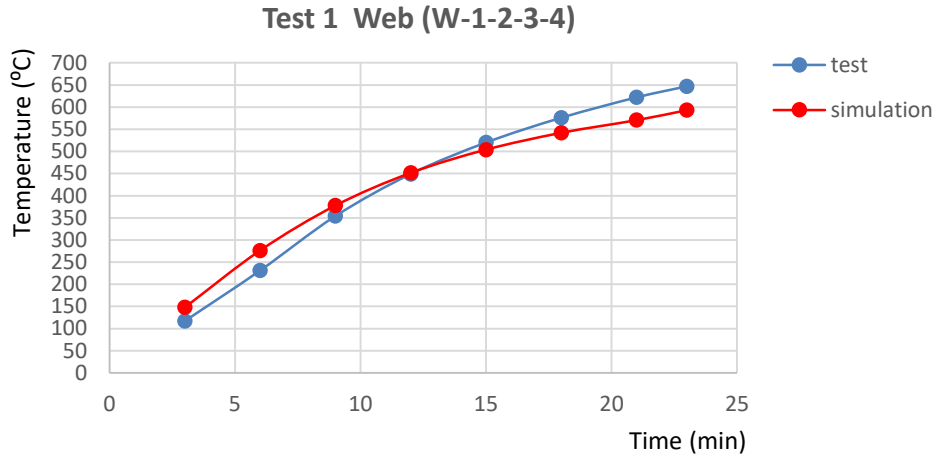

Figure 5-19 Temperature distribution with time at points W-1-2-3-4

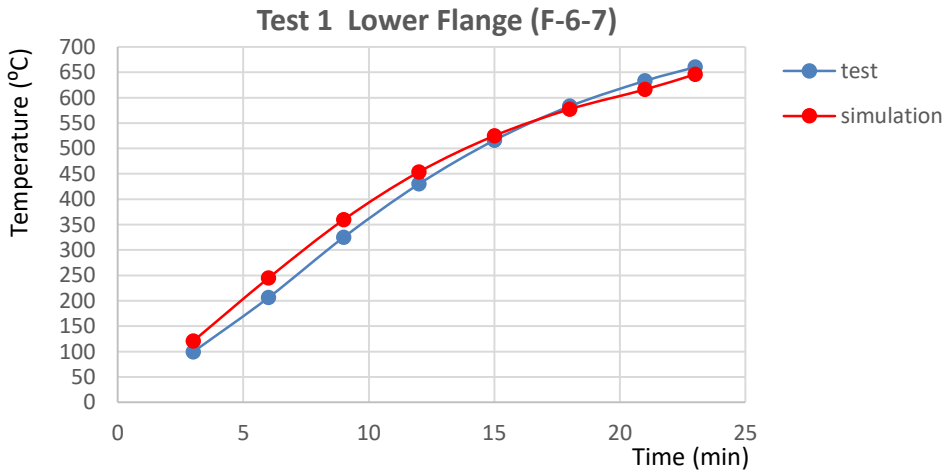

Figure 5-20 Temperature distribution with time at points F-6-7

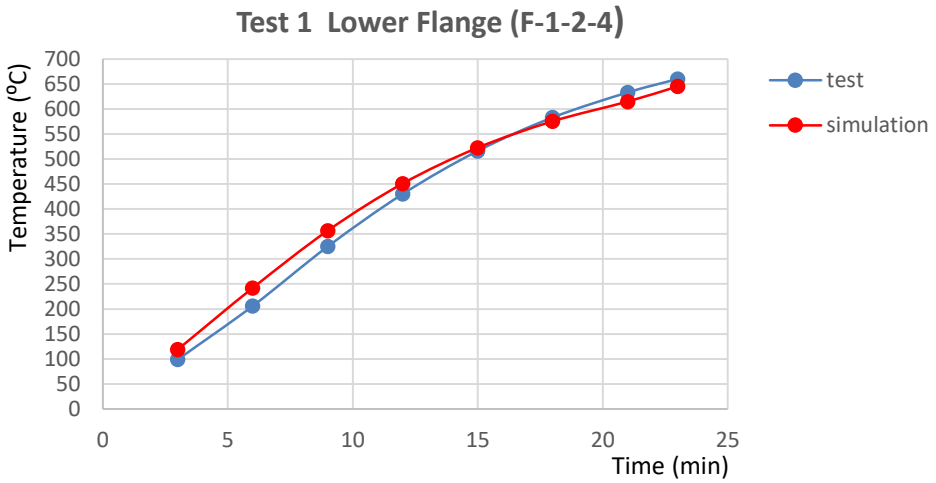

Figure 5-21 Temperature distribution with time at points F-1-2-4

5.5.4.2 Test 2

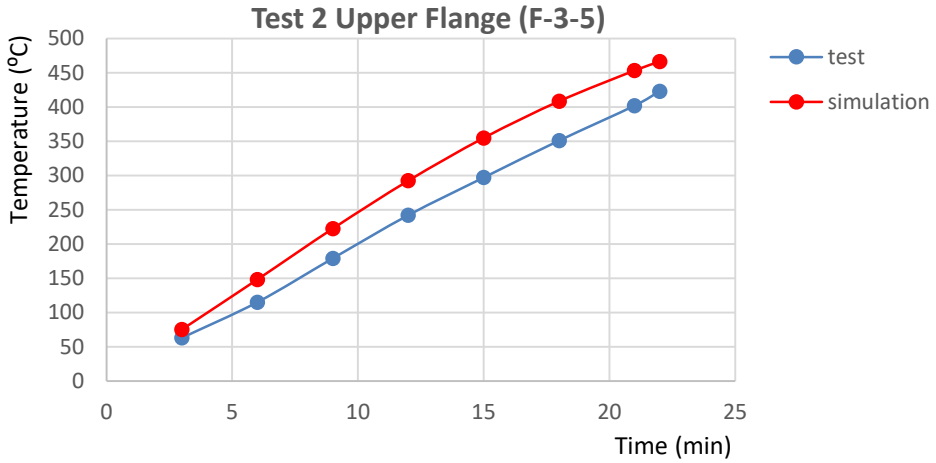

Figure 5-22 Temperature distribution with time at points F-3-5

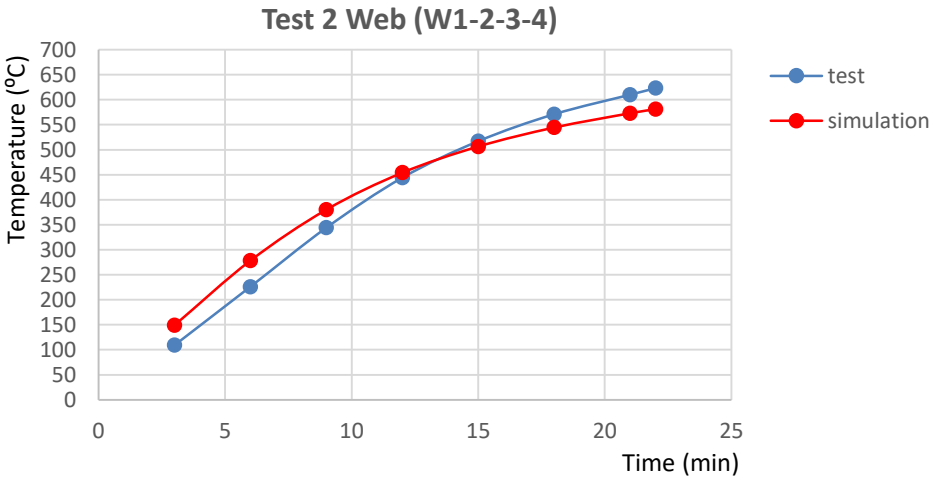

Figure 5-23 Temperature distribution with time at points W-1-2-3-4

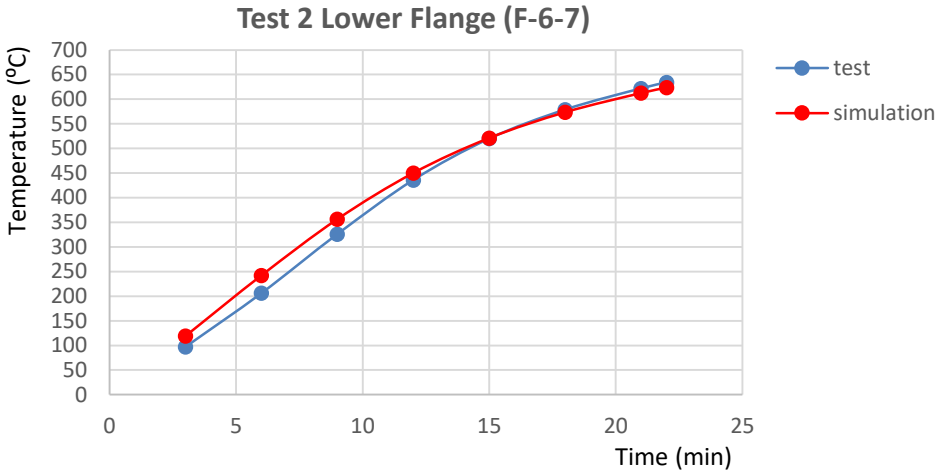

Figure 5-24 Temperature distribution with time at points F-6-7

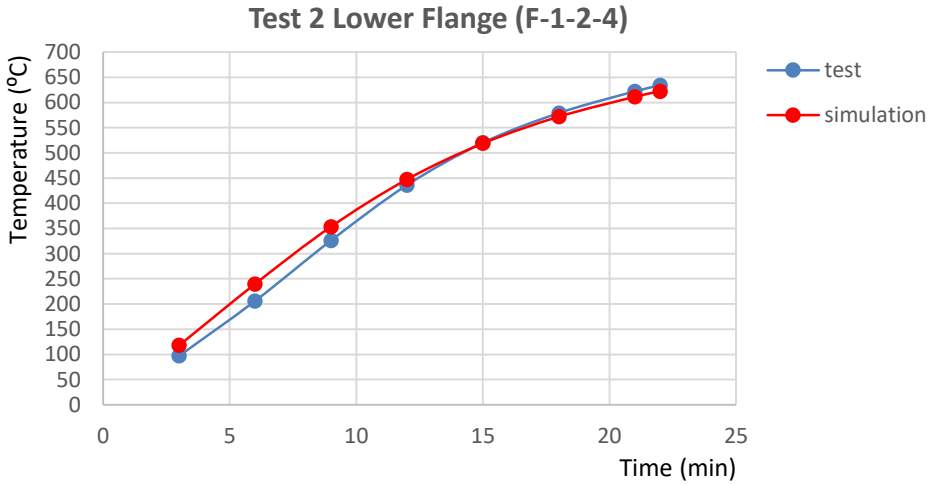

Figure 5-25 Temperature distribution with time at points F-1-2-4

5.5.4.3 Test 3

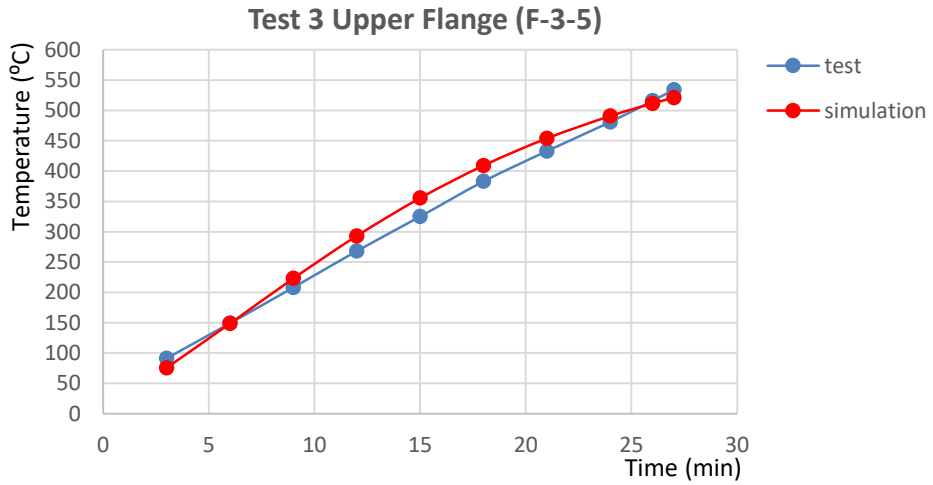

Figure 5-26 Temperature distribution with time at points F-3-5

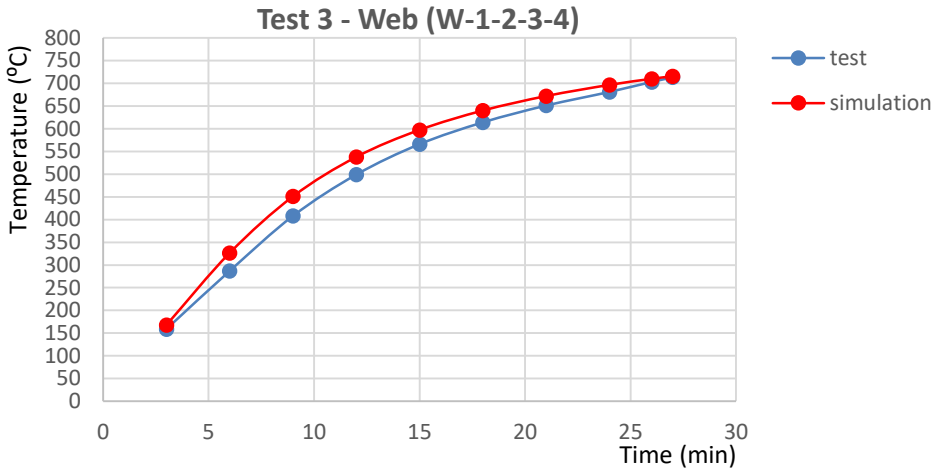

Figure 5-27 Temperature distribution with time at points W-1-2-3-4

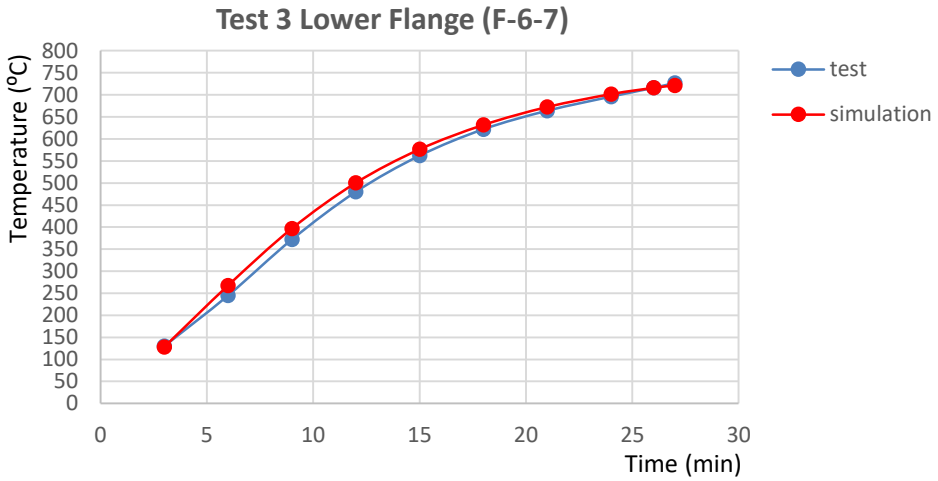

Figure 5-28 Temperature distribution with time at points F-6-7

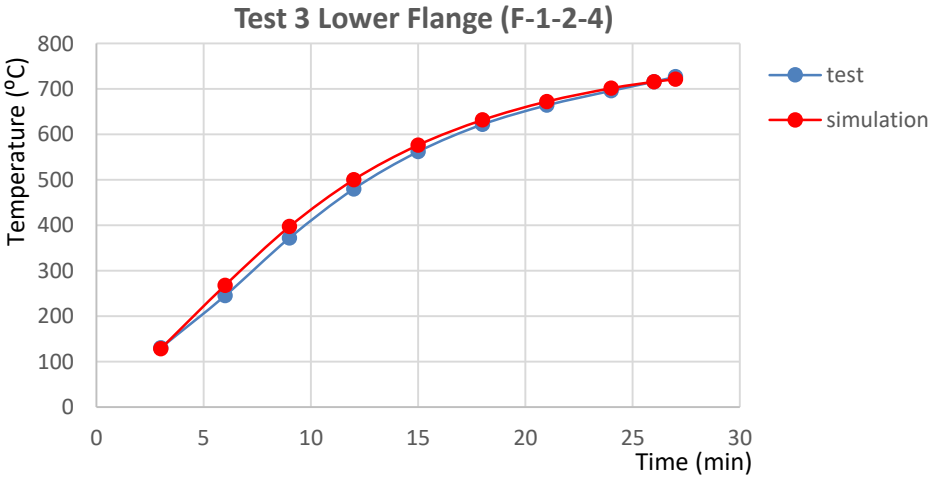

Figure 5-29 Temperature distribution with time at points F-1-2-4

It is observed that temperature of the lower flange predicted by the numerical model is almost identical with the test results. Slight differences are observed in web and upper flange, probably due to the coefficient of thermal conduction and specific heat adopted during the

numerical simulation. According to the above the temperature distribution of the simulation in most of the cases gives well enough predictions. The boundary condition being used and the material properties entered as software input are properly chosen.

CHAPTER 6. RESULTS

In this chapter the results of the numerical analysis are presented. The analysis is divided in two parts, the first part contains the first 24 models of one burning and one target tank, and the second part contains 12 models with multiple burning tanks and one target tank. The analysis results are shown in a set of three or four, and the temperature distribution is presented along the circumference of the target tank at various heights and along the most heated meridian. The temperature distribution of each model is given separately and then a comparison is conducted between corresponding models. The temperature distribution of the target tanks is also compared to the autoignition temperature of the containing fuel. The same autoignition temperature is also used by NFPA 30:2012 in order to define the safety distance between the tanks.

6.1 Results of the models with one burning tank

As mentioned before the first 24 models analyzed contain only one burning tank, which is also indicated by the last symbol of the name of each model (_1).

The results from the first part are shown in sets of three. The temperature distribution is presented along the circumferential plane of the tank every 5 m in height and along the meridian where the maximum temperature value occurs.

The temperature distribution of each model is compared to the temperature distribution of the other corresponding models, in order to get more accurate conclusions. The same time the results of the analysis are compared with the autoignition temperature which is used by NFPA 30:2012 in order to define the safety distance between the burning tank and the adjacent one.

Autoignition temperature is the minimum temperature required to ignite the fuel contained in the adjacent tank without a spark or flame being present. Failure of the target tank is expected to occur when the external sidewall temperature of the target tank gets equal to or bigger than the autoignition temperature. The temperature responsible for the autoignition of the contained fuel is the internal temperature of the tank wall. In the analysis the external and the internal temperature of the tank wall is assumed to be the same, due to the small thickness of the shell. Based on experimental values, autoignition temperature is found to be equal to 392^{o}C for Ethanol and 298,9°C for Gasoline.

In this chapter are presented the results for 6 of the 24 models of one burning and one target tank. The results of the rest 18 models are given in the Annex. In the first 3 models the fuel is Ethanol and at the later 3 Gasoline. The first three models presented are 15_15_E_W_1, 15_20_E_W_1 and 15_25_E_W_1. They vary only on the distance between the burning and the adjacent tank - (d) equals to 15, 20 and 25 m - while the rest of the tank characteristics remain the same - the diameter (D) of the burning tank equals to 15 m, Ethanol is used as a storage fuel (E), the fire takes place under wind conditions (W).

In Figure 6.1 is illustrated the burning and the adjacent tank, and the reference directions along the circumference of the target that are used in the simulation. The most heated meridian of the target tank that is at 180^{o}.

The temperature distribution on the sidewall of the target tank of the model 15_15_E_W_1 calculated by the analysis using the MSC-MSC Marc (2014) software is shown in Figure 6.2. The face presented is directly opposite of the burning tank, with the center being at 180 ^{o}.

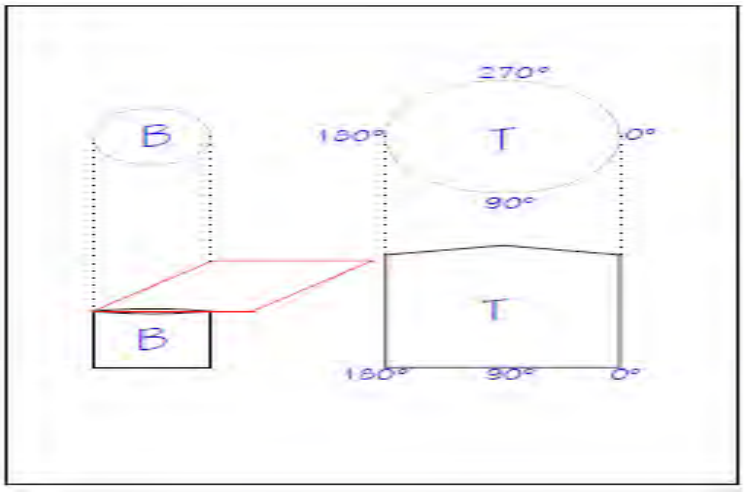

Figure 6-1 Temperature distribution of the target tank as result output from the analysis

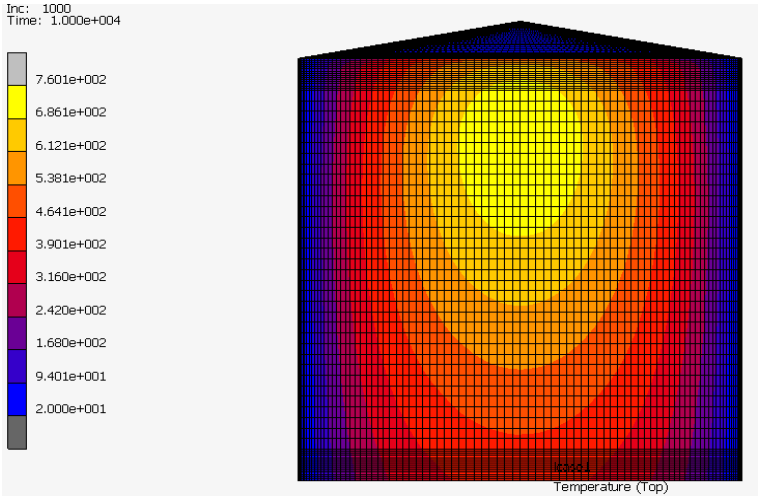

Figure 6-2 Temperature distribution of the target tank as result output from the analysis

The following figures (6.3, 6.4, 6.5) present the temperature distribution of the models 15_15_E_W_1, 15_20_E_W_1 and 15_25_E_W_1 respectively, along the circumferential plane for every 5m in height, at 0m, 5m, 10m, 15m and 20m. The autoignition temperature of Ethanol is also presented.

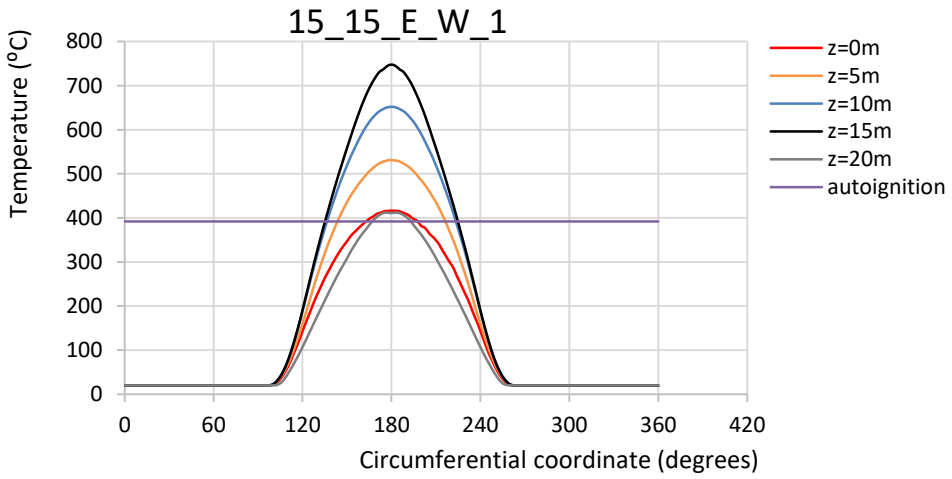

Figure 6-3 Temperature distribution along the circumferential plane for model 15_15_E_W_1

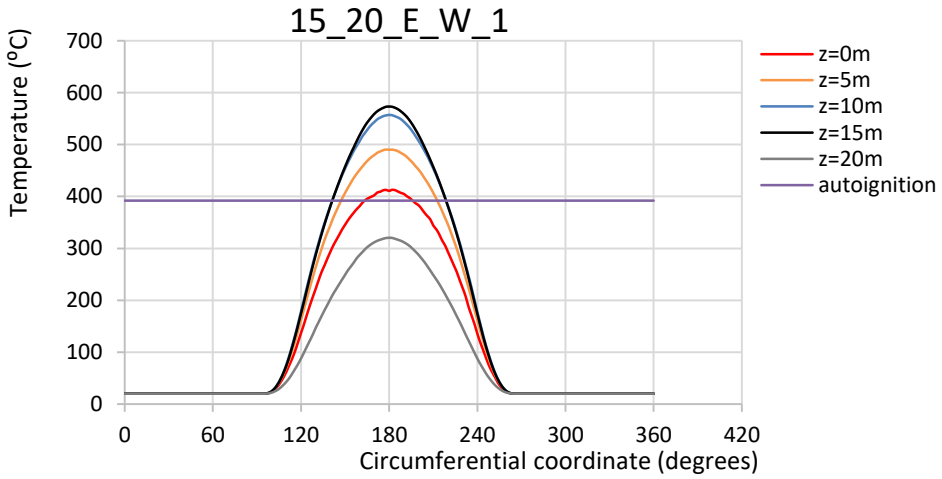

Figure 6-4 Temperature distribution along the circumferential plane for model 15_20_E_W_1

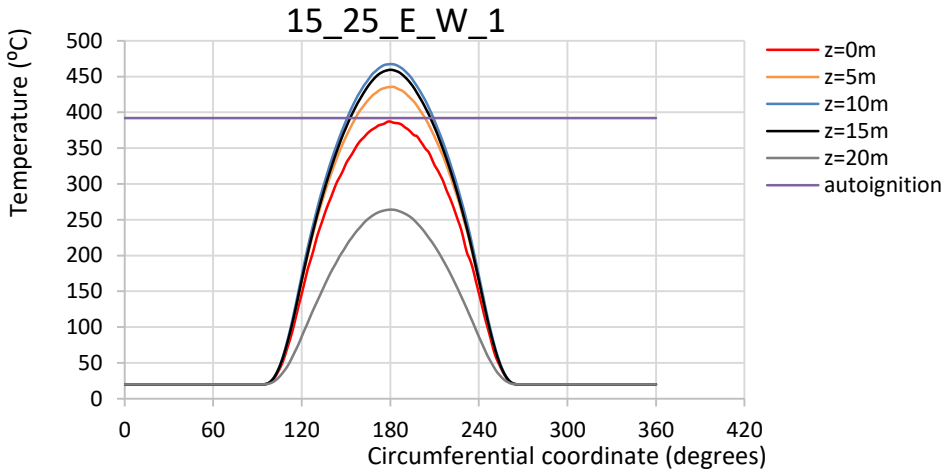

Figure 6-5 Temperature distribution along the circumferential plane for model 15_25_E_W_1

As expected, in all three models the temperature distribution on the tank wall of the adjacent tank is not uniform. The temperature is higher on the side of the tank wall facing the source tank while the opposite side is not affected by the pool fire. It can be concluded from the temperature distribution along the circumferential plane that approximately 1/3 of the circumference of the target tank is affected by the fire, which corresponds to 120^{o} on the presented diagrams.

In the model 15_15_E_W_1 the highest temperatures are observed at the height of 15 m. The temperature distribution at the levels of 0 m and 20 m is almost the same, and are the least affected by the pool fire. At the levels of 5m and 10m the temperatures are in the mid-range. In this model the temperature distribution exceeds the autoignition temperature, at all levels.

In the model 15_20_E_W_1 the highest temperatures are observed at 10 m and 15 m high, with small difference between them, with the level of 15m having slightly higher temperatures. The level of 20 m, is less affected by the flame and is followed by the level of 0m and 5m. In this model the temperature distribution surpasses the autoignition temperature at all levels, except from the level of 20m.

In the model 15_25_E_W_1 the temperatures are higher at the levels of 10 m and 15 m, with the level of 10m to having slightly higher temperatures. The level of 5m has also quite elevated temperatures. The level of 20 m, is less affected, and is followed by level 0 m. The temperature at levels 5 m, 10 m and 15 m is exceeds the autoignition temperature.

The following figures (6.6 - 6.10) show the comparison of temperature distribution between the three models, 15_15_E_W_1, 15_20_E_W_1 and 15_25_E_W_1 along the circumferential plane at height 0m, 5m, 10m, 15,m and 20m. The autoignition temperature of Ethanol is also presented.

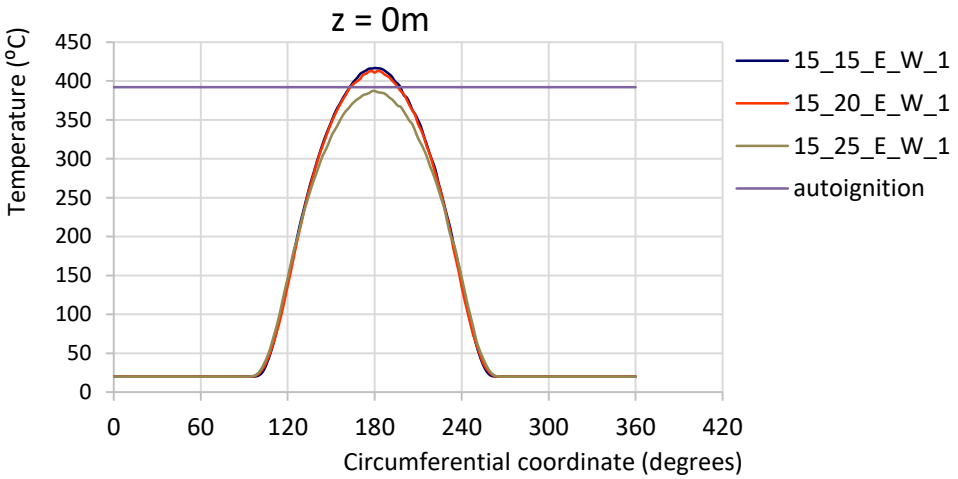

Figure 6-6 Temperature distribution along the circumferential plane for models 15_15_E_W_1, 15_20_E_W_1 and 15_25_E_W_1 at height 0m

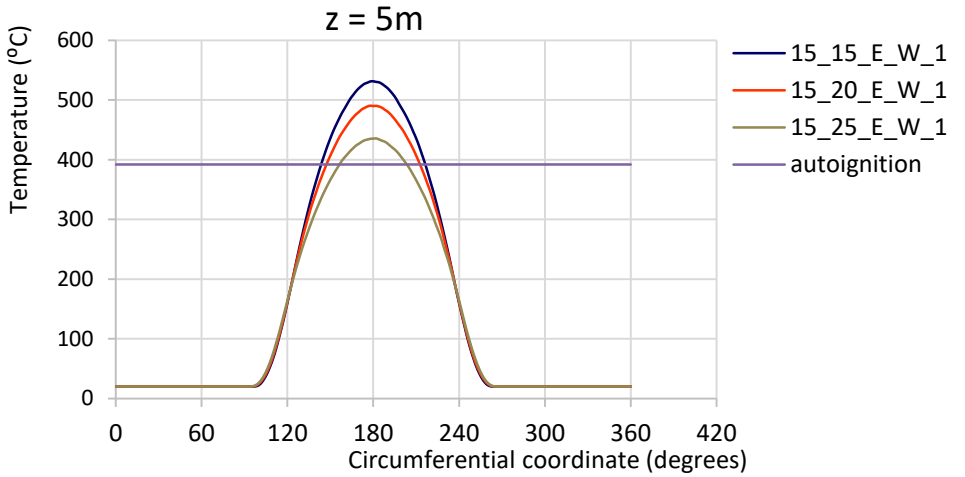

Figure 6-7 Temperature distribution along the circumferential plane for models 15_15_E_W_1, 15_20_E_W_1 and 15_25_E_W_1 at height 5m

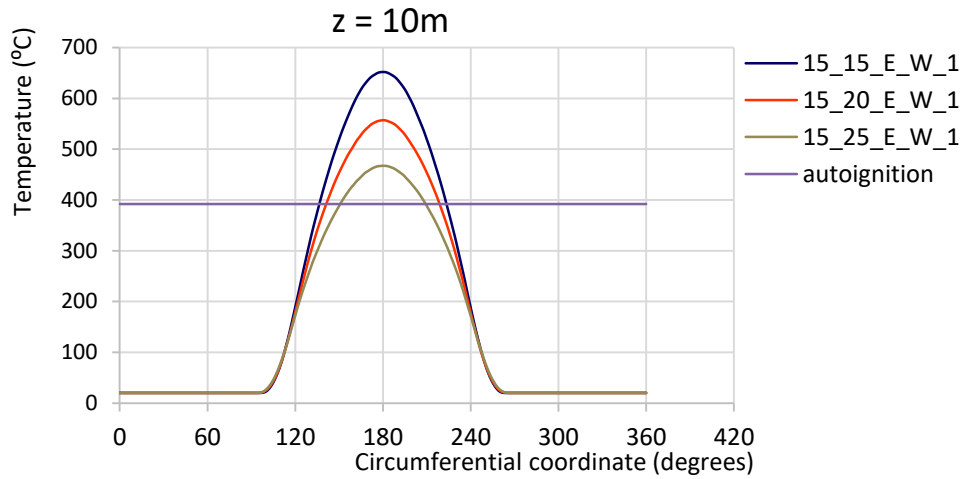

Figure 6-8 Temperature distribution along the circumferential plane for models 15_15_E_W_1, 15_20_E_W_1 and 15_25_E_W_1 at height 10m

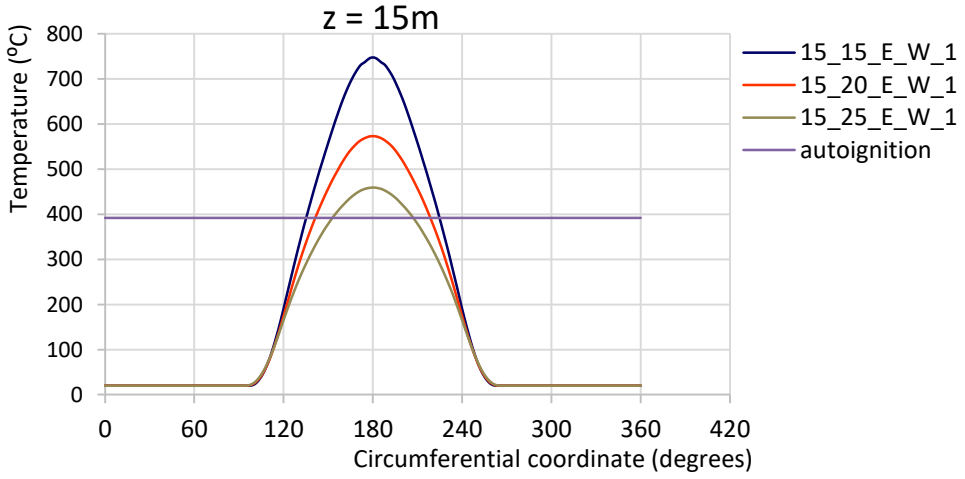

Figure 6-9 Temperature distribution along the circumferential plane for models 15_15_E_W_1, 15_20_E_W_1 and 15_25_E_W_1 at height 15m

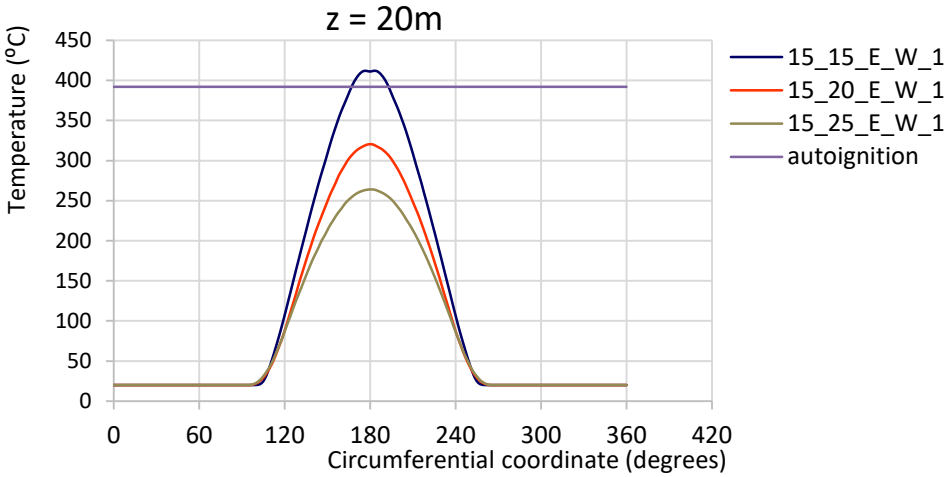

Figure 6-10 Temperature distribution along the circumferential plane for models 15_15_E_W_1, 15_20_E_W_1 and 15_25_E_W_1 at height 20m

At all levels the model 15_15_E_W_1 develops the highest temperatures, while in model 15_25_E_W_1 the tempeerature rise is the lowest. The temperature rise in model 15_20_E_W_1 is between the temperature values of the other two models. Autoignition temperature is reached at heights 5 m, 10 m and 15 m by all models, at height 0 m is reached by the models 15_15_E_W_1 and 15_20_E_W_1, and at height 20 m is reached only by the model 15_15_E_W_1.

The following figure (6.11) shows the comparison of temperature distribution between the three models, 15_15_E_W_1, 15_20_E_W_1 and 15_25_E_W_1 along the vertical plane. The temperature distribution is plotted along the meridian that develops the highest temperatures. The autoignition temperature is also presented.

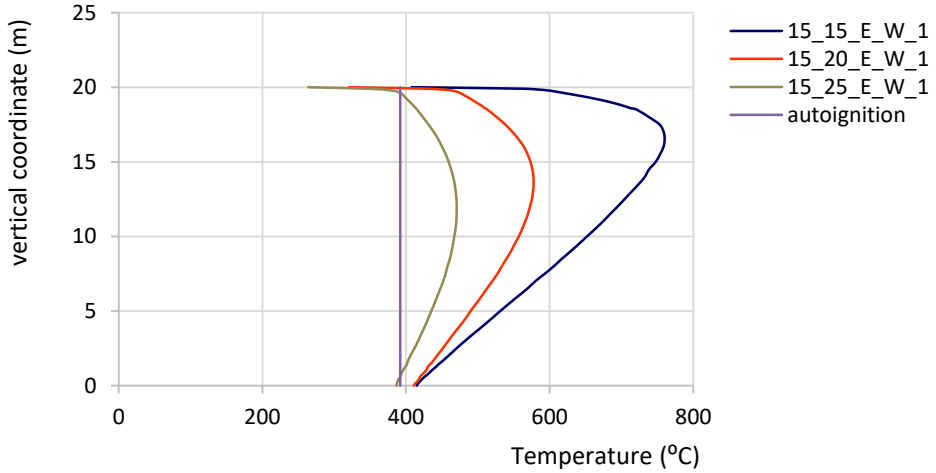

Figure 6-11 Temperature distribution along the vertical plane for models 15_15_E_W_1, 15_20_E_W_1 and 15_25_E_W_1

For model 15_15_E_W_1 the maximum temperature is equal to 760,11°C, at 16,5 m height, for model 15_20_E_W_1 is equal to 577,65°C, at 13,5 m height and for model 15_25_E_W_1 is equal to 470,61°C, at 12 m height.

The next three models presented are 15_15_G_W_1, 15_20_G_W_1 and 15_25_G_W_1.

The parameters of the models are the same to the models presented above - distance between tanks (d) is equal to 15, 20 and 25 m, diameter (D) of the burning tank equals to 15 m, and the fire takes place under wind conditions (W). The different parameter is the burning fuel which in this case is Gasoline (G).

The temperature distribution on the sidewall of the model of target tank is presented in the next figure. The side shown is the side opposite the burning tank, with the center being at 180°.

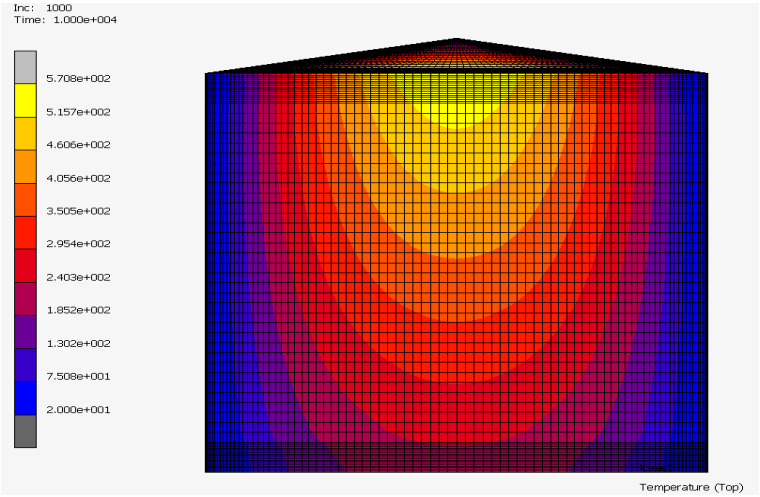

Figure 6-12 Temperature distribution of the target tank as result output from the analysis

The following figures (6.13, 6.14, 6.15) present the temperature distribution of the models 15_15_G_W_1, 15_20_G_W_1 and 15_25_G_W_1 respectively, along the circumferential plane for every 5m in height, that is 0m, 5m, 10m, 15,m and 20m. The autoignition temperature of Gasoline is also indicated.

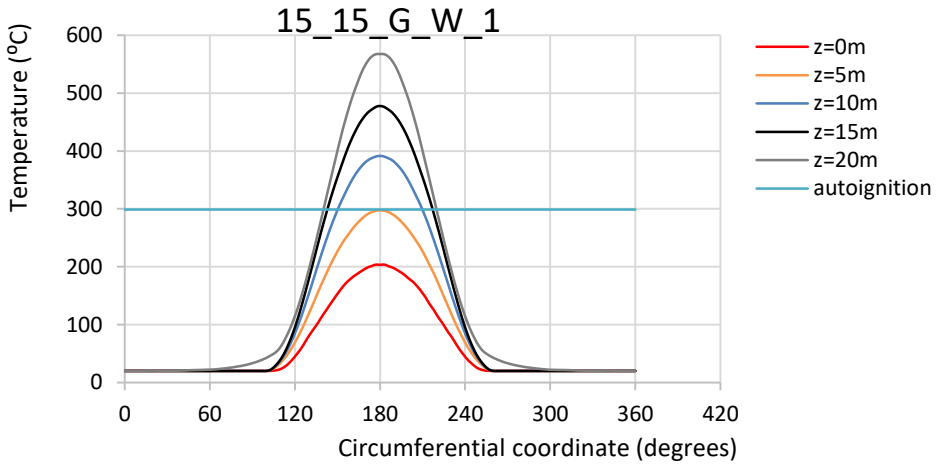

Figure 6-13 Temperature distribution along the circumferential plane for model 15_15_G_W_1

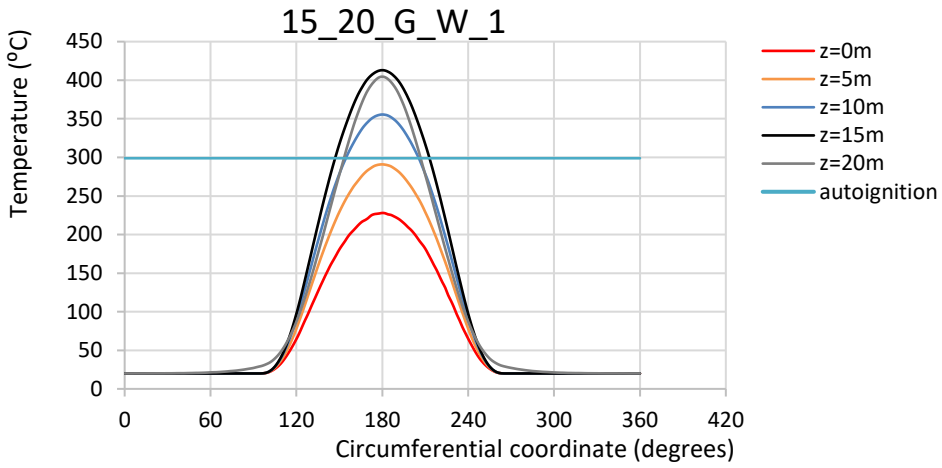

Figure 6-14 Temperature distribution along the circumferential plane for model 15_20_G_W_1

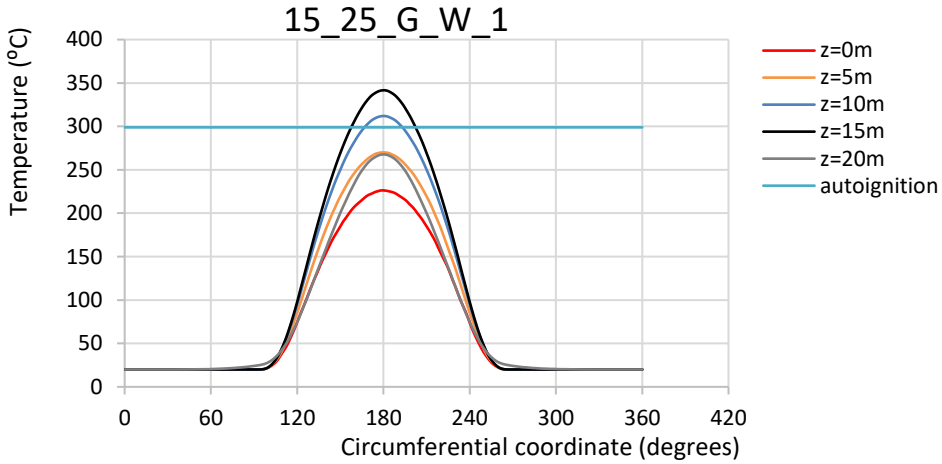

Figure 6-15 Temperature distribution along the circumferential plane for model 15_25_G_W_1

As we mentioned before, the temperature distribution on the tank wall of the adjacent tank of these three models is not uniform and only 1/3 of the circumference of the target tank is affected (angle of 120^{o}).

In model 15_15_G_W_1 the highest temperatures are observed at 20 m. The temperature distribution is relative to the height. Level 0 m is the least affected by the flame, and is followed by the levels of 5 m, 10 m and 15 m. In this model the autoignition temperature is exceeded at levels 10 m, 15 m and 20 m.

In model 15_20_G_W_1 the most elevated temperatures are observed at 15 m and 20 m high, with small differences between them, with the level of 15m having slightly higher temperatures. The level of 0 m, is the least affected by the flame and is followed by the level of 5 m and 10 m. In this model the temperature distribution surpasses the autoignition temperature at levels 10 m, 15 m and 20 m.

In model 15_25_G_W_1 the highest temperatures are observed at 15 m. The level of 10m has also quite elevated temperatures. The level of 0 m, is least affected by the pool fire, and is

followed by levels 5m and 20m with similar temperature distributions. Only the temperature developed at levels 10 m and 15 m is found to exceed the autoignition temperature.

The following figures (6.16 - 6.20) show the comparison of temperature distributions between the three models, 15_15_G_W_1, 15_20_G_W_1 and 15_25_G_W_1 along the circumferential plane at heights 0m, 5m, 10m, 15m and 20m. The autoignition temperature of Gasoline is also presented.

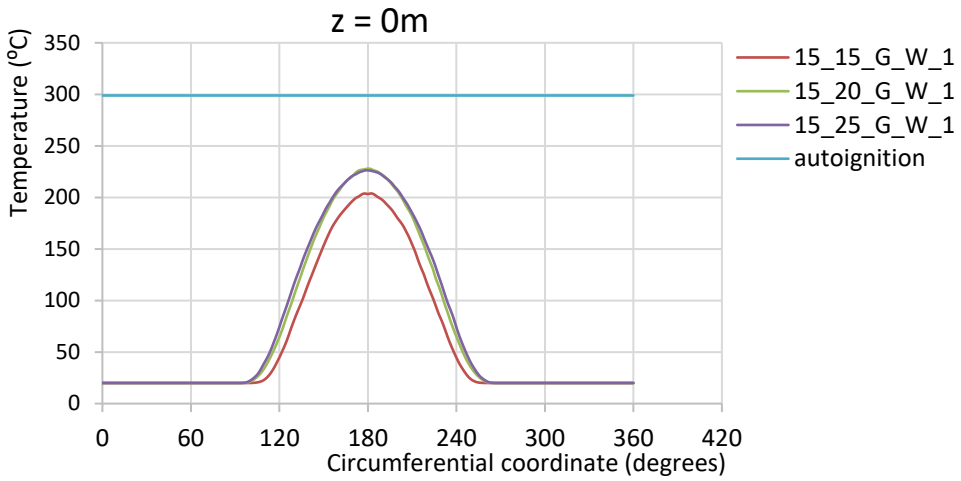

Figure 6-16 Temperature distribution along the circumferential plane for models 15_15_G_W_1, 15_20_G_W_1 and 15_25_G_W_1 at height 0m

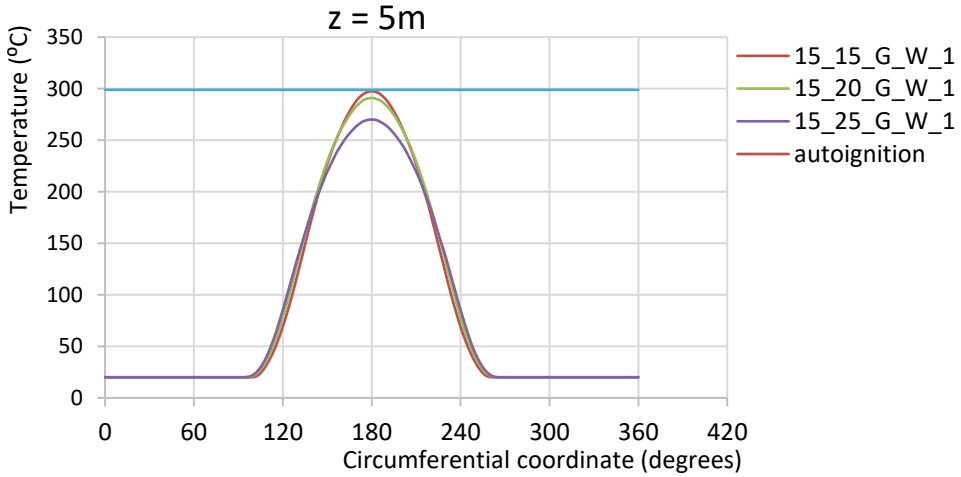

Figure 6-17 Temperature distribution along the circumferential plane for models 15_15_G_W_1, 15_20_G_W_1 and 15_25_G_W_1 at height 5m

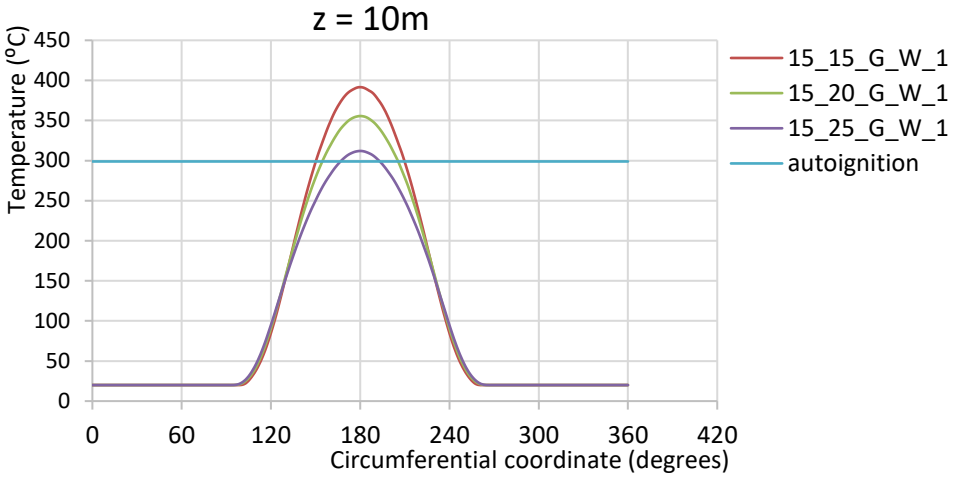

Figure 6-18 Temperature distribution along the circumferential plane for models 15_15_G_W_1, 15_20_G_W_1 and 15_25_G_W_1 at height 10m

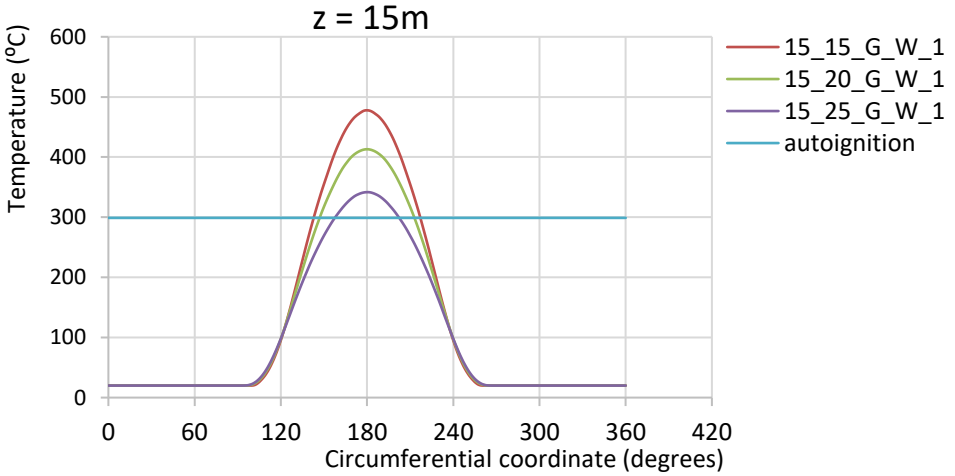

Figure 6-19 Temperature distribution along the circumferential plane for models 15_15_G_W_1, 15_20_G_W_1 and 15_25_G_W_1 at height 15m

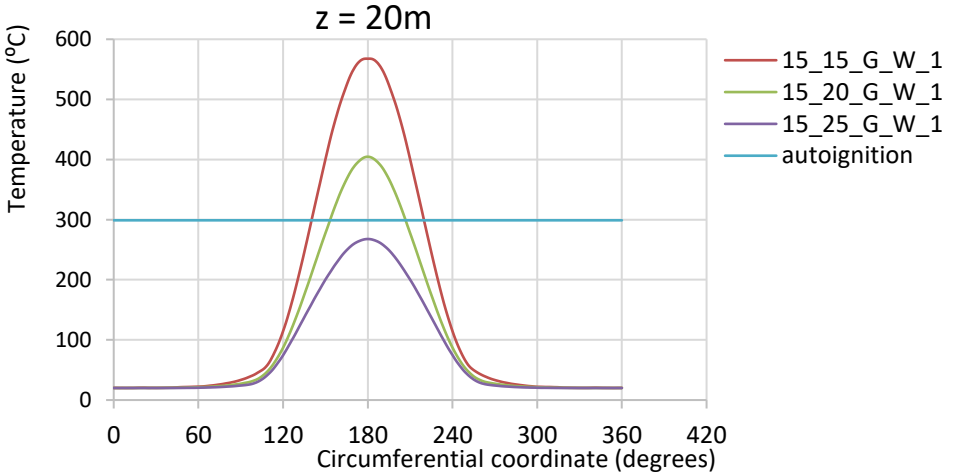

Figure6-20 Temperature distribution along the circumferential plane for models 15_15_G_W_1, 15_20_G_W_1 and 15_25_G_W_1 at height 20m

At all levels the model 15_15_G_W_1 develops the most elevated temperatures, while the model 15_25_G_W_1 develops the least elevated. The temperature distribution of model 15_20_G_W_1 is in the middle. Autoignition temperature is reached at heights 10 m and 15 m by all models, at height 20 m is reached by models 15_15_G_W_1 and 15_20_G_W_1, and at height 0 m and 5m is not reached by any model.

The following figure (6.21) shows the comparison of temperature distribution between the three models, 15_15_G_W_1, 15_20_G_W_1 and 15_25_G_W_1 along the vertical plane. The temperature distribution is captured at the meridian that develops the highest temperatures. The autoignition temperature is also shown.

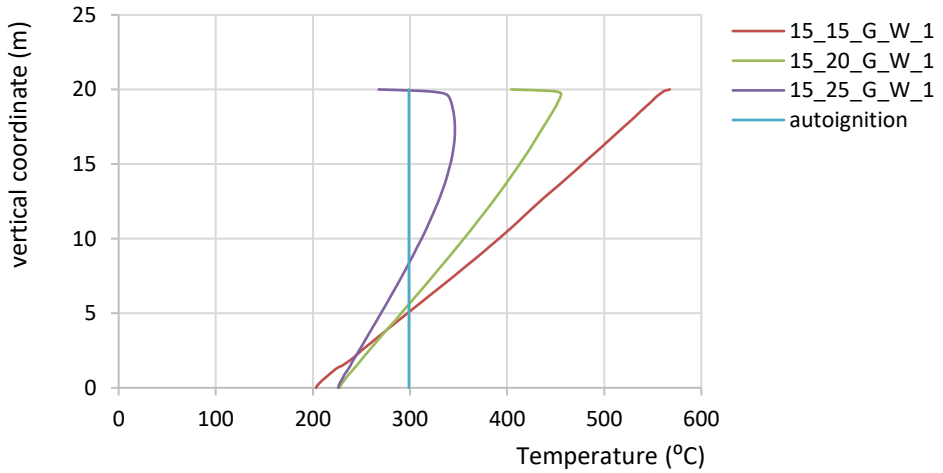

Figure 6-21 Temperature distribution along the vertical plane for models 15_15_G_W_1, 15_20_G_W_1 and 15_25_G_W_1

For model 15_15_G_W_1 the maximum temperature is equal to 567,59ºC, at 20,0m height, for model 15_20_G_W_1 is equal to 455,65ºC, at 19,7m height and for the model 15_25_G_W_1 is equal to 346,23ºC, at 17,5m height. The autoignition temperature as previously mentioned is exceeded at all models.

According to the above results as the distance between the burning and the target tank increases the temperatures become lower and also the point where the maximum temperature occurs is at a lower height.

Table 6.1 presents the maximum temperature of the first 24 models and the height it is observed.

Name	**max Temperature**	**Heigth**
	(m)	(m)
10_15_E_W_1	568.52	16.5
10_20_E_W_1	428.86	13.5
10_25_E_W_1	342.46	12.0
15_15_E_W_1	760.11	16.5
15_20_E_W_1	577.65	13.5
15_25_E_W_1	470.61	12.0
10_15_G_W_1	476.10	18.5
10_20_G_W_1	315.29	14.5

10_25_G_W_1	235.60	12.5
15_15_G_W_1	567.64	20.0
15_20_G_W_1	455.65	19.7
15_25_G_W_1	346.23	17.5
10_15_E_NW_1	451.16	10.0
10_20_E_NW_1	370.66	15.0
10_25_E_NW_1	312.90	15.0
15_15_E_NW_1	554.08	17.5
15_20_E_NW_1	466.90	17.0
15_25_E_NW_1	402.04	16.5
10_15_G_NW_1	285.52	18.0
10_20_G_NW_1	228.77	18.0
10_25_G_NW_1	187.09	18.5
15_15_G_NW_1	356.46	19.4
15_20_G_NW_1	296.14	19.4
15_25_G_NW_1	251.06	18.9

Table 6-1 maximum temperature of each model and the height it is observed

6.2 Results of the models considering multiple burning tanks

The 12 models that were analyzed in the second part of our study were derived from the most critical cases examined in the first part of the study. These models contain more than one burning tank, which is indicated by the last symbol (number) in the name of each model.

The results from this part are shown in sets of four, and the temperature distribution is presented along the circumferential plane of the target tank every 5 m in height and along the vertical plane at the meridian where the maximum temperature occurs.

The temperature distribution of each model is compared with the temperature distribution of the other three models of the set. Again, the temperature results of the analysis are compared with the autoignition temperature of the fuel.

The first four models presented are 15_15_G_W_2, 15_15_G_W_2 and 15_15_E_NW_2 and 15_15_G_NW_2. In these four models the diameter of the target tank (D), the distance between them (d) and the number of the burning tanks remains stable while the fuel type and the wind conditions vary. The diameter (D) of the burning tank is equal to 15 m, they are placed at a distance (d) of 15m and they consist of 2 tanks burning. Two models have Ethanol (E) as fuel, two models use Gasoline (G) and the scenarios take place either under wind conditions or no wind.

The following figures (6.22 - 6.25) present the temperature distribution of the models 15_15_E_W_2, 15_15_G_W_2, 15_15_E_NW_2 and 15_15_G_NW_2 respectively, along the circumferential plane for the levels of 0m, 5m, 10m, 15,m and 20m. The autoignition temperature of Ethanol and Gasoline are also presented.

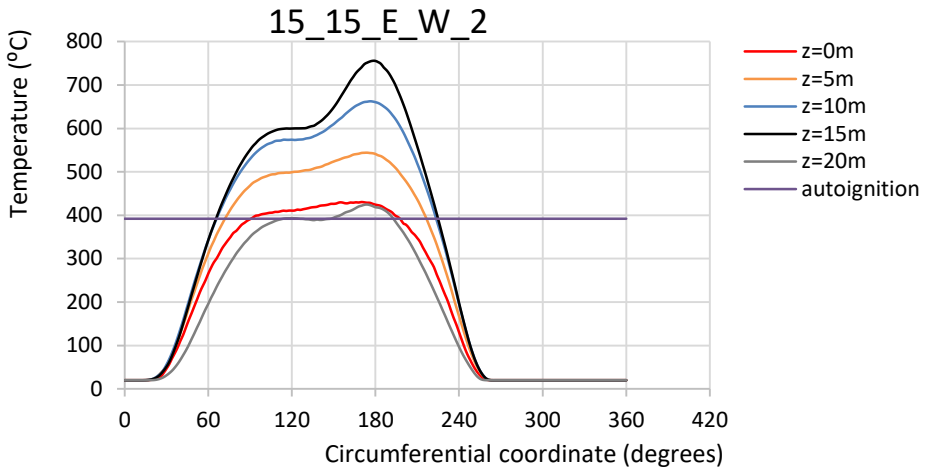

Figure 6-22 Temperature distribution along the circumferential plane for model 15_15_E_W_2

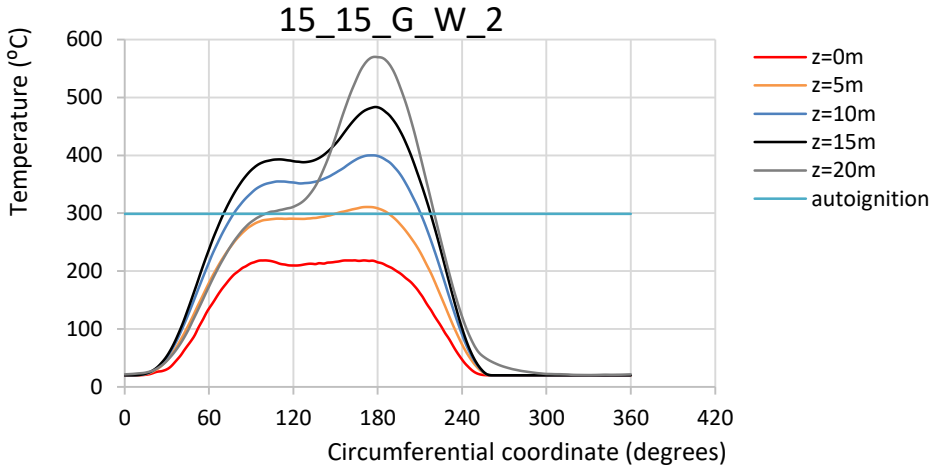

Figure 6-23 Temperature distribution along the circumferential plane for model 15_15_G_W_2

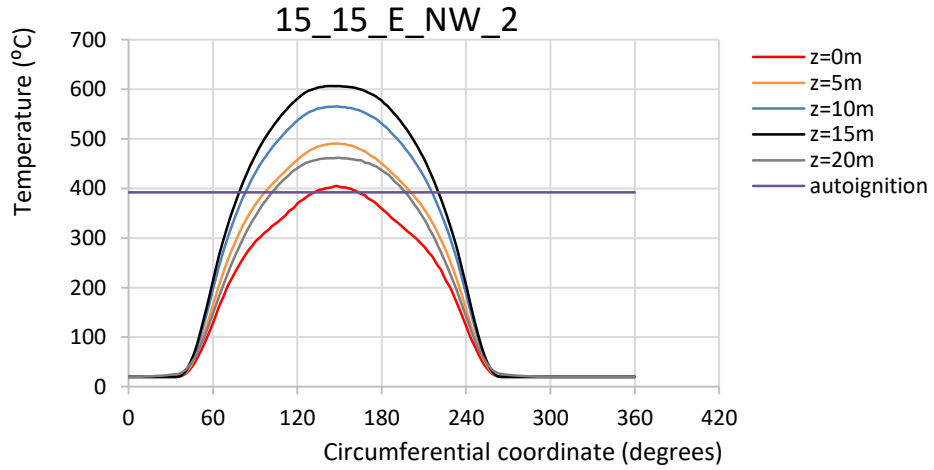

Figure 6-24 Temperature distribution along the circumferential plane for model 15_15_E_NW_2

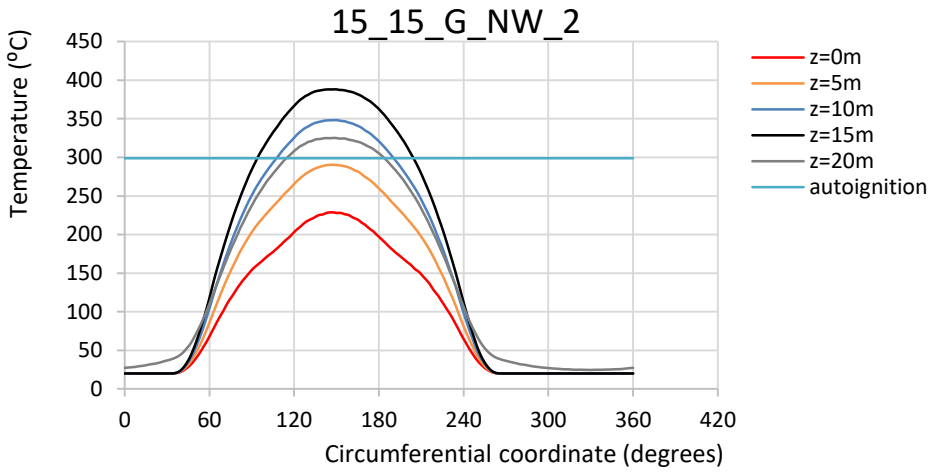

Figure 6-25 Temperature distribution along the circumferential plane for model 15_15_G_NW_2

As mentioned before, the temperature distribution on the tank wall of the target tank of these four models is not uniform. When two adjacent tanks are burning, almost doubled the range of the circumference affected by the fire, from 1/3 to 64%, that corresponds to 230°.

In the model 15_15_E_W_2 the highest temperatures are observed at 15 m high. The levels 0 m and 20 m are less affected by the flame and are followed by the levels at 5 m and 10 m. In this model the temperature distribution exceeds the autoignition temperature at all levels.

In the model 15_15_G_W_2 the highest temperatures are observed at 15 m and 20m. The level of 0 m, is less affected by the pool fire, and is followed by the level of 5m and 10m. Only at levels 0 m the temperature doesn't exceed the autoignition temperature of the fuel.

In the model 15_15_E_NW_2 the level with the highest temperatures is at 15m. The level of 0 m, is again the least affected by the flame and is followed by the levels of 5 m and 20 m, with similar temperatures. Level 10 m has also high temperatures. In this model the temperature distribution surpasses the autoignition temperature at all levels.

In the model 15_15_G_NW_2 the most elevated temperatures are observed at 15 m. The level of 0 m, is the least affected by the flame and is followed by the level of 5m and 20m and 10 m. In this model the autoignition temperature is exceeded at levels 10 m, 15 m and 20 m.

At this point it should be noted that at models 15_15_E_NW_2 and 15_15_G_NW_2 where there is no wind, the curves are smoother. The curves at all heights increase linearly until a plateu appears at the top for about 60° and then start to decrease linearly until 20°C where they become stable. At models 15_15_E_W_2 and 15_15_G_W_2, where wind is present, at the lower temperatures the curves are also smoother. At elevated temperature though, the temperature curves increase linearly, a platue appears for about 40° and then again start to increase rapidly. When the curve of the temperature distribution reaches the maximum value, then starts to decrease immediately until becomes stable at 20°C.

The following figure (6.26) shows the comparison of temperature distribution between the four models, 15_15_E_W_2, 15_15_G_W_2, 15_15_E_NW_2 and 15_15_G_NW_2 along the vertical plane. The temperature distribution is taken at the meridian that develops the highest temperatures. The autoignition temperatures of Ethanol and Gasoline are also shown.

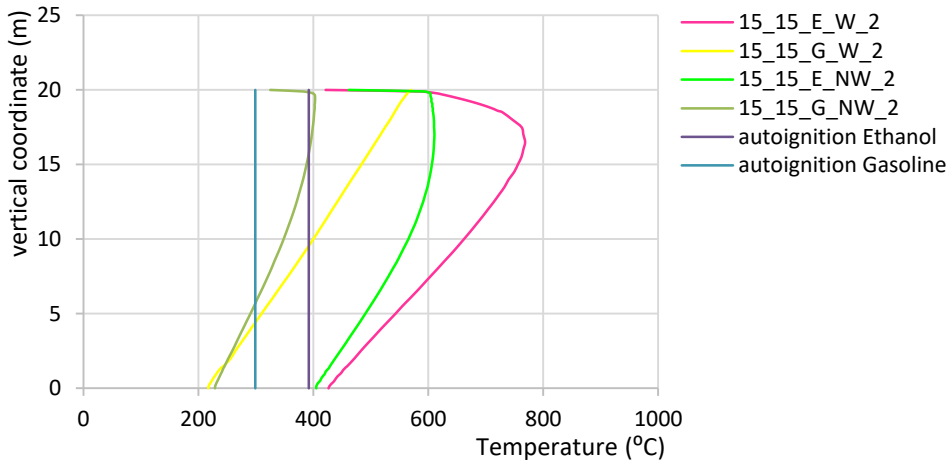

Figure 6-26 Temperature distribution along the vertical plane for models 15_15_E_W_2, 15_15_G_W_2, 15_15_E_NW_2 and 15_15_G_NW_2

For the model 15_15_E_W_2 the maximum temperature is equal to 768,45°C, at 16,5m height, for the model 15_15_G_W_2 is equal to 570,16°C, at 20,0m height, for the model 15_15_E_NW_2 is equal to 610,65°C at 17m height and for the model 15_15_G_NW_2 is equal to 402,95°C, at 19,4m height. The autoignition temperature is exceeded at all models.

The next figures illustrate models 15_15_E_W_3, 15_15_G_W_3, 15_15_E_NW_3 and 15_15_G_NW_3. These models contain 3 burning tanks, while the other variables are the same the were at the previous models.

The following figures (6.27 - 6.30) present the temperature distribution of the models 15_15_E_W_3, 15_15_G_W_3, 15_15_E_NW_3 and 15_15_G_NW_3 respectively, along the circumferential plane every 5m in height, that is 0m, 5m, 10m, 15m and 20m. The autoignition temperature of Ethanol and Gasoline are given also.

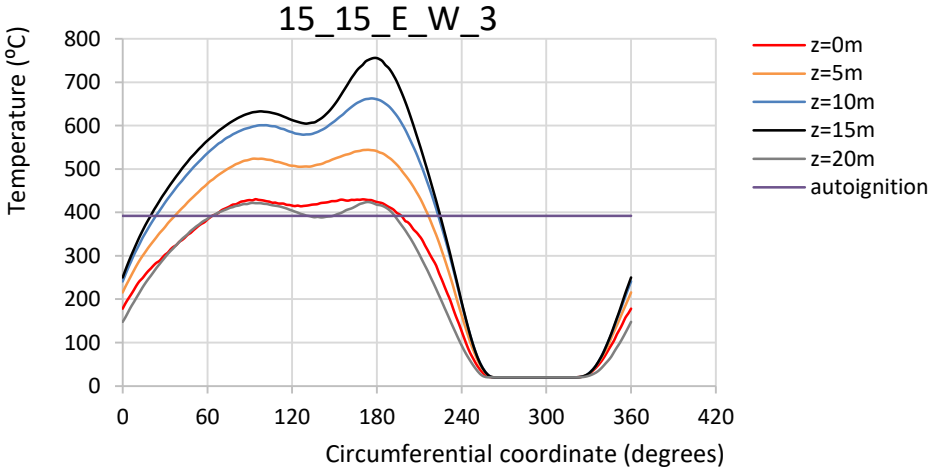

Figure 6-27 Temperature distribution along the circumferential plane for model 15_15_E_W_3

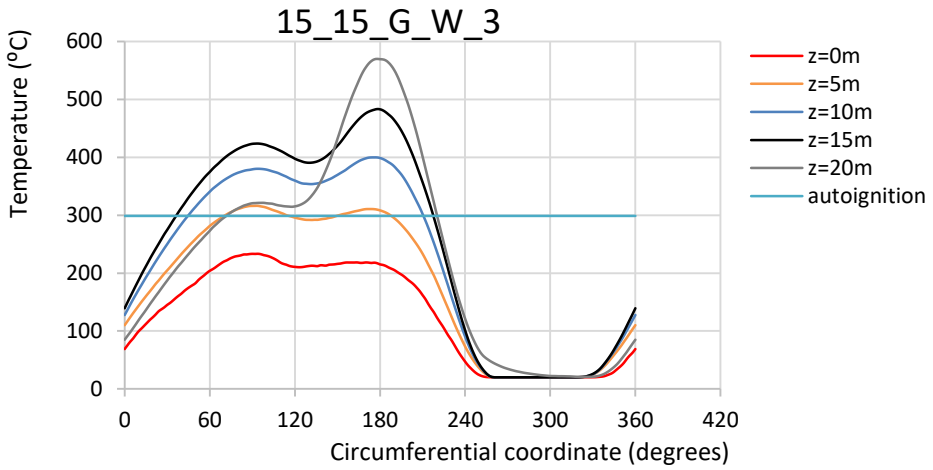

Figure 6-28 Temperature distribution along the circumferential plane for model 15_15_G_W_3

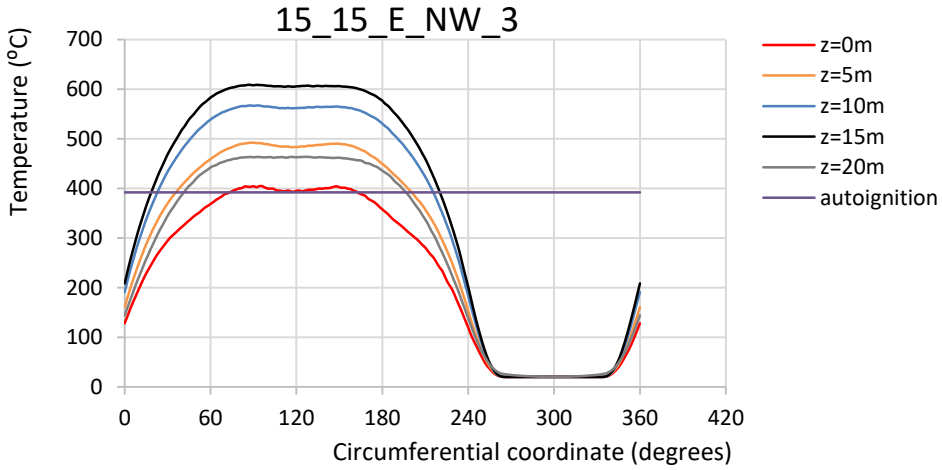

Figure 6-29 Temperature distribution along the circumferential plane for model 15_15_E_NW_3

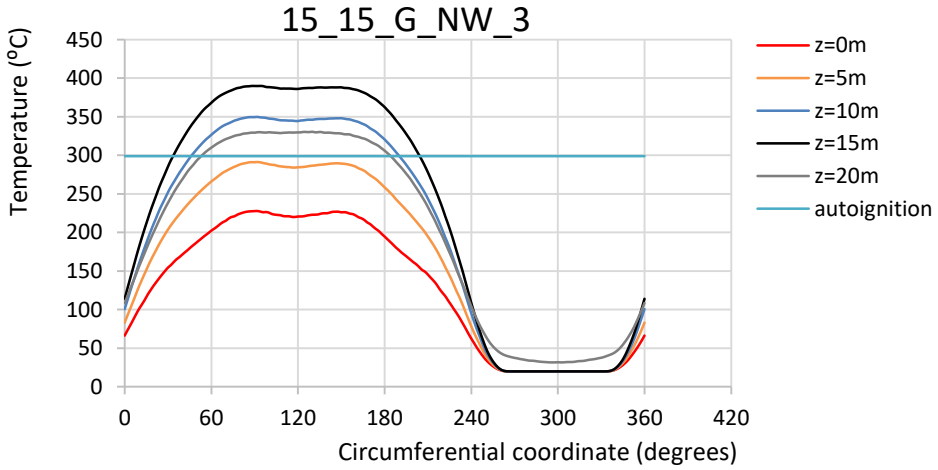

Figure 6-30 Temperature distribution along the circumferential plane for model 15_15_G_NW_3

The temperature distribution on the tank wall of the adjacent tank of the models containing 3 burning tanks is not uniform, while the range of the perimeter affected by the flame increases to exactly 2/3, that corresponds to 240^{o}.

In the model 15_15_G_W_3 the most elevated temperatures are observed at the level of 15m. The levels of 0 m and 20 m have similar temperatures and are less affected by the flame. The temperatures at the levels of 5 m and 10 m are higher. In this model the temperature distribution exceeds the autoignition temperature, at all levels.

In the model 15_15_G_W_3 the more elevated temperatures are observed at 15 m and 20m. The level of 0 m, is less affected by the pool fire, and is followed by the levels of 5 m and 10 m. Only the temperature developed at levels 0 m doesn't exceed the autoignition temperature.

In the model 15_15_E_NW_3 the most elevated temperatures are observed at 15 m. The level of 0 m, is less affected by the flame and is followed by the levels of 5 m and 20 m, that are almost the same. The level of 10 m has also high temperatures. In this model the temperature distribution surpasses the autoignition temperature at all levels.

In the model 15_15_G_NW_3 the most elevated temperatures are observed at 15 m. The level of 0 m, is the least affected by the flame and is followed by the levels of 5 m, 20 m and 10 m. In this model the autoignition temperature is exceeded at levels 10 m, 15 m and 20 m.

At this point it can be noted that at models 15_15_E_NW_2 and 15_15_G_NW_2 where there is no wind, the temperature curves are smoother. The curves at all heights increase linearly until a plateau appears at the top at 60^{o} and then at 180^{o} start to decrease linearly until 20^{o}C where they become stable. At models 15_15_E_W_2 and 15_15_G_W_2, where there is wind present, at lower temperatures the curves exhibit the same pattern. At elevated temperatures though, the curves increase linearly until a plateau appears between 60^{o} and 120^{o}C and then start to increase rapidly. When the curve of the temperature distribution reaches the maximum, then the temperature starts to decrease immediately until it becomes stable at 20^{o}C.

The following figure (6.31) shows the comparison of temperature distribution between the four models, 15_15_E_W_3, 15_15_G_W_3, 15_15_E_NW_3 and 15_15_G_NW_3 along the vertical plane. The temperature distribution is given at the meridian that develops the highest temperatures. The autoignition temperature curves of Ethanol and Gasoline are also shown.

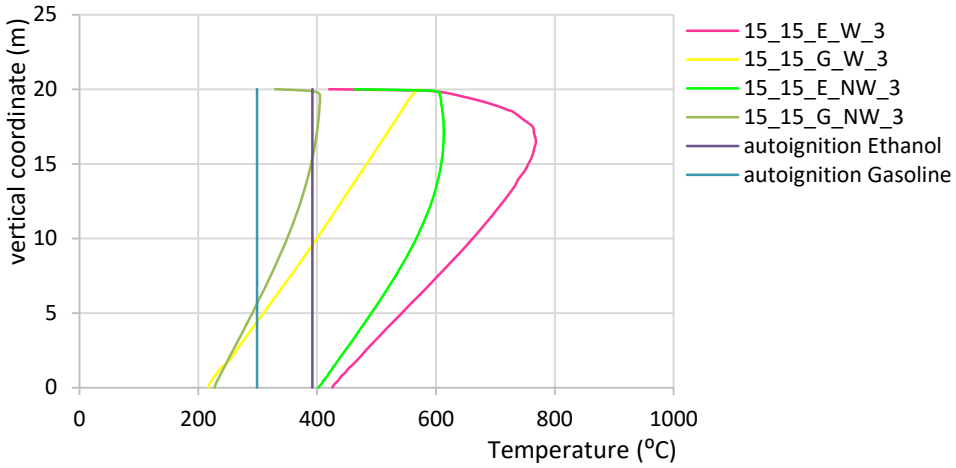

Figure 6-31 Temperature distribution along the vertical plane for models 15_15_E_W_3, 15_15_G_W_3, 15_15_E_NW_3 and 15_15_G_NW_3

For the model 15_15_E_W_3 the maximum temperature is equal to 768,35°C, at 16,5m height, for the model 15_15_G_W_3 is equal to 570,19°C, at 20,0 m height, for the model 15_15_E_NW_3 is equal to 613,05°C at 17 m height and for the model 15_15_G_NW_3 is equal to 404,85°C, at 19,3 m height. The autoignition temperature is reached and exceeded at all models.

The next set of models is 15_15_E_W_4, 15_15_G_W_4, 15_15_E_NW_4. These models contain 4 burning tanks, while the rest variables remain the same.

The following figures (6.32 - 6.34) present the temperature distribution of the models 15_15_E_W_4, 15_15_G_W_4, 15_15_E_NW_4 respectively, along the circumferential plane every 5m in height, at 0m, 5m, 10m, 15,m and 20m. The autoignition temperatures of Ethanol and Gasoline are also presented.

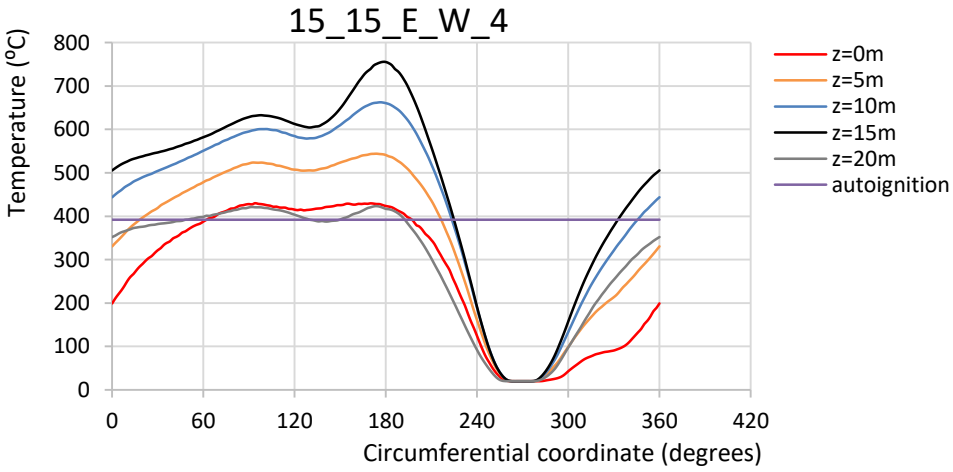

Figure 6-32 Temperature distribution along the circumferential plane for model 15_15_E_W_4

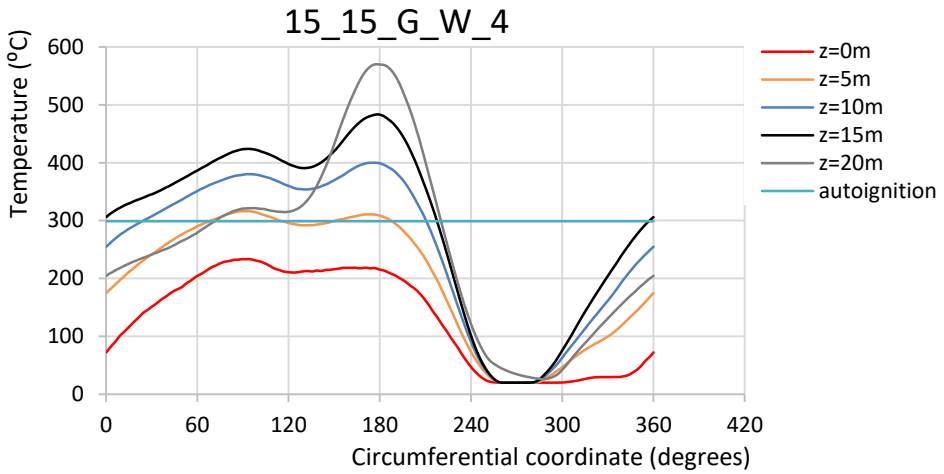

Figure 6-33 Temperature distribution along the circumferential plane for model 15_15_G_W_4

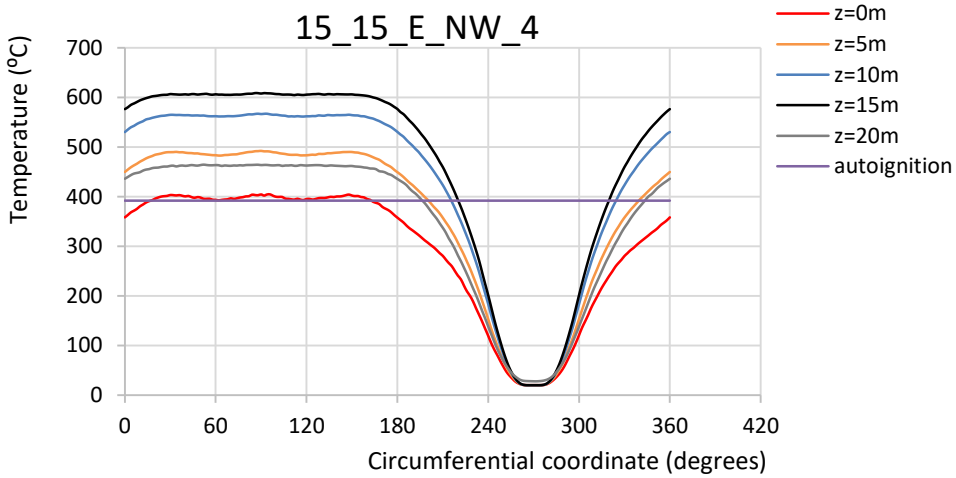

Figure 6-34 Temperature distribution along the circumferential plane for model 15_15_E_NW_4

The temperature distribution on the tank wall of the target tank of the models containing 4 burning tanks is again not uniform, but in these models the whore perimeter is affected by the flame.

In model 15_15_E_W_4 the most elevated temperatures are observed at the level of 15m. The temperatures at levels 0 m and 20 m are similar and less affected by the flame, while are the temperatures at 5 m and 10 m are higher. The temperature at height 10m is quite close to the ones at level 15m. In this model the temperature distribution exceeds the autoignition temperature at all levels.

In the model 15_15_G_W_4 the most elevated temperatures are observed at 15 m and 20m. The level of 0 m, is the least affected by the pool fire and the levels of 5 m and 10 m follow. Only the temperature of level 0 m doesn't exceed the autoignition temperature.

In the model 15_15_E_NW_4 the most elevated temperatures are observed at 15 m. The level of 0 m, is the least affected by the flame and is followed by the level of 5 m and 20 m that

have almost the same temperatures. Level 10 m has also high temperatures. In this model the temperature distribution exceeds the autoignition temperature at all levels.

The following figure (6.35) shows the comparison of temperature distribution between the three models, 15_15_E_W_4, 15_15_G_W_4 and 15_15_E_NW_4 along the vertical plane. The temperature distribution is displayed along the meridian that develops the highest temperatures. The autoignition temperature is also shown.

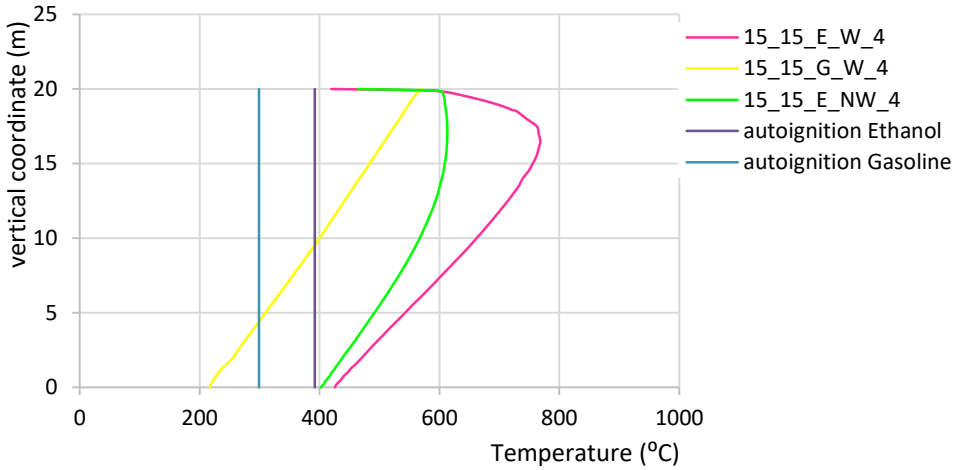

Figure 6-35 Temperature distribution along the vertical plane for models 15_15_E_W_3, 15_15_G_W_4 and 15_15_E_NW_4

For the model 15_15_E_W_4 the maximum temperature is equal to 768,26°C, at 16,5m height, for the model 15_15_G_W_4 is equal to 570,16°C, at 20,0m height and for the model 15_15_E_NW_4 is equal to 613,05°C at 17m height. The autoignition temperature is reached and exceeded at all models.

6.3 Aggregated results

As it is mentioned before, the temperature distribution on the external surface of the target tank depends on various factors such as the diameter of the burning tank (D=10 m and D=15 m), the type of the fuel (Ethanol and Gasoline), the presence of wind (w=0m/s and w=5m/s), the separation distance between the burning tank and the adjacent tank, (15 m, 20 m and 25 m) and at last the number of the burning tanks (1, 2, 3 & 4). In order to reveal the key factors that mainly affect the temperature distribution on the external surface of the target tank, the following figures were developed, that show the aggregated results.

Again, first, are illustrated the aggregated results of the 24 models that contain only one burning tank and subsequently are shown the rest 12 models that contain multiple burning tanks.

6.3.1 Aggregated results of models with one burning tank

It can be easily observed from the above results that when the target tank is closer to the burning tank, the maximum temperature is higher, and as the separation distance increases the maximum temperature decreases. This reduction is present in all cases, independent of the burning tank diameter, the fuel type, the wind conditions or the number of the burning tanks.

In order to investigate and confirm the above conclusion, extra analyses were conducted for the intermediate separation distances of 17,5 m and 22,5 m, for both fuel cases (Ethanol and Gasoline), both wind conditions and for the burning tank diameter equal to 10m.

In Figure 6-36 is illustrated the maximum temperature on the external surface of the target tank versus the separation distance between the source and the target tank for both fuel types, Ethanol and Gasoline, for both wind scenarios, and for burning tank diameter equal to D=10 m.

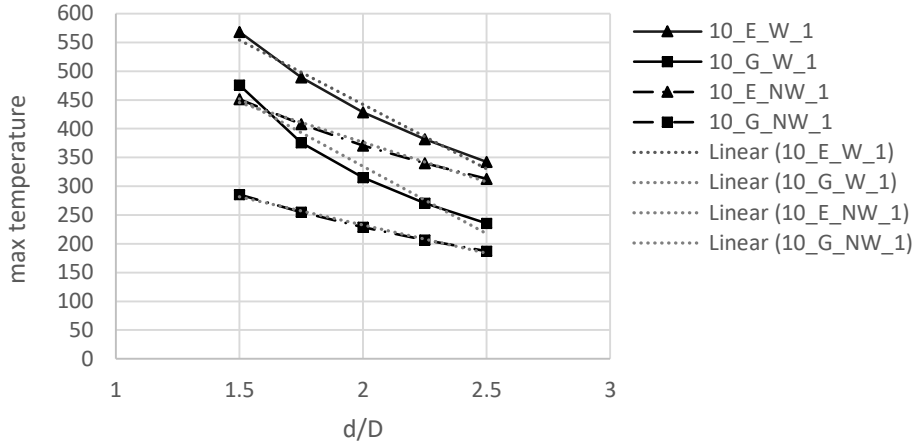

Figure 6-36 Maximum temperature variation with the different separation distances

For every curve illustrated in Figure 6-36 the trend line is also plotted, which is found to be linear. It can be noticed that the trend line coincides with the corresponding curve. The only case that the trend line diverges slightly is the case of Gasoline under wind conditions. That can be explained by the overshadowing effect the Gasoline flame has on the target tank for smaller separation distances, due to the flame tilt and the flame length. Thus it can be concluded that the maximum temperature decreases linearly as the separation distance increases.

In Figure 6-37 is illustrated the maximum temperature of the external surface of the target tank versus the separation distance between the source and the target tank for both wind scenarios and for both diameters of the burning tank, for fuel type Ethanol.

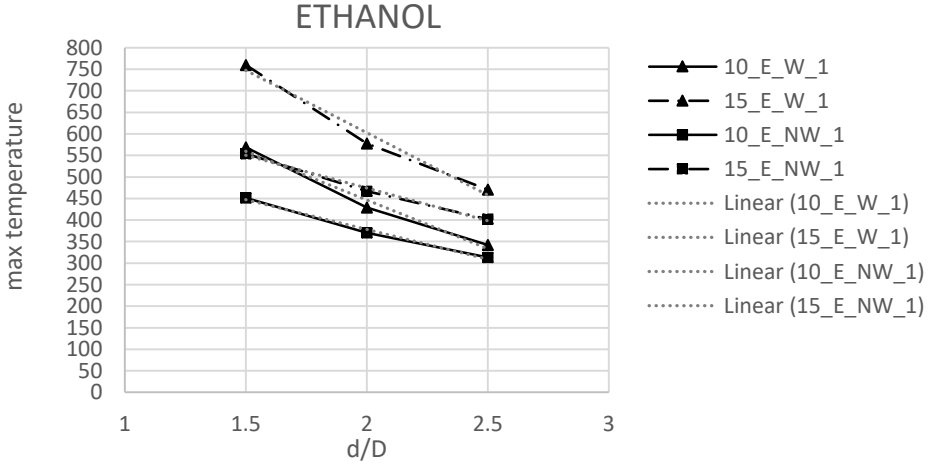

Figure 6-37 Maximum temperature variation with the different separation distances, for Ethanol models

It can be easily observed that when the target tank is closer to the burning tank, the maximum temperature is higher, and as the separation distance increases the maximum temperature decreases linearly.

In order to find which of the factors influence more the temperature decrease apart from the distance between them, the slope of the curves was examined. The ratio of the slope of the curve with the diameter of the burning tank at D=15m, to the slope of the curve with diameter of the burning tank D=10 m, under wind conditions is 1,28 while the same ratio under no wind conditions is equal to 1. Also, the slope of the curve with diameter of the burning tank D=10m under wind conditions to the slope of the curve with the same diameter under no wind conditions is 1,64. The same ratio for the curve for the 15m diameter burning tank (D= 15m) is 1,90.

One can obtain from the above estimations that in the case of Ethanol the rate of reduction of the maximum temperature as the separation distance increases is more affected by the presence of the wind than of the diameter of the burning tank.

In Figure 6-38 is illustrated the maximum temperature values on the external surface of the target tank against the separation distance between the source and the target tank for both wind scenarios and for both diameters of the burning tank, for fuel type Gasoline.

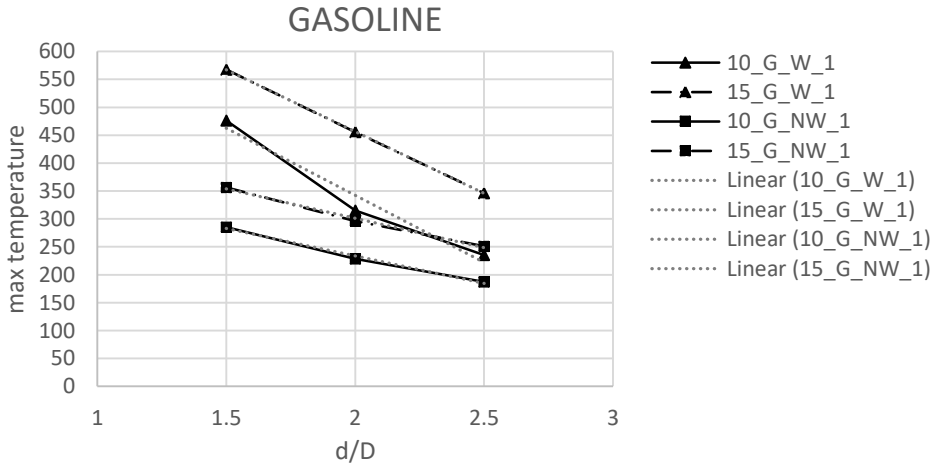

Figure 6-38 Maximum temperature variation with the different separation distances, for Gasoline models

It can be also seen for Gasoline that the closer the burning tank is to the target tank, the maximum temperature is higher, and decreases linearly as the separation distance increases.

The ratio of the slope of the curve with diameter of the burning tank D=10m to the slope of the curve with diameter of the burning tank D=15 m, under wind conditions is 1,28 while the same ratio under no wind conditions is equal 1. Also, the ratio of the slope of the curve with diameter of the burning tank D=10m, under wind conditions to the slope of the curve with the same diameter under no wind conditions is 1,64. The same ratio for diameter of the burning tank D= 15 m is 1,90.

It can be concluded that in the case of Gasoline too, the rate of reduction of the maximum temperature as the separation distance increases is more influenced by the wind conditions than of the diameter of the burning tank.

In Figure 6-39 is illustrated the maximum temperature values on the external surface of the target tank versus the separation distance between the source and the target tank for both fuel types, Ethanol and Gasoline, for both diameters of the burning tank, under wind conditions.

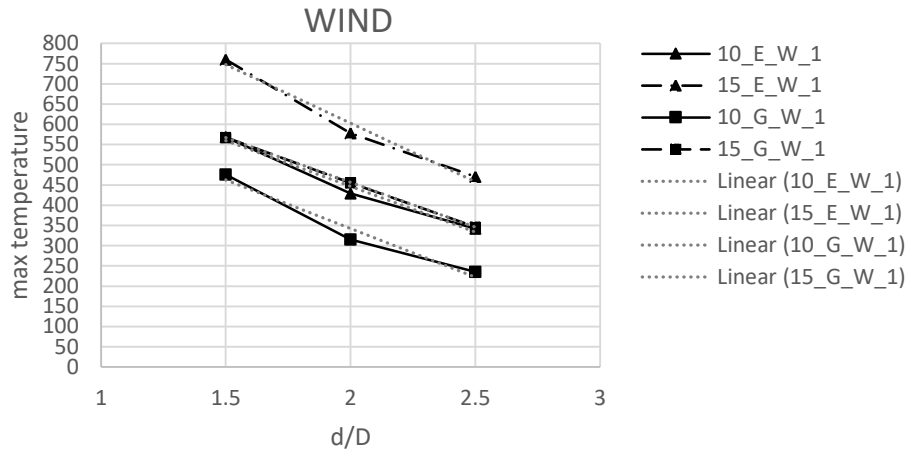

Figure 6-39 Maximum temperature variation with the different separation distances, for models under wind conditions

As it mentioned before, it can also be concluded from the above figure that as the target tank is further from the source tank, the maximum temperature decreases linearly.

Under wind conditions, when the diameter of the burning tank is equal to D=15 m, the ratio of the slope of the curve of Ethanol to Gasoline is 1,30 while the same ratio for the 10m diameter of the burning tank, is equal to 0,93.

It can be deduced that under wind conditions, in smaller diameters of the source tank the rate of temperature reduction with the separation distance is not affected by the fuel type, while when the diameter of burning tank rises, the temperature variation is influenced by the fuel type.

Figure 6-40 shows the maximum temperature variation on the external surface of the target tank with the separation distance between the source and the target tank for both fuel types (Ethanol and Gasoline), for both diameters of the burning tank, under no wind conditions.

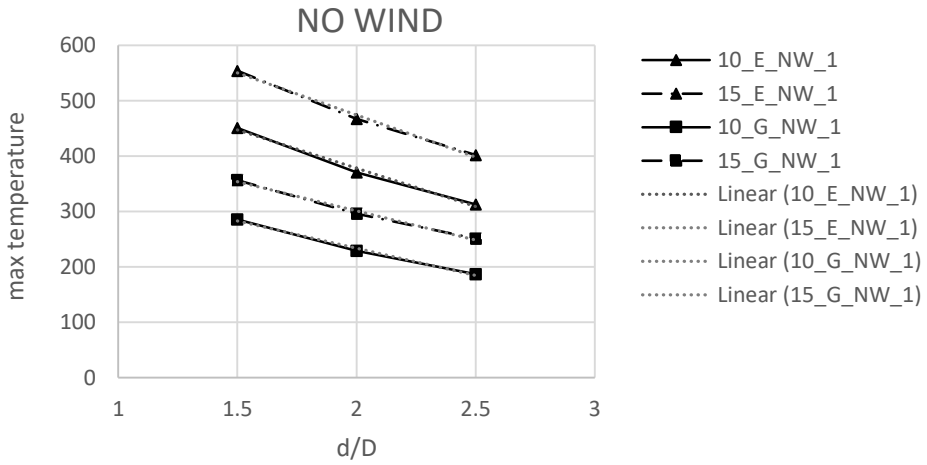

Figure 6-40 Maximum temperature variation with the different separation distances, for models under no wind conditions

Linearity in temperature reduction with the separation distance is also observed in this figure.

Under no wind conditions, when the diameter of the burning tank is D=15 m, the ratio of the slope of the curve of Ethanol to Gasoline is 1,44 while the same ratio for the 10m burning tank is 1,40. When the fuel type is Ethanol the ratio of the slope of the curve for the 15m burning tank to 10 m burning tank is 1,10. When the fuel type is Gasoline the same ratio is 1,07.

According to the above results, under no wind conditions, the rate of temperature reduction with the separation distance in not affected by the diameter of burning tank, but slightly affected by the fuel type.

6.3.2 Aggregated results of models with multiple burning tanks

In the next 12 models the number of the burning tanks increases and a more complicated scenario takes place. It has been mentioned before that in the cases of more than one burning tanks the length of the affected circumference changes while the maximum temperature is not affected by the number of burning tanks.

The maximum temperature is obtained at exactly the same meridian as the first 24 models and the rate of maximum temperature decrease follows the previous trends.

6.4 Comparison indexes

In order to quantify the results of the analyses of the models, in a more consistent, dimensionless way, appropriate indexes were adopted.

The first index proposed is the *ambient temperature index*. This index actually estimates the ratio of the external surface of the target tank where the calculated temperature is higher than the ambient temperature, to the total surface of the tank. The ambient temperature is considered to be equal to 20^{o}C.

The next index which also takes into account the autoignition temperature, is the *autoignition temperature index*. This index calculates the percentage of the external surface of the target tank that the temperature exceeds the autoignition temperature, to the total surface of the tank. As mentioned before the autoignition temperature for Ethanol is equal to 392ºC and for Gasoline is equal to 298,9ºC.

The last but not least index being adopted for the comparison of the pool fire scenarios is the *fire risk index*. The fire risk index takes into account both a) the spatial distribution of the temperature values exceeding the autoignition temperature along the external surface of the target tank, and b) the degree that these temperature values exceed the autoignition temperature.

6.4.1 Comparison indexes for the models with one burning tank

6.4.1.1 Ambient temperature index of models with one burning tank

In Table 6.2 can be observed the *ambient temperature index* (T>20ºC) for every model arranged in descending order.

MODEL	AMBIENT TEMPERATURE INDEX T>20oC
15_25_G_NW_1	55.69%
15_20_G_NW_1	55.27%
15_15_G_NW_1	54.86%
15_20_G_W_1	54.30%
15_25_E_NW_1	50.69%
10_25_G_NW_1	50.69%
15_15_E_NW_1	50.55%
10_20_G_NW_1	50.28%
15_20_E_NW_1	50.21%
10_15_G_NW_1	50.21%
15_15_G_W_1	48.89%
15_25_G_W_1	48.89%
15_25_E_W_1	47.91%
15_20_E_W_1	47.78%
10_25_E_NW_1	47.78%
15_15_E_W_1	46.80%
10_25_E_W_1	46.66%
10_25_G_W_1	46.66%
10_20_E_NW_1	46.66%
10_20_E_W_1	45.55%
10_20_G_W_1	45.55%
10_15_E_NW_1	45.00%
10_15_E_W_1	44.44%
10_15_G_W_1	41.94%

Table 6-2 Ambient temperature index arranged in descending order

It can be seen that the ambient temperature index varies from 41,94% to 55,69%. This means that for many tanks more than half of the tank perimeter exhibits temperatures greater that 20ºC, while for the rest of the tanks more than 40% of the tank perimeter is affected.

It can also be observed that under no wind conditions the ambient temperature index is higher than under wind conditions. When there is no wind, there is no flame tilt, and the flame affects more of the tanks surface, although the maximum temperatures may be lower.

6.4.1.2 Autoignition temperature index of models with one burning tank

In Table 6.3 can be observed the *autoignition temperature index* (T>Taut) for every model arranged in descending order.

MODEL	AUTOIGNITION TEMPERATURE INDEX T≥Taut
15_15_E_W_1	19.03%
15_20_E_W_1	17.08%
15_15_E_NW_1	15.00%
15_15_G_W_1	12.36%
15_25_G_W_1	12.36%
10_15_E_W_1	11.94%
15_25_E_W_1	11.39%
15_20_G_W_1	10.28%
15_20_E_NW_1	8.06%
10_15_G_W_1	7.22%
10_15_E_NW_1	6.39%
10_20_E_W_1	4.17%
15_15_G_NW_1	4.17%
10_20_G_W_1	1.94%
15_25_E_NW_1	1.67%
10_25_E_W_1	0.00%
10_25_G_W_1	0.00%
10_20_E_NW_1	0.00%
10_25_E_NW_1	0.00%
10_15_G_NW_1	0.00%
10_20_G_NW_1	0.00%
10_25_G_NW_1	0.00%
15_20_G_NW_1	0.00%
15_25_G_NW_1	0.00%

Table 6-3 Autoignition temperature index arranged in descending order

It can be seen that the autoignition temperature index varies from 0% to 19,03%. Only in 9 out of 24 models, there is no part of the external surface of the target tank that exceeds the autoignition temperature and it mainly happens under no wind conditions. The higher autoignition indexes occur under wind conditions.

6.4.1.3 Fire risk index of models with one burning tank

In Table 6.4 can be seen the fire risk index for every model arranged in descending order.

model	FIRE RISK INDEX
15_15_E_W_1	1.437
15_20_E_W_1	0.747
15_15_G_W_1	0.662
15_15_E_NW_1	0.501
10_15_E_W_1	0.483
15_20_G_W_1	0.300
15_25_E_W_1	0.230
10_15_G_W_1	0.218
15_20_E_NW_1	0.150
10_15_E_NW_1	0.095
15_25_G_W_1	0.052
15_15_G_NW_1	0.046
10_20_E_W_1	0.031
10_20_G_W_1	0.010
15_25_E_NW_1	0.005
10_25_E_W_1	0.000
10_25_G_W_1	0.000
10_20_E_NW_1	0.000
10_25_E_NW_1	0.000
10_15_G_NW_1	0.000
10_20_G_NW_1	0.000
10_25_G_NW_1	0.000
15_20_G_NW_1	0.000
15_25_G_NW_1	0.000

Table 6-4 Fire risk index arranged in descending order

It can be noted that the fire risk index varies from 0 to 1.437. The fire risk index is 0.00 for 9/24 models, because in this models the autoignition temperature is never reached.

Figure 6-41 shows the fire risk index of the target tank versus the separation distance between the source and the target tank for both diameters of the burning tank and wind conditions, for Ethanol models.

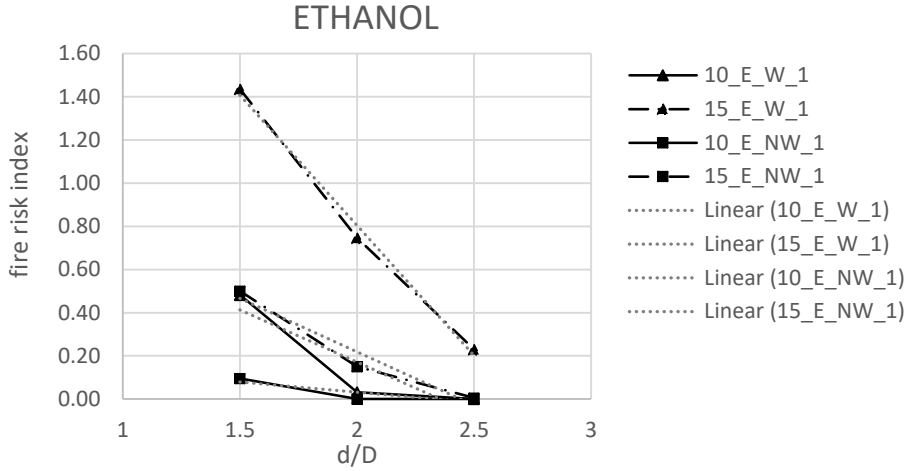

Figure 6-41 Fire risk index with the different separation distances, for Ethanol models

In the smaller diameters of the burning tank with Ethanol the fire risk index rate decreases rapidly as the separation distance increases and for d/D values >2 the fire risk becomes zero. In larger diameters of the source tank the fire risk rate decreases linearly, under both wind conditions. In the case of wind presence the decrease rate is higher.

Figure 6-42 illustrates the fire risk index of the target tank with the separation distance between the source and the target tank for both diameters of the burning tank and wind conditions, for Gasoline models.

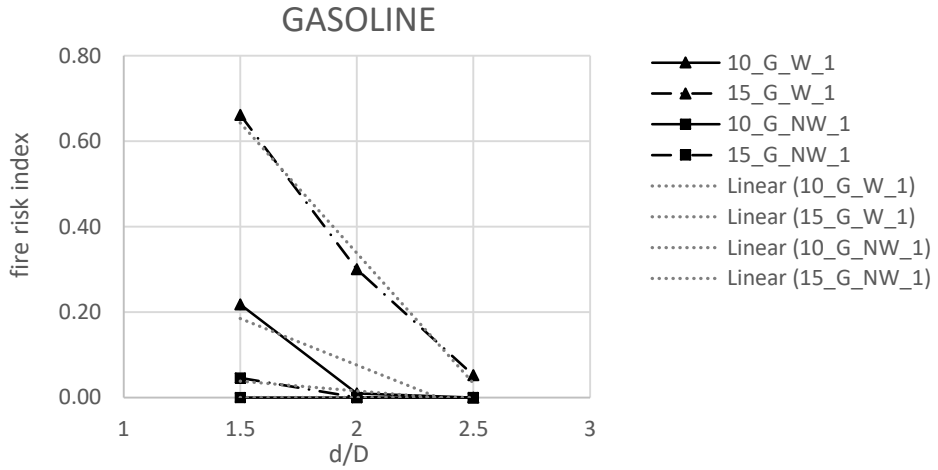

Figure 6-42 Fire risk index with the different separation distances, for Gasoline models

In Gasoline models in most scenarios examined the fire risk index is very small and as the separation distance increases it becomes zero. Higher values occur only in the large diameter models at distances d/D <2 and under wind condition, but they decrease rapidly as the separation distance increases.

Figure 6-43 illustrates the fire risk index of the target tank with the separation distance between the source and the target tank for both diameters of the burning tank and for both fuel types under wind conditions.

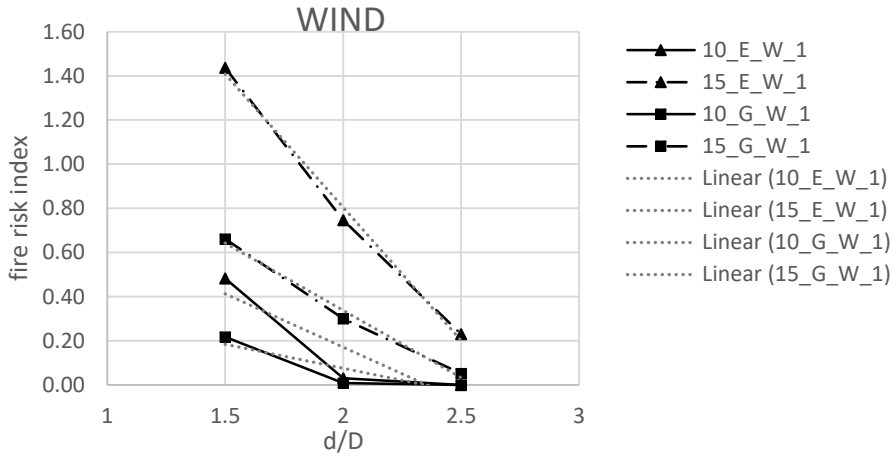

Figure 6-43 Fire risk index with the different separation distances, for models under wind conditions

Under wind conditions, for both fuel types' at large diameters, the fire risk rate declines in a linear way. For larget source tanks the reduction rate is higher as the separation distance increases and the higher reduction rate is for ethanol fuel.

Figure 6-44 illustrates the fire risk index of the target tank with the separation distance between the source and the target tank for both diameters of the burning tank and for both fuel types under no wind conditions.

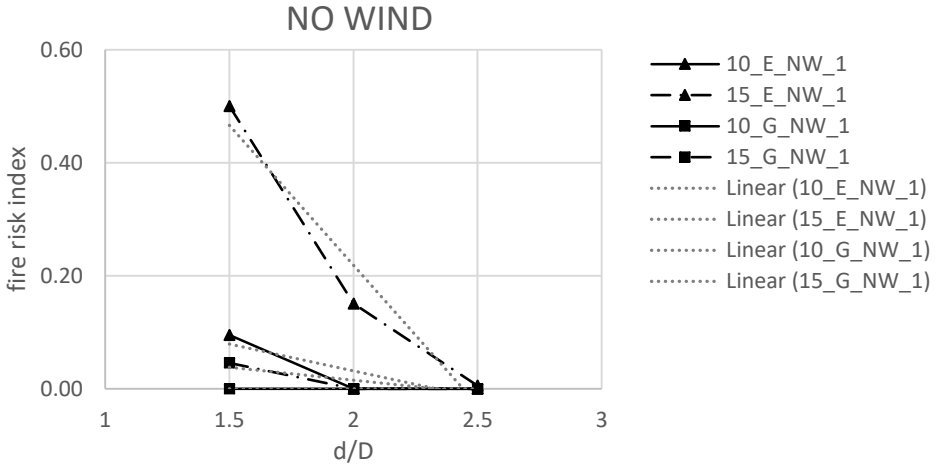

Figure 6-44 Fire risk index with the different separation distances, for models under no wind conditions

Under no wind conditions in almost every scenario examined the fire risk index is very small and as the separation distance increases it becomes zero. Only the large diameter Ethanol model exhibits higher fire risk indexes which decrease to zero as the separation distance increases.

6.4.2 Comparison indexes for the models with multiple burning tanks

Table 6-5 illustrates the ambient temperature index, the autoignition temperature index and the fire risk index of the target tank for Ethanol models, under wind conditions, for 1, 2, 3 & 4 burning tanks

MODEL	AMBIENT TEMPERATURE INDEX T>20	AUTOIGNITION TEMPERATURE INDEX T≥Taut	FIRE RISK INDEX
15_15_E_W_1	46.80%	19.03%	1.44
15_15_E_W_2	69.72%	38.05%	2.73
15_15_E_W_3	84.16%	49.86%	3.50
15_15_E_W_4	96.04%	57.43%	3.94

Table 6-5 Comparison indexes for Ethanol models, under wind conditions for 1, 2, 3 & 4 burning tanks

It can be deduced from the above table that all indexes increase when a burning tank is added. The ambient temperature index varies from 46,80% when only one tank is burning to 96,04% when 4 tanks are burning. The autoignition temperature index ranges from 19,03 % to 57,43%. The fire risk index increases from 1,44 to 3,94.

Table 6-6 shows the ambient temperature index, the autoignition temperature index and the fire risk index of the target tank for Gasoline models, under wind conditions, for 1, 2, 3 & 4 burning tanks

MODEL	AMBIENT TEMPERATURE INDEX T>20	AUTOIGNITION TEMPERATURE INDEX T≥Taut	FIRE RISK INDEX
15_15_G_W_1	48.89%	12.36%	0.66
15_15_G_W_2	74.72%	27.50%	1.11
15_15_G_W_3	86.18%	37.15%	1.38
15_15_G_W_4	95.62%	40.14%	1.47

Table 6-6 Comparison indexes for Gasoline models, under wind conditions for 1, 2, 3 & 4 burning tanks

As indicated in the previous models all indexes increase when a burning tank is added. It can be seen that the ambient temperature index varies from 48,89% when only one tank is burning to 95,62% when 4 tanks are burning. The autoignition temperature index ranges from 12,36 % to 40,14%. Last but not least fire risk index increases from 0,66 to 1,47 that shows that Gasoline compared to Ethanol causes lower temperatures.

Table 6-7 illustrates the ambient temperature index, the autoignition temperature index and the fire risk index of the target tank for Ethanol models, under no wind conditions, for 1, 2, 3 & 4 burning tanks

MODEL	AMBIENT TEMPERATURE INDEX T>20	AUTOIGNITION TEMPERATURE INDEX T≥Taut	FIRE RISK INDEX
15_15_E_NW_1	50.55%	15.00%	0.50
15_15_E_NW_2	67.29%	31.18%	1.60
15_15_E_NW_3	83.47%	49.44%	2.70
15_15_E_NW_4	98.05%	64.02%	3.73

Table 6-7 Comparison indexes for Ethanol models, under wind no conditions for 1, 2, 3 and 4 burning tanks

Again, the addition of burning tanks leads to higher indexes. It can be seen that the ambient temperature index varies from 50,55% when only one tank is burning to 98,05% when 4 tanks are burning. The autoignition temperature index ranges from 15,00% to 64,02%. The fire risk index rises from 0,50 to 3,73.

Table 6-8 illustrates the ambient temperature index, the autoignition temperature index and the fire risk index of the target tank for Gasoline models, under no wind conditions, for 1, 2, 3 & 4 burning tanks

model	AMBIENT TEMPERATURE INDEX T>20	AUTOIGNITION TEMPERATURE INDEX T≥Taut	FIRE RISK INDEX
15_15_G_NW_1	54.86%	4.17%	0.05
15_15_G_NW_2	69.86%	16.46%	0.35
15_15_G_NW_3	83.95%	28.61%	0.68
15_15_G_NW_4	96.57%	39.26%	0.98

Table 6-8 Comparison indexes for Gasoline models, under no wind conditions for 1, 2, 3 and 4 burning tanks

As noted in the previous models, all indexes increase when a burning tank is added. It can be seen that the ambient temperature index varies from 54,86% when only one tank is burning to 96,57% when 4 tanks are burning. The autoignition temperature index ranges from 4,17 % to 39,26%. The fire risk index increases from 0,05 to 0.98 which shows that Gasoline compared to Ethanol causes lower temperatures.

At this point it must be noted that according to the ambient temperature index, in all models with one burning tank half of the external surface is affected, while with four burning tanks 95% of the target tank surface is affected.

Figure 6-45 illustrates the fire risk index of the target tank with the number of the burning tanks for Ethanol models for both wind conditions.

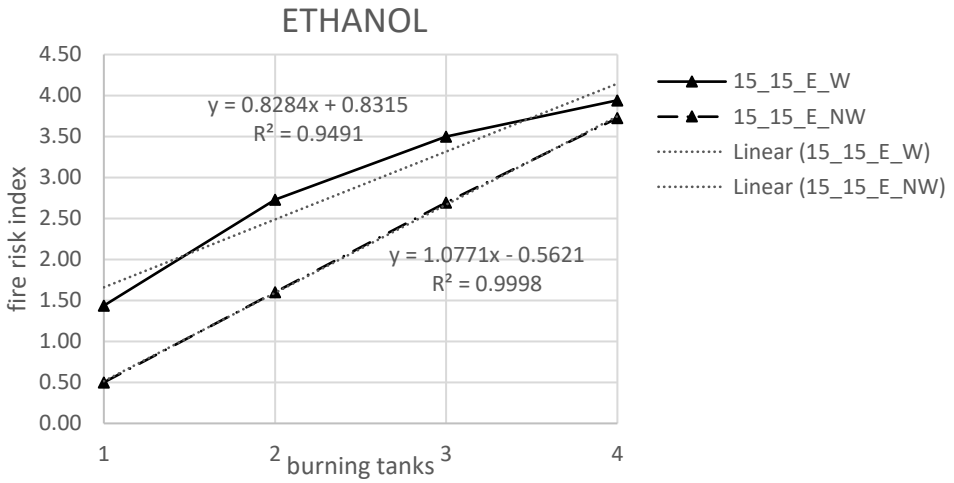

Figure 6-45 Fire risk index with the number of burning tanks for Ethanol models

It has been already mentioned that as the number of burning tanks the fire risk index increases too. Although the values of the fire risk index under wind conditions are bigger than under no wind conditions, the fire risk increase rate under no wind conditions is slightly bigger. Both curves rise linearly, as noted by the trend line.

Figure 6-46 presents the fire risk index of the target tank with the number of the burning tanks for Gasoline models for both wind conditions.

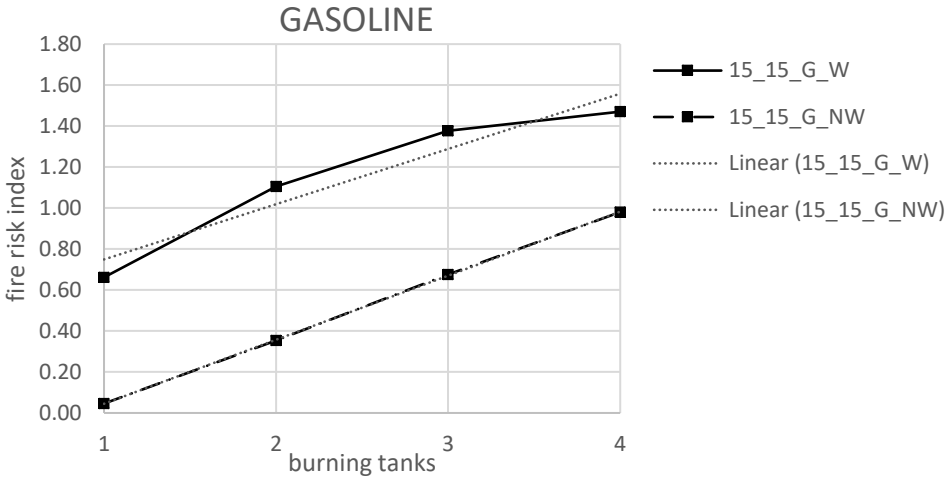

Figure 6-46 Fire risk index with the number of burning tanks for Gasoline models

When a burning tank is added the fire risk index increases linearly too in Gasoline models. The absence of wind conditions leads to lower values of the fire risk index, though the rate of increase the curve is higher.

Figure 6-47 presents the fire risk index of the target tank with the number of the burning tanks under wind conditions for both fuel types.

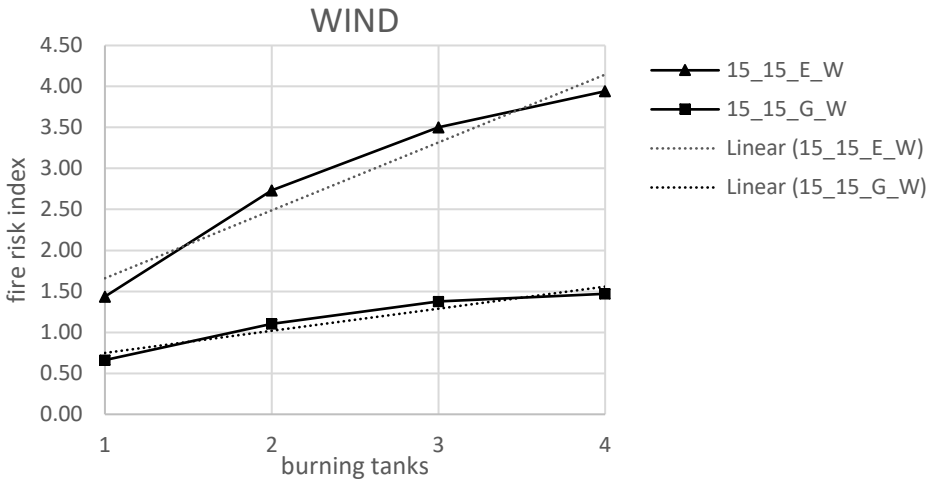

Figure 6-47 Fire risk index with the number of burning tanks for models under wind conditions

The fire risk in Ethanol is bigger than the fire risk in Gasoline models as the number of burning tanks increases under wind conditions. The curve of Ethanol models shows a rapid rise as the burning tanks increase from 1 to 2 and gets smoother afterwards. The same trend is observed in Gasoline too, but in a smaller scale. The ratio of the fire risk rate in Ethanol is 4 times bigger than the Gasoline rate.

Figure 6-48 presents the fire risk index of the target tank with the number of the burning tanks under no wind conditions for both fuel types.

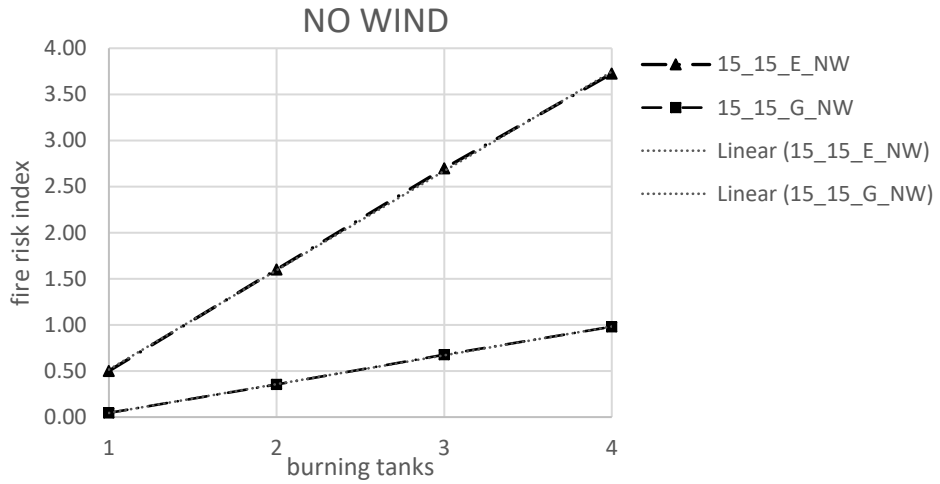

Figure 6-48 Fire risk index with the number of burning tanks for models under no wind conditions

The fire risk in Gasoline models is smaller than the fire risk in Ethanol models as the number of burning tanks increases under no wind conditions. Both curves increase linearly while the fire risk rate is 3,5 times bigger in Ethanol models.

Figure 6-49 illustrates the fire risk index of the target tank with the number of the burning tanks for both fuel types under both wind conditions.

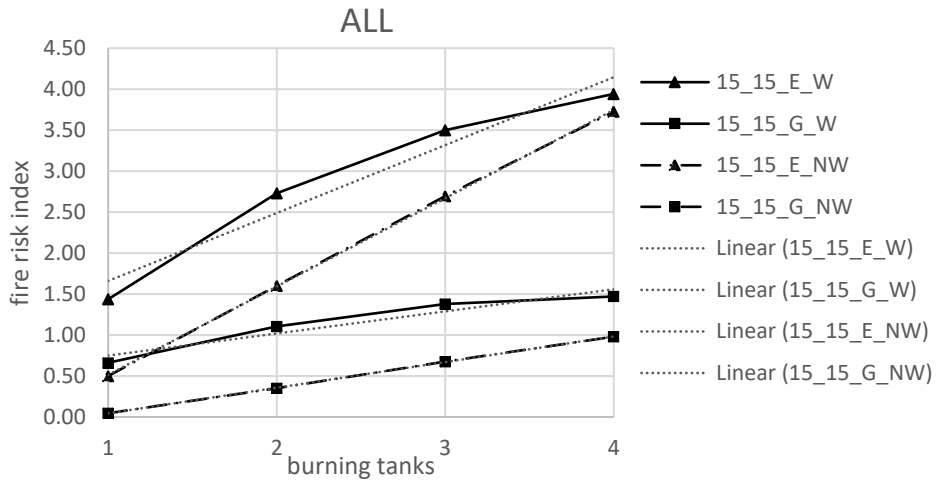

Figure 6-49 Fire risk index with the number of burning tanks for all models

In Figure 6-49 is observed that the curve fire risk is more affected by the fuel type when the number of burning tanks increases. The presence or absence of wind conditions affects only the magnitude of fire risk.

CHAPTER 7. CONCLUSIONS

The present thesis addresses the thermal behavior of steel fixed-roof oil storage tanks heated by an adjacent tank. The study is divided in two parts. The first part focuses on the characteristics and parameters that describe the burning tank. In the second part the heated tank is examined in order to reveal the key factors that mainly affect the temperature distribution on the external surface. The problem is solved numerically using the Finite Element method. Thirty six, three dimensional models are developed for the investigation of the temperature fields of the target storage tank. A flame pattern, available in the literature, is used to simulate the burning tank by the adjacent fire-engulfed tank. Parametric analyses are conducted to investigate the influence of a combination of various parameters: diameter of the burning tank, type of stored fuel (gasoline or ethanol), presence of wind, distance between the tanks and the number of burning tanks involved. Out of the various findings obtained during this work, the following ones should be especially mentioned:

- The temperature distribution on the tank wall of the adjacent tank is not uniform. The temperature rise takes place on the side of the tank wall which is on the face of the source tank while the opposite side is not affected by the pool fire. This pattern becomes more complicated as more burning tanks are added.
- When the target tank is closer to the burning tank, the maximum temperature is higher, and as the separation distance increases the maximum temperature decreases. This reduction is observed in all cases, regardless of the burning tank diameter, the fuel type, the wind conditions or the number of the burning tanks and is found to be linear.
- In both fuel types - Ethanol and Gasoline - the rate of reduction of the maximum temperature as the separation distance increases is more affected by the presence of wind than of the diameter of the burning tank.
- Under wind conditions, in smaller diameters of the source tank the rate of temperature reduction with the increase of the separation distance is not affected by the fuel type. In bigger burning tank diameters it has an effect. Under no wind conditions, the rate of temperature reduction with the separation distance is more influenced by the fuel type.
- The ambient temperature index is higher under no wind conditions. That can be by the absence of flame tilt under no wind conditions. When there is no wind, the vertical flame affects more evenly the adjacent tank.
- In 9 out of 24 models, no part of the external surface of the target tank that exceeds the autoignition temperature and it mainly happens under no wind conditions. The highest autoignition indexes take place under wind conditions.
- In small diameters of the burning tank in Ethanol models the fire risk rate decreases rapidly as the separation distance increases and as the tanks get more separated fire risk becomes zero. In large diameters of the source tank the fire risk rate decreases linearly under both wind conditions.
- In Gasoline models in almost every scenario examined the fire risk index is very small and as the separation distance increases it becomes zero. Only in large burning diameters and under wind condition the fire risk rate is higher and decreases linearly until the fire risk becomes zero.
- Under wind conditions, for both fuel types at large diameters, the fire risk rate declines in a linear way. In small diameters for both fuel types the fire risk rate

shows a rapid reduction in closer separation distances. When the two tanks become more separated, the fire risk becomes zero.

- Under no wind conditions in almost every scenario examined the fire risk index is very small and as the separation distance increases it becomes zero. Only in large diameter Ethanol models the fire risk rate decreases linearly until the fire risk becomes zero.
- All indexes increase when a burning tank is added.
- According to the ambient temperature index, in all models when there is one burning tank half of the external surface is affected while when there are four burning tanks burning almost 95% of the external surface is affected.
- The fire risk index increases linearly as the number of burning tanks rises.
- The fire risk index in Ethanol is bigger than the fire risk index in Gasoline models as the number of burning tanks increases under both wind conditions.
- The fire risk index is more affected by the fuel type when the number of burning tanks increases. The presence or absence of wind conditions affects only the magnitude of the fire risk index.

REFERENCES

American Gas Association (AGA), 1974. *LNG Safety Research Programme, Report* IS 3-1. Arlington, VA: Battelle Columbus Laboratories.

API STD 650:2013, Welded tanks for oil storage, 12 ed., American Petroleum Institute, 2013

Babrauskas V., 1983. *Estimating Large Pool Fire Burning Rates. Fire Technology*,19, pp.251–261.

Bathe K.J. (1996) “Finite Element Procedures.” Prentice Hall Inc, New Jersey

Beyler, C. L. (2004b). "Industrial fire protection engineering." Fire Technology, 40(3): 297-298

BS EN 14015:2004 Specification for the design and manufacture of site built, vertical, cylindrical, flat-bottomed, above ground, welded, steel tanks for the storage of liquids at ambient temperature and above (BS EN14015:2004).

Casal J., (2008). "Evaluation of the effects and consequences of major accidents in industrial plants", Industrial Safety Series, v.8, Elsevier 1–363.

Considine, M., 1984. *Thermal Radiation Hazard Ranges from Large Hydrocarbon Pool Fires*. Wigshaw: Safety & Reliability Directorate, UK Atomic Energy Authority

Cook, J., Bahrami, Z., Whitehouse, R. J, 1990. *A comprehensive program for calculation of flame radiation levels*, J. Loss Prevention. Process Industry, 3, pp 150-155.

Cowley, L. T. and Johnson, A. D., 1992. Oil and Gas Fires: Characteristics and Impact. Chester: Shell Research Limited.

Daniel, A., Crowl, J., & Louvar, F. (2002). Chemical process safety e fundamentals with applications. In B. Goodwin (Ed.) (2nd ed..).Prentice Hall international series.

Ditali, S., Rovati, A. and Rubino, F. 1992. *Experimental Model to Assess Thermal Radiation from Hydrocarbon Pool Fires*. In Proceedings of the 7th International Symposium on Loss Prevention and Safety Promotion in the Process Industries, Volume 1.

EN 1993-1-6 Eurocode 3: Design of steel structures, Part 1-6: General rules - Strength and

stability of shell structures (EN1993 1-6, 2007).

EN 1993-4-2 Eurocode 3- Design of steel structures, Part 4-2: Tanks (EN1993 4-2, 2007).

EN1993 1-2 (2007). Eurocode 3: Design of steel structures, Part 1-2: General rules - Structural fire design. Brussels, CEN

European Model Code of Safe Practice, 1981. *The Storage and Handling of Petroleum Products*. Concawe Product Dossier 98/109

Fontenelle F.M.A., Thermal Analysis of Ethanol Storage Tanks Under Fire Conditions (M.Sc. Dissertation), Federal University of Rio de Janeiro (COPPE/ UFRJ), Rio de Janeiro, RJ, Brazil, 2012.

Hankinson, G., 1986. "*A Method for Calculating the Configuration Factor between a Flame and a Receiving Target for a Wide Range Of Flame Geometries Relevant to Large Scale Fires"*. Fire Safety Science, Proceeding of the first international symposium. Hemisphere Publishing Corporation, Nueva York.1, pp.197-206.

Hughes O. Ship Structural Design: "A rationally-based, computer-aided optimization procedure." SNAME, New York (1996)

Institute of Petroleum, 1981. *Refining Safety Code, Part 3 of Model Code of Safe Practice in the Petroleum Industry*.

Johnson, A. D., 1992. *A Model for Predicting Thermal Radiation Hazards from Large-Scale Pool Fires*. IChemE Symposium Series, 130, pp.507-524.

Lees, F. P. (1995) (2nd ed.).Loss prevention in process industries, Vol. 3 Butterworth Heinemann.

Liu Ying Doctor of Philosophy in The University of Edinburgh (2011) Thermal buckling of metal oil tanks subject to an adjacent fire

Mansour K.A (2012), Fires in Large Atmospheric Storage Tanks and Their Effect on Adjacent tanks, Doctoral Dissertation, Loughborough University

MSC Software Corporation, MSC Marc, Volume A: Theory and User Information, Version 2014.

McGrattan, K. B., Baum, H. R., and Hamins, A. (2000). "Thermal radiation from large pool fires." NIST Technology Administration U.S. Department of Commerce.

Moorhouse, J., 1982. *Scaling Laws for Pool Fires Determined from Large Scale Experiments*. IChemE Symposium Series, 71, pp.165-179

Moorhouse, J. and Pritchard, M.J., 1982. *Thermal Radiation Hazards from Large Pool Fires and Fireballs: A Literature Review*. IChemE Symposium Series, 71, p.123

Mudan, K.S., 1984. *Thermal Radiation Hazards from Hydrocarbon Pool Fires*. Progress in Energy and Combustion Science, 10(1), pp.59-80.

Mudan, K.S. and Croce, P.A., 1988. *Fire Hazard Calculations for Large Open Hydrocarbon Fires*. In the SFPE Handbook of Fire Protection Engineering, 1995. Quincy, Massachusetts: National Fire Protection Association.

NFPA 30 (1996). "Flammable and Combustible Liquids Code." National fire protection association, Quincy, MA.

NFPA 30:2012, Flammable and Combustible Liquids Code, National Fire Protection Association, Quincy, MA, USA, 2012.

Pantousa D. Dr. Ing. Civil Engineer (2015) ‘’Numerical simulation of oil steel tank structural behavior under fire conditions’’ in State-of-the-Art Design and Analysis Methods in Industry´´

prEN 14015-1: Specification for the Design and Manufacture of Site Built Vertical Cylindrical Flat-Bottomed Above Ground Welded Metallic Tanks for the Storage of Liquids at Ambient Temperature and Above - Part 1: Steel Tanks EN 14015, draft issued for public comment in 2000 (prEN 14015-1 2000).

Pritchard, M.J. and Binding, T. M., 1992. FIRE2: *A New Approach for Predicting Thermal Radiation Levels from Hydrocarbon Pool Fires*. IChemE Symposium, 130, pp. 491-505.

Rew, P. J., and Hulbert, W. G. (1996). "Development of pool fire thermal radiation model." *HSE Contract Research Report*.

Santos F.S., Landesmann A. (2014) Thermal performance-based analysis of minimum safe distances between fuel storage tanks exposed to fire, Fire Safety Journal 69, 57–68

Sengupta, A., Gupta, A. K., and Mishra, I. M. (2010). "Engineering layout of fuel tanks in a tank farm." Journal of Loss Prevention in the Process Industries

SFPE (1999). Engineering guide for assessing flame radiation to external targets from pool fires. Bethesda, Maryland.

Thomas P. H. (1963). "The size of flames from natural fires." Elsevier, 844-859.

TNO (1980). "Methods for calculation of the physical effects of the escape of dangerous materials (liquids and gases)", Netherlands Organization for Applied Scientific Research (TNO)

Wayne, F. D. 1991. *An Economical Formula for Calculating Atmospheric Infrared Transmissivities* Journal of Loss Prevention in the Process Industries, Vol. 4, pp.86-92.

Welker, J.R. and Sliepcevich, C.M. 1966. *Bending of wind-blown flames from liquid pools*. Fire Technology 2, 127-135

ANNEX

The following figures (A.1, A.2, A.3) present the temperature distribution of the models 10_15_E_W_1, 10_20_E_W_1 and 10_25_E_W_1 respectively, along the circumferential plane for every 5m high, that is 0m, 5m, 10m, 15m and 20m. The autoignition temperature of Ethanol is also captured.

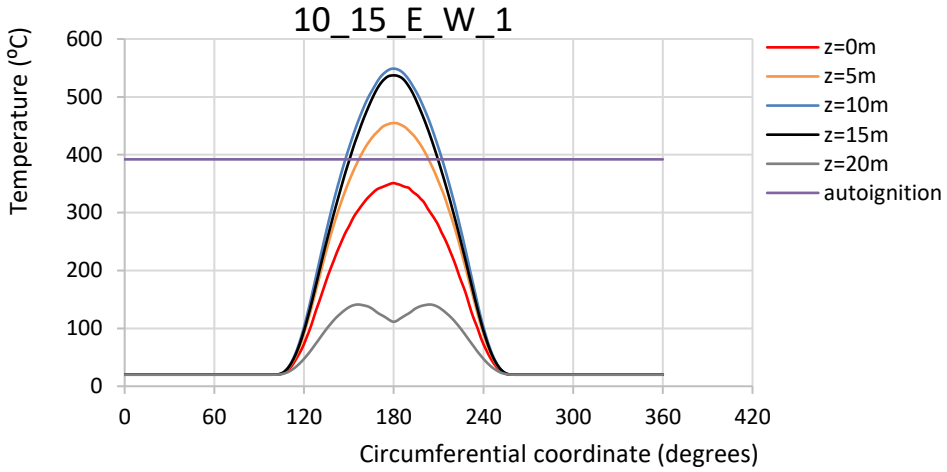

Figure A-1 Temperature distribution along the circumferential plane for model 10_15_E_W_1

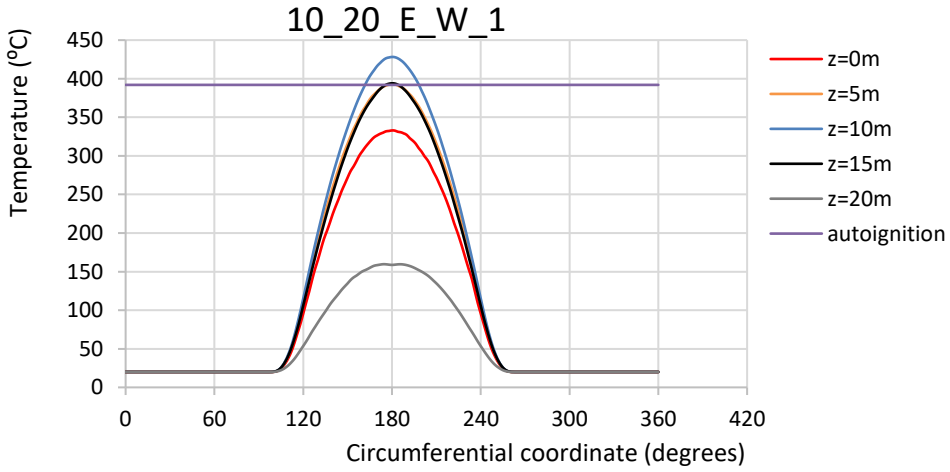

Figure A-2 Temperature distribution along the circumferential plane for model 10_20_E_W_1

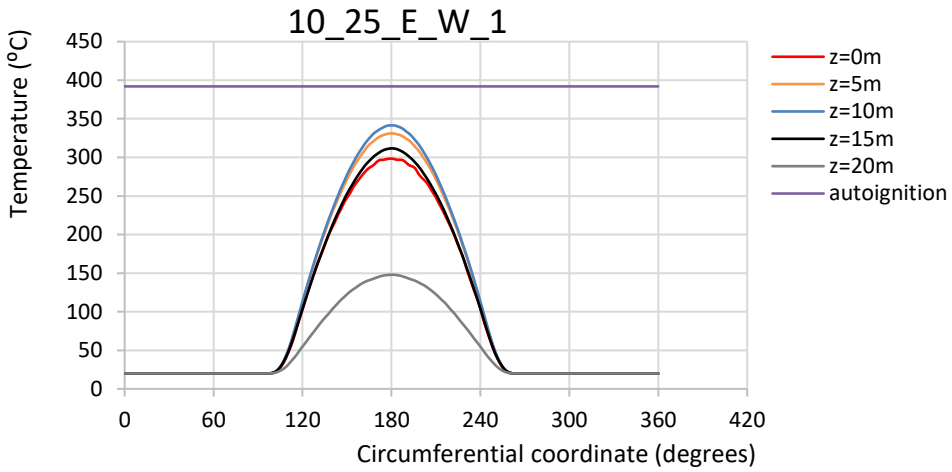

Figure A-3 Temperature distribution along the circumferential plane for model 10_25_E_W_1

The following figures (A.4 – A.8) show the comparison of temperature distribution between the three models, 10_15_E_W_1, 10_20_E_W_1 and 10_25_E_W_1 along the circumferential plane at height 0m, 5m, 10m, 15m and 20m. The autoignition temperature of Ethanol is also captured.

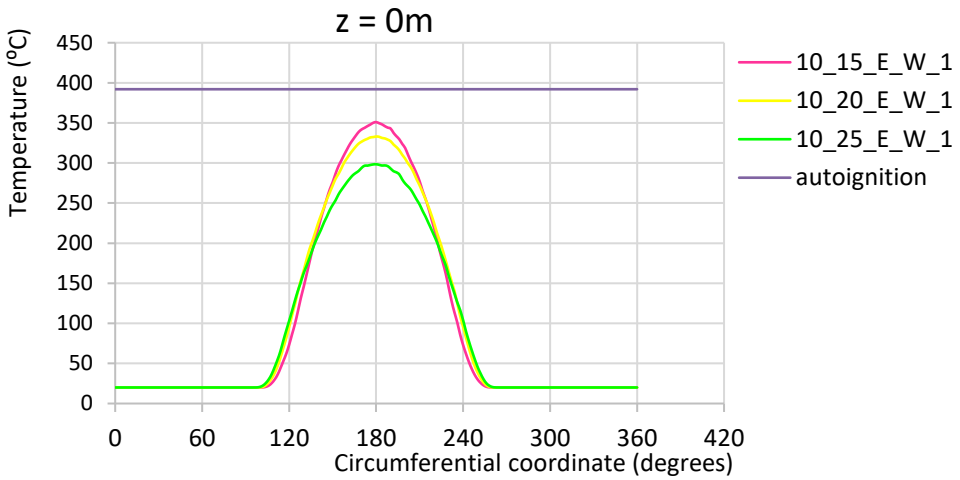

Figure A-4 Temperature distribution along the circumferential plane for models 10_15_E_W_1, 10_20_E_W_1 and 10_25_E_W_1 at height 0m

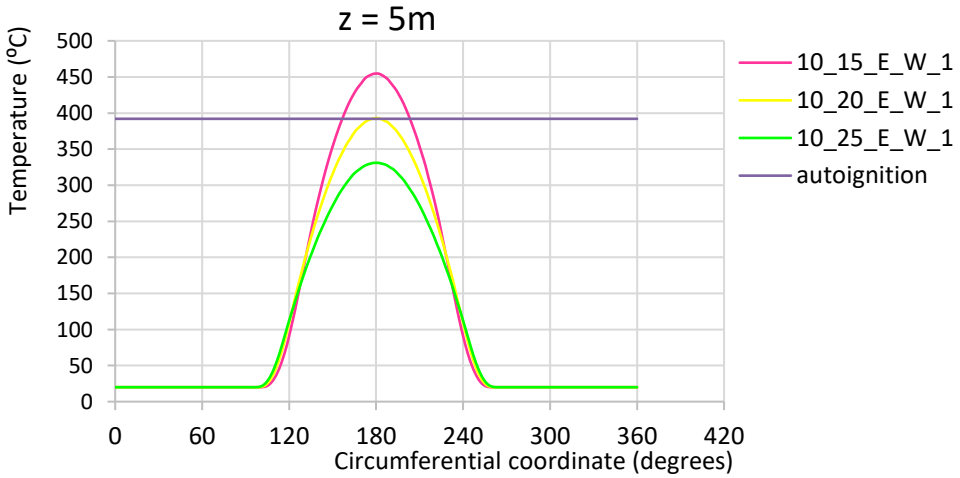

Figure A-5 Temperature distribution along the circumferential plane for models 10_15_E_W_1, 10_20_E_W_1 and 10_25_E_W_1 at height 5m

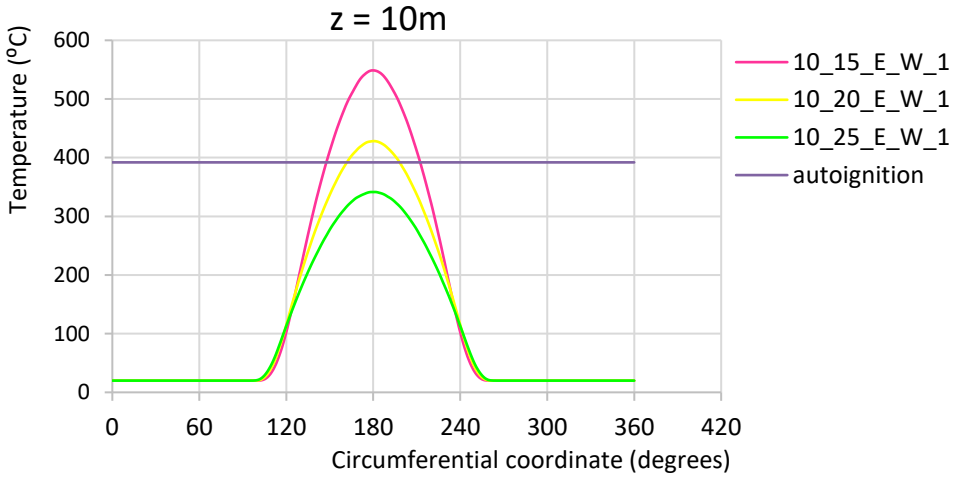

Figure A-6 Temperature distribution along the circumferential plane for models 10_15_E_W_1, 10_20_E_W_1 and 10_25_E_W_1 at height 10m

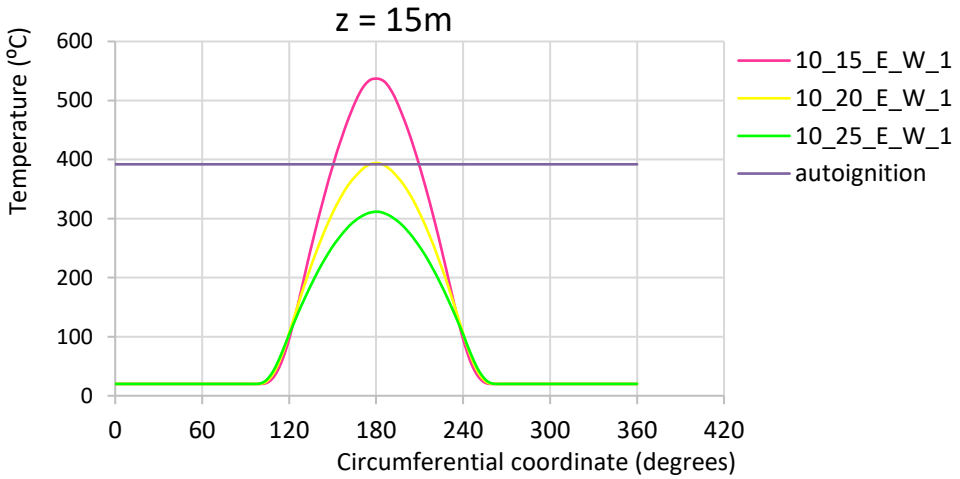

Figure A-7 Temperature distribution along the circumferential plane for models 10_15_E_W_1, 10_20_E_W_1 and 10_25_E_W_1 at height 15m

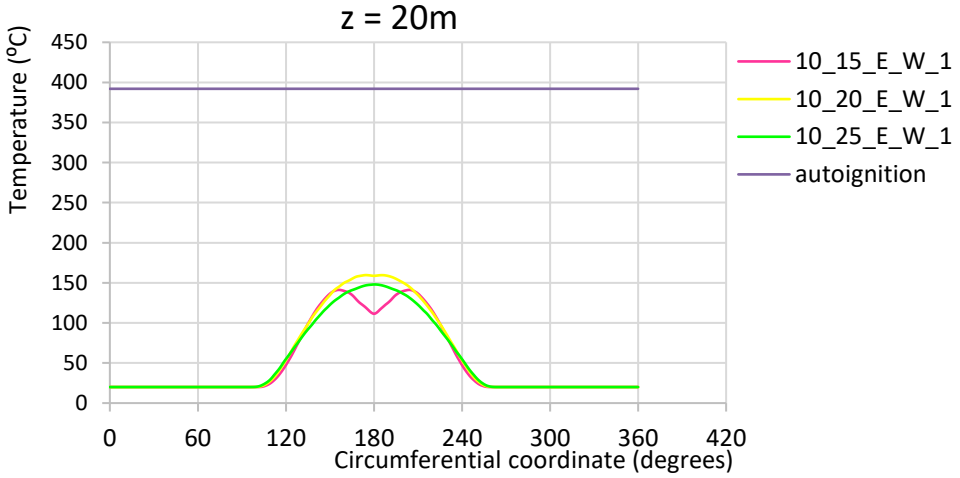

Figure A-8 Temperature distribution along the circumferential plane for models 10_15_E_W_1, 10_20_E_W_1 and 10_25_E_W_1 at height 20m

The following figure (A.9) shows the comparison of temperature distribution between the three models, 10_15_E_W_1, 10_20_E_W_1 and 10_25_E_W_1 along the vertical plane. The temperature distribution is captured at the meridian that develops the highest temperatures. The autoignition temperature curve is also shown.

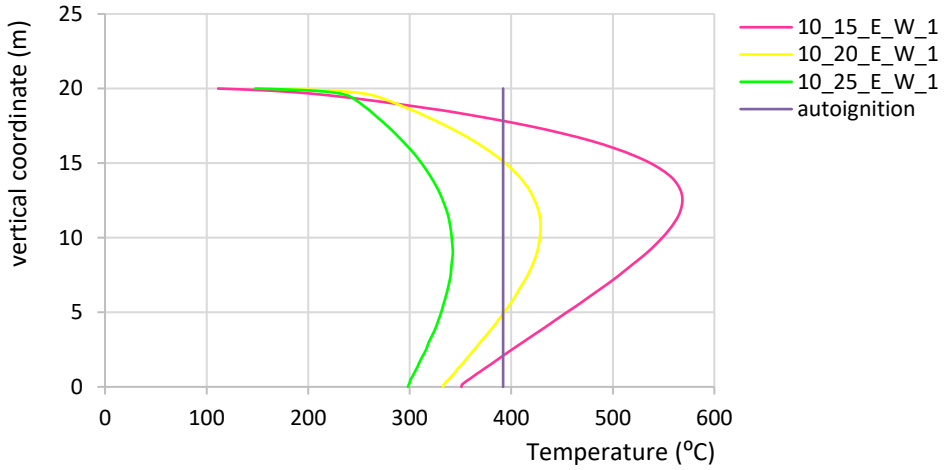

Figure A-9 Temperature distribution along the vertical plane for models 10_15_E_W_1, 10_20_E_W_1 and 10_25_E_W_1

The following figures (A.10, A.11, A.12) present the temperature distribution of the models 10_15_G_W_1, 10_20_G_W_1 and 10_25_G_W_1 respectively, along the circumferential plane for every 5m high, that is 0m, 5m, 10m, 15m and 20m. The autoignition temperature of Gasoline is also captured.

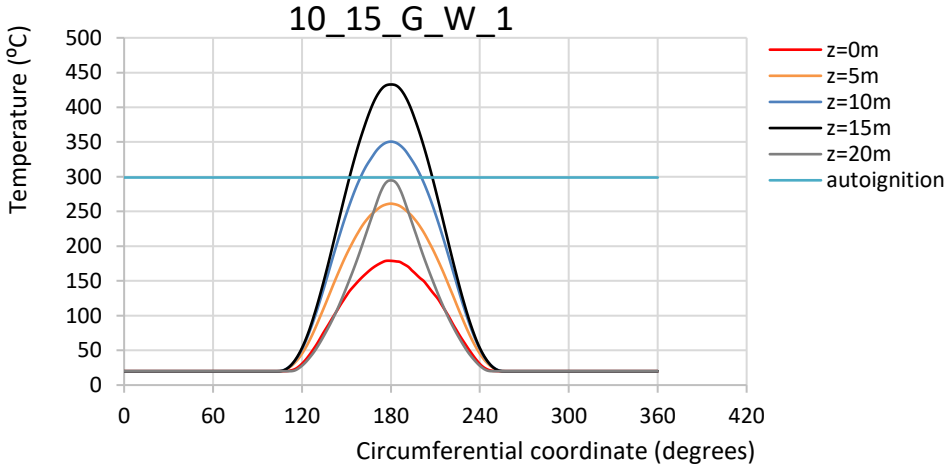

Figure A-10 Temperature distribution along the circumferential plane for model 10_15_G_W_1

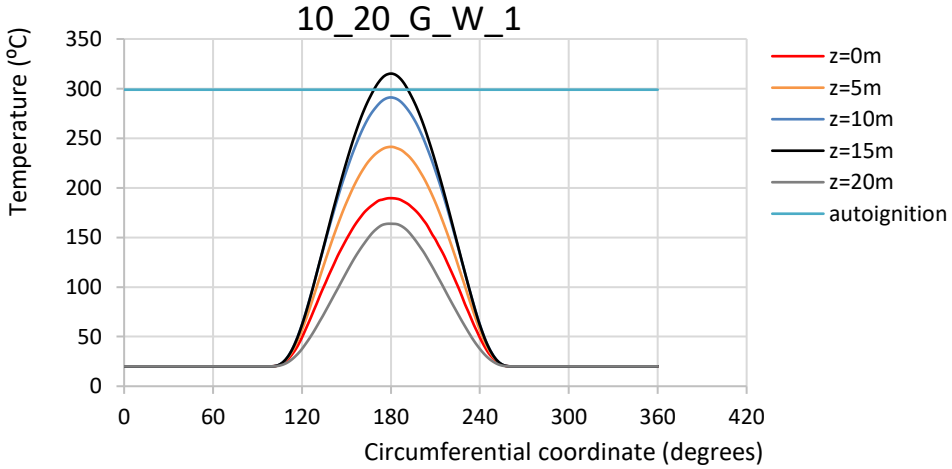

Figure A-11 Temperature distribution along the circumferential plane for model 10_20_G_W_1

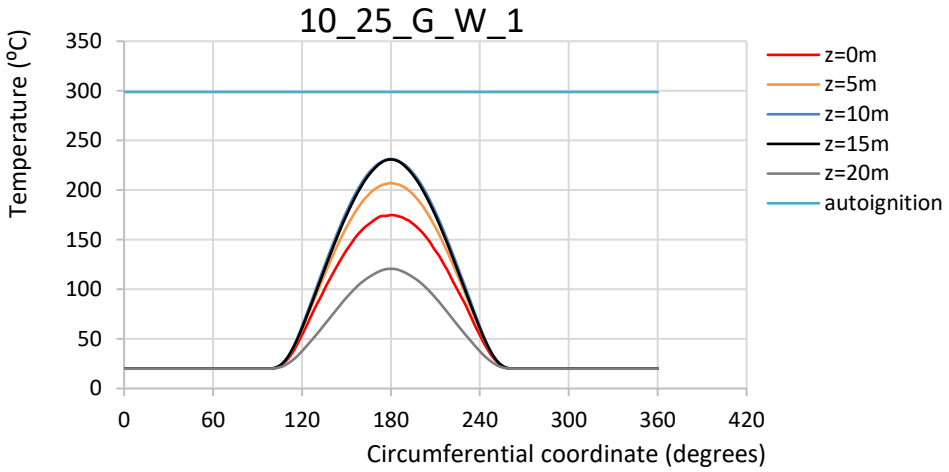

Figure A-12 Temperature distribution along the circumferential plane for model 10_25_G_W_1

The following figures (A.13 - A.17) show the comparison of temperature distribution between the three models, 10_15_G_W_1, 10_20_G_W_1 and 10_25_G_W_1 along the circumferential plane at height 0m, 5m, 10m, 15m and 20m. The autoignition temperature of Gasoline is also captured.

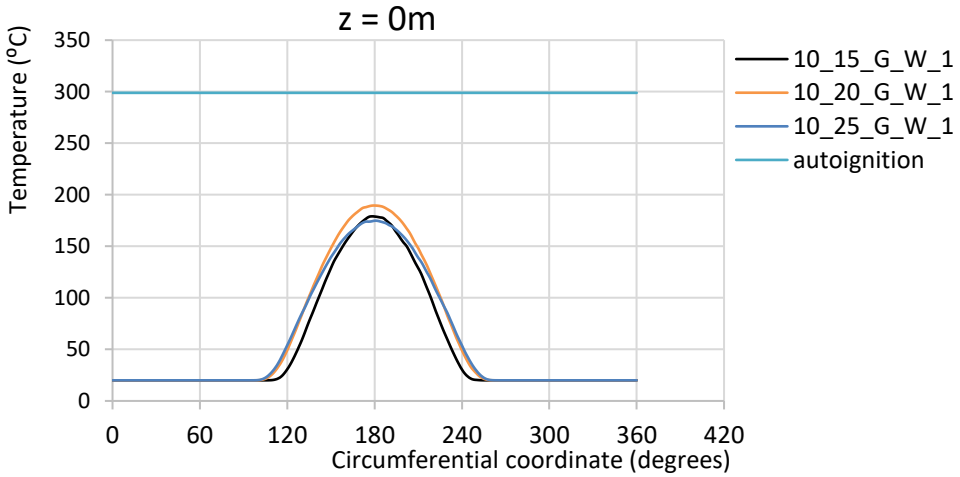

Figure A-13 Temperature distribution along the circumferential plane for models 10_15_G_W_1, 10_20_G_W_1 and 10_25_G_W_1 at height 0m

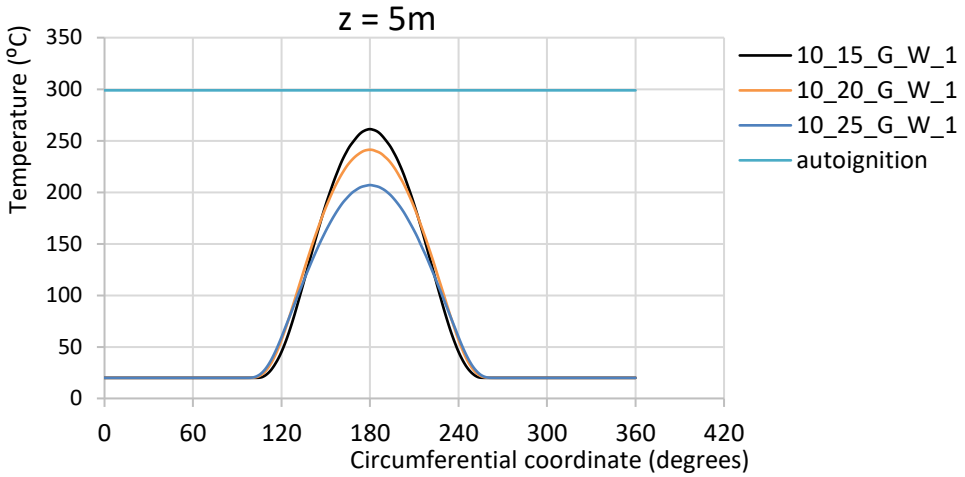

Figure A-24 Temperature distribution along the circumferential plane for models 10_15_G_W_1, 10_20_G_W_1 and 10_25_G_W_1 at height 5m

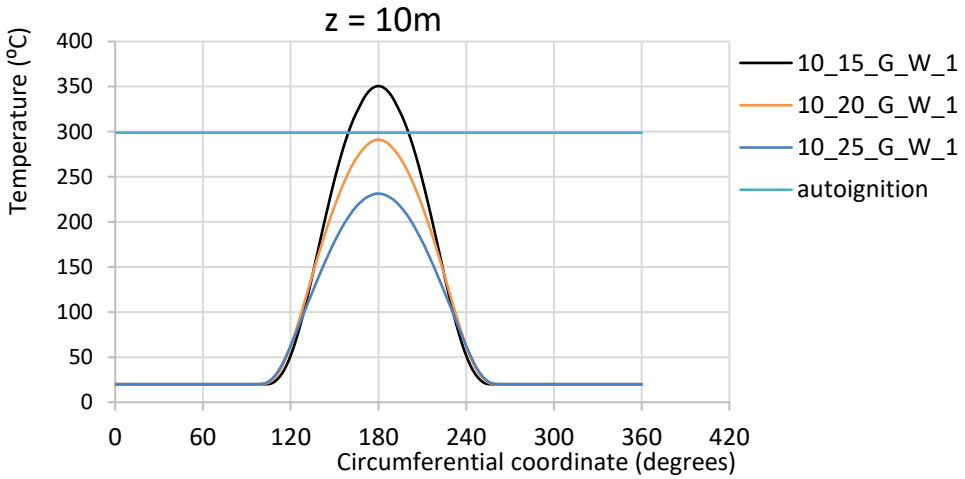

Figure A-35 Temperature distribution along the circumferential plane for models 10_15_G_W_1, 10_20_G_W_1 and 10_25_G_W_1 at height 10m

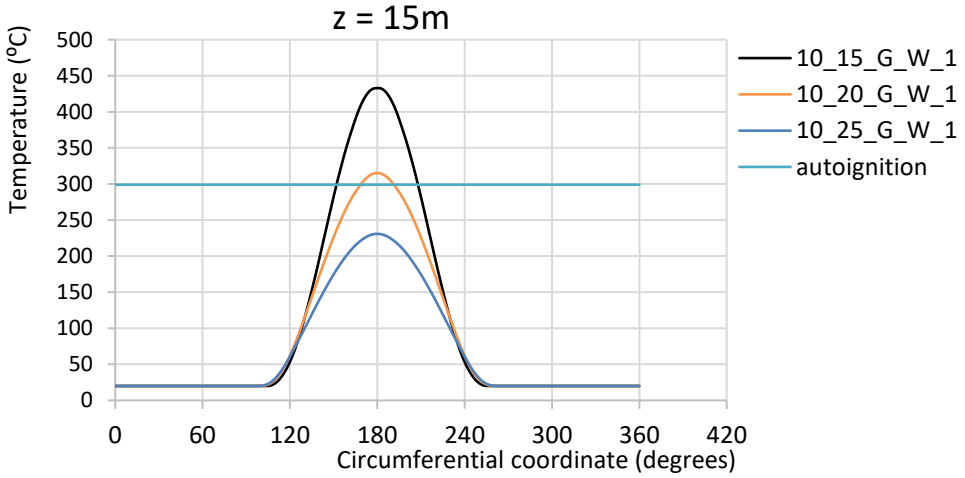

Figure A-46 Temperature distribution along the circumferential plane for models 10_15_G_W_1, 10_20_G_W_1 and 10_25_G_W_1 at height 15m

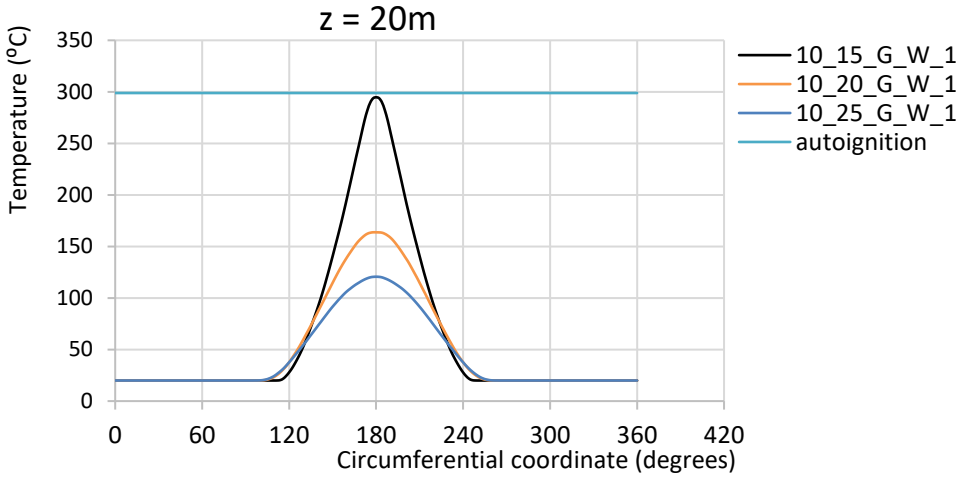

Figure A-57 Temperature distribution along the circumferential plane for models 10_15_G_W_1, 10_20_G_W_1 and 10_25_G_W_1 at height 20m

The following figure (A.18) shows the comparison of temperature distribution between the three models, 10_15_G_W_1, 10_20_G_W_1 and 10_25_G_W_1 along the vertical plane. The temperature distribution is captured at the meridian that develops the highest temperatures. The autoignition temperature curve is also shown.

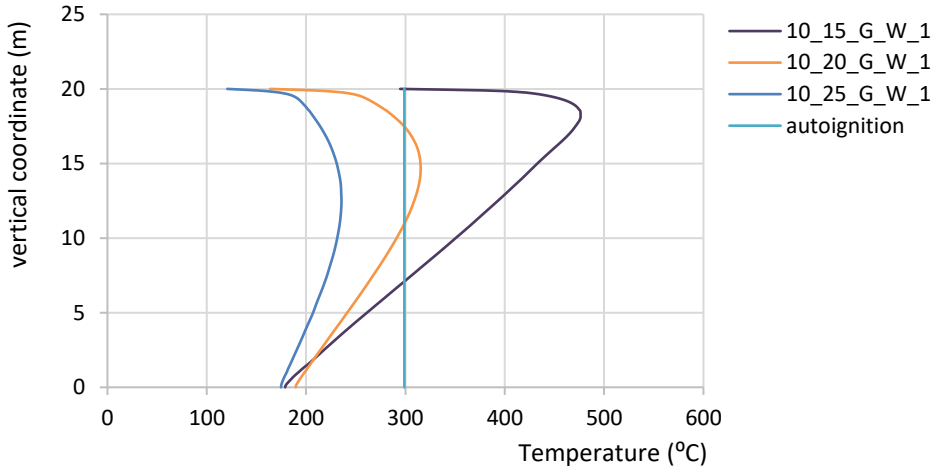

Figure A-18 Temperature distribution along the vertical plane for models 10_15_G_W_1, 10_20_G_W_1 and 10_25_G_W_1

The following figures (A.19, A.20, A.21) present the temperature distribution of the models 10_15_E_NW_1, 10_20_E_NW_1 and 10_25_E_NW_1 respectively, along the circumferential plane for every 5m high, that is 0m, 5m, 10m, 15m and 20m. The autoignition temperature of Ethanol is also captured.

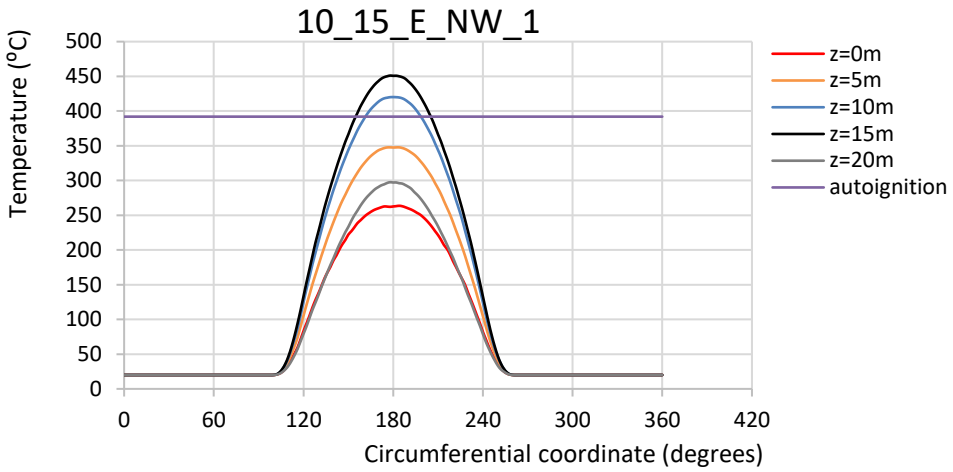

Figure A-19 Temperature distribution along the circumferential plane for model 10_15_E_NW_1

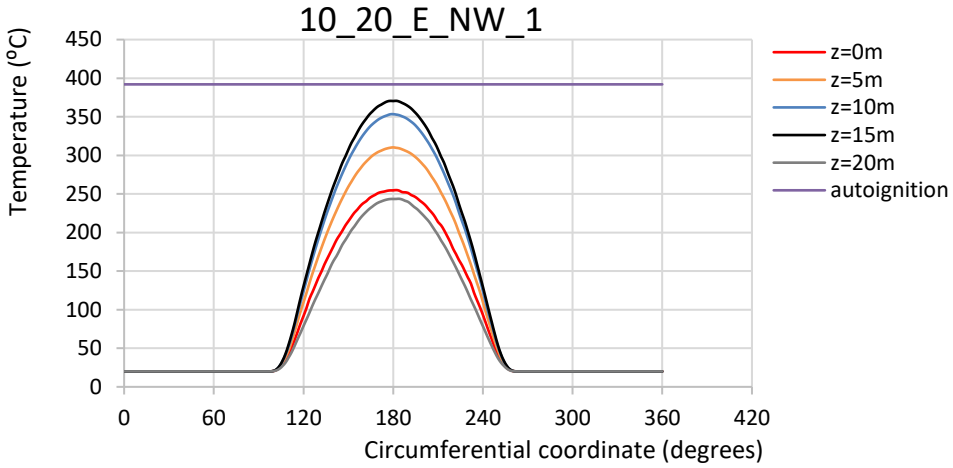

Figure A-20 Temperature distribution along the circumferential plane for model 10_20_E_NW_1

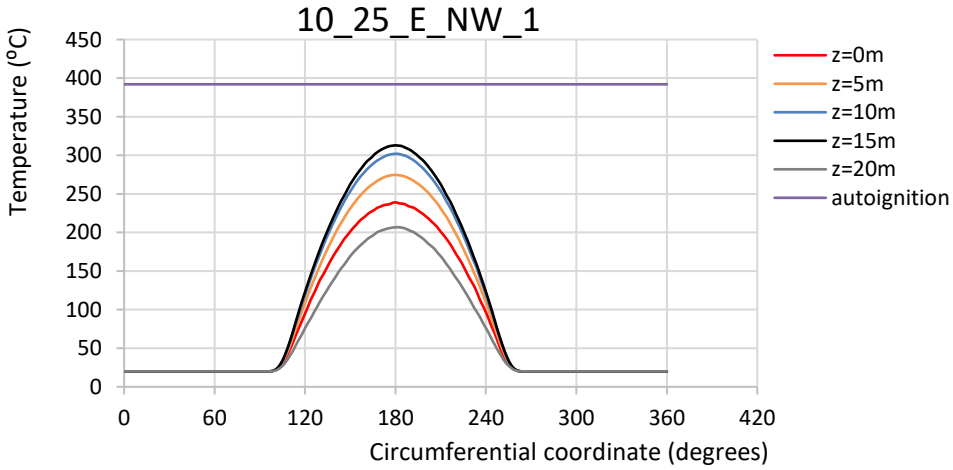

Figure A-21 Temperature distribution along the circumferential plane for model 10_25_E_NW_1

The following figures (A.22 – A.26) show the comparison of temperature distribution between the three models, 10_15_E_NW_1, 10_20_E_NW_1 and 10_25_E_NW_1 along the

circumferential plane at height 0m, 5m, 10m, 15m and 20m. The autoignition temperature of Ethanol is also captured.

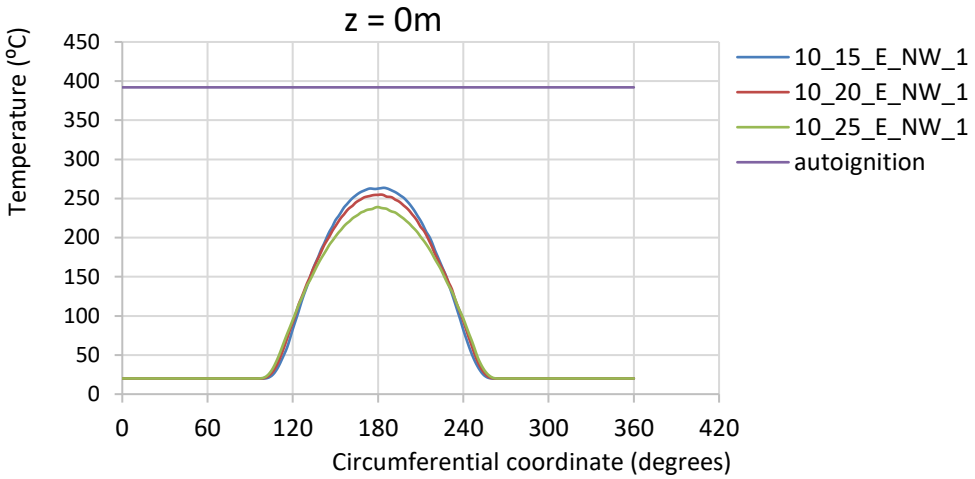

Figure A-22 Temperature distribution along the circumferential plane for models 10_15_E_NW_1, 10_20_E_NW_1 and 10_25_E_NW_1 at height 0m

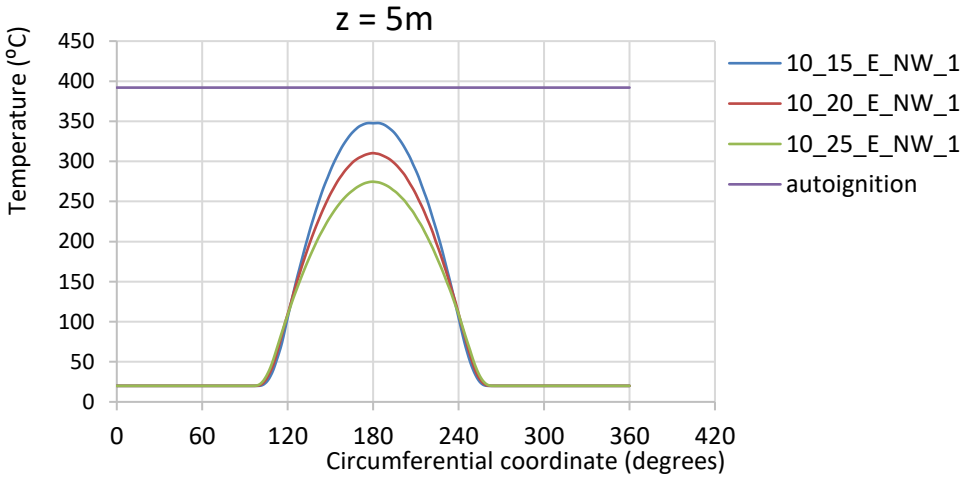

Figure A-23 Temperature distribution along the circumferential plane for models 10_15_E_NW_1, 10_20_E_NW_1 and 10_25_E_NW_1 at height 5m

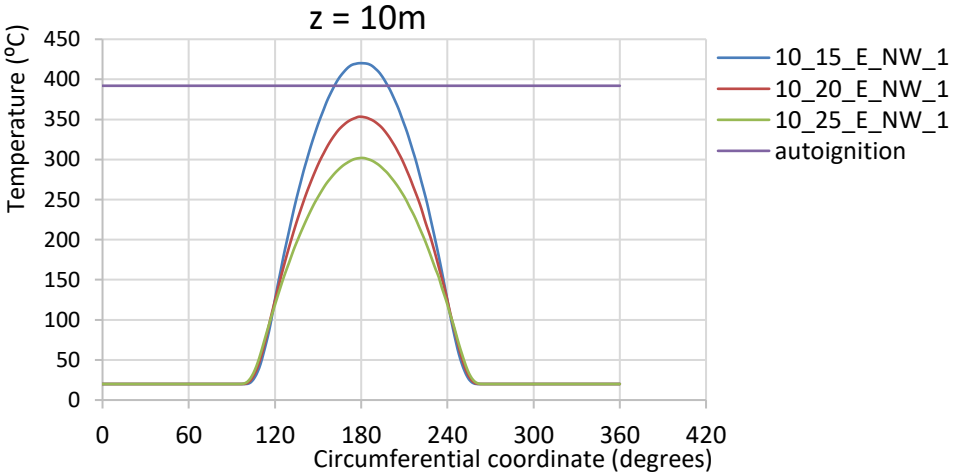

Figure A-24 Temperature distribution along the circumferential plane for models 10_15_E_NW_1, 10_20_E_NW_1 and 10_25_E_NW_1 at height 10m

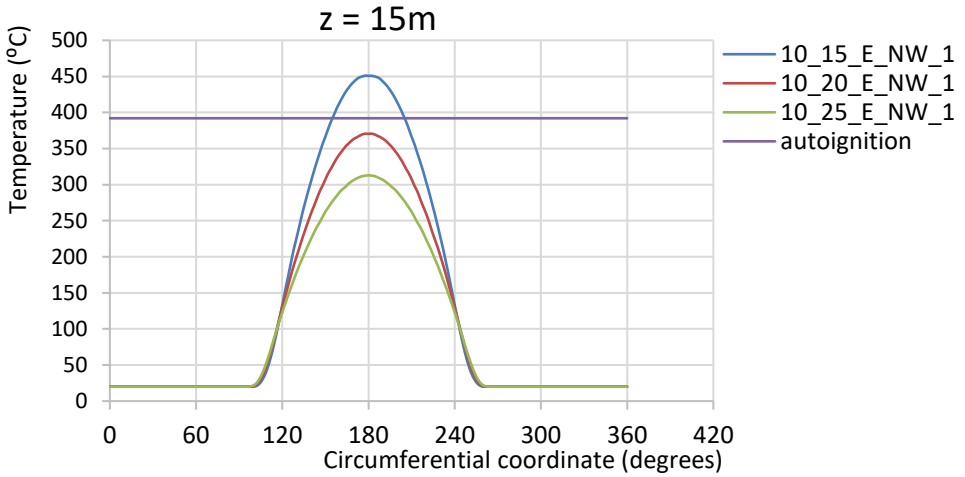

Figure A-25 Temperature distribution along the circumferential plane for models 10_15_E_NW_1, 10_20_E_NW_1 and 10_25_E_NW_1 at height 15m

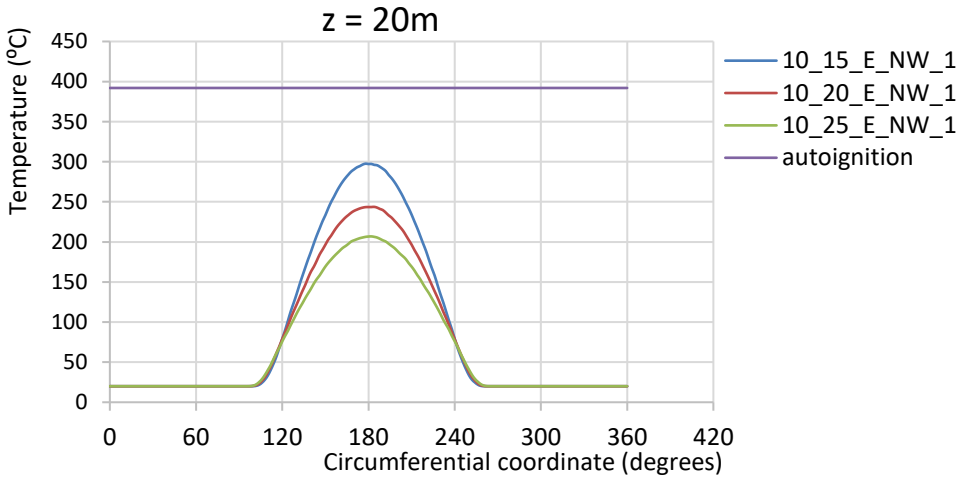

Figure A-26 Temperature distribution along the circumferential plane for models 10_15_E_NW_1, 10_20_E_NW_1 and 10_25_E_NW_1 at height 20m

The following figure (A.27) shows the comparison of temperature distribution between the three models, 10_15_E_NW_1, 10_20_E_NW_1 and 10_25_E_NW_1 along the vertical plane. The temperature distribution is captured at the meridian that develops the highest temperatures. The autoignition temperature curve is also shown.

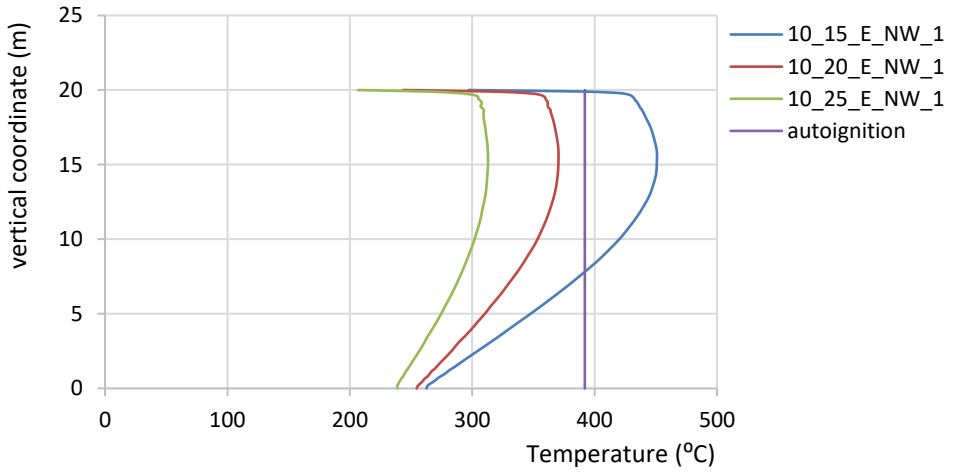

Figure A-27 Temperature distribution along the vertical plane for models 10_15_E_NW_1, 10_20_E_NW_1 and 10_25_E_NW_1

The following figures (A.28, A.29, A.30) present the temperature distribution of the models 10_15_G_NW_1, 10_20_G_NW_1 and 10_25_G_NW_1 respectively, along the circumferential plane for every 5m high, that is 0m, 5m, 10m, 15m and 20m. The autoignition temperature of Gasoline is also captured.

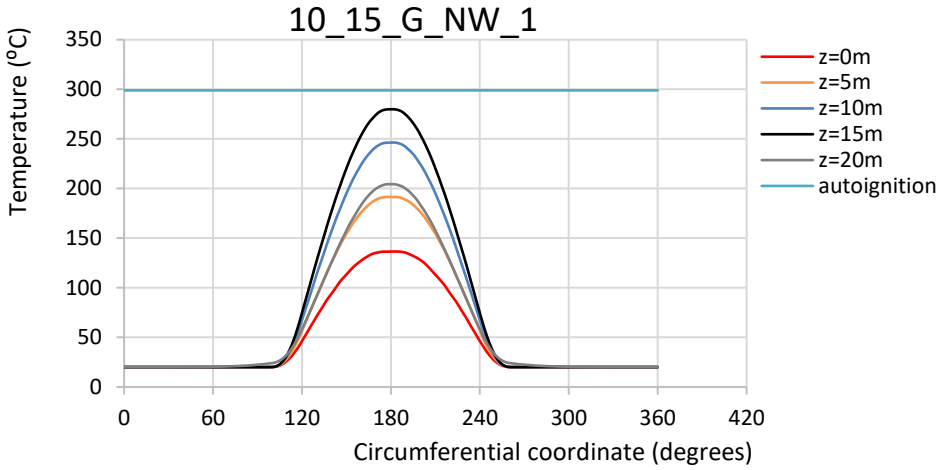

Figure A-28 Temperature distribution along the circumferential plane for model 10_15_G_NW_1

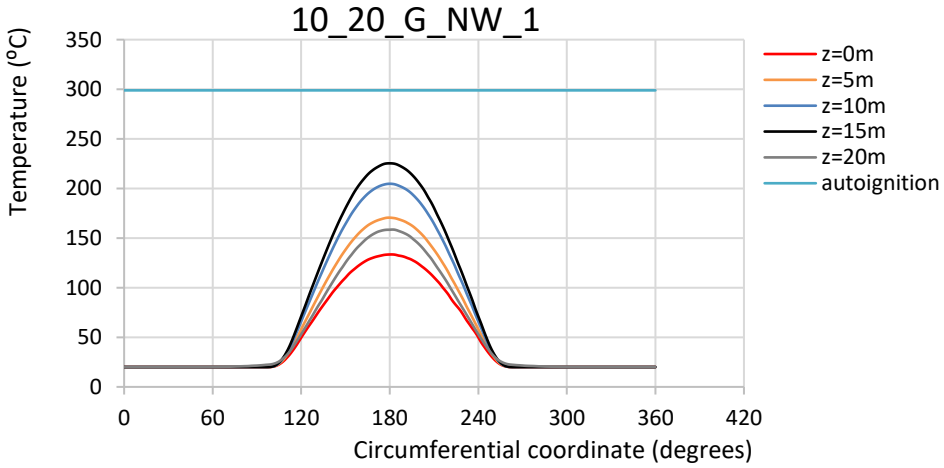

Figure A-29 Temperature distribution along the circumferential plane for model 10_20_G_NW_1

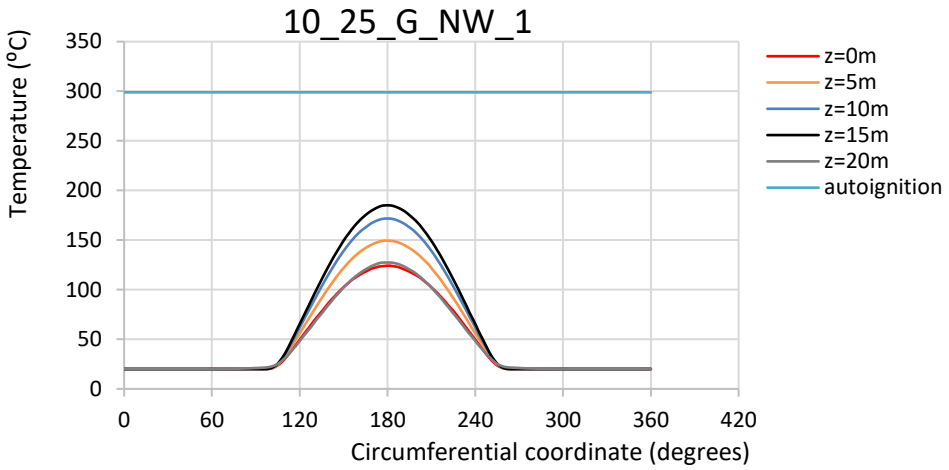

Figure A-30 Temperature distribution along the circumferential plane for model 10_25_G_NW_1

The following figures (A.31 - A.35) show the comparison of temperature distribution between the three models, 10_15_G_NW_1, 10_20_G_NW_1 and 10_25_G_NW_1 along the circumferential plane at height 0m, 5m, 10m, 15m and 20m. The autoignition temperature of Gasoline is also captured.

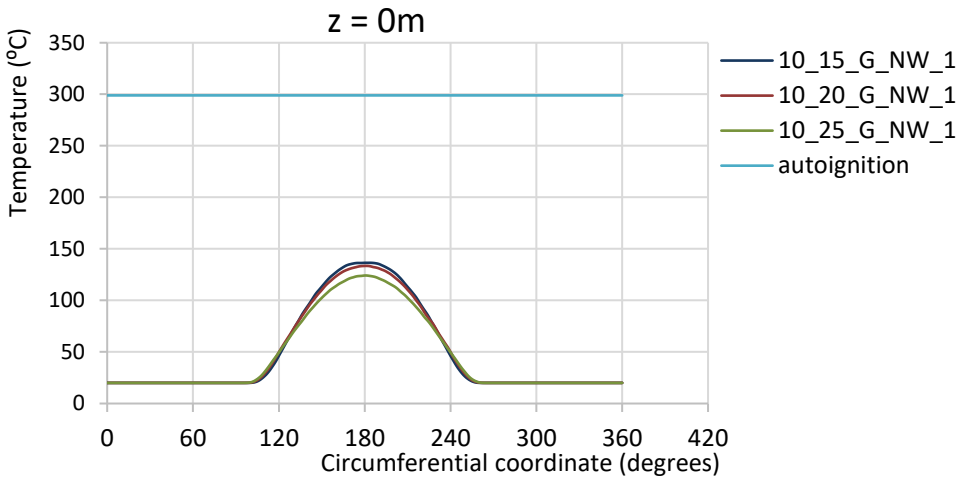

Figure A-31 Temperature distribution along the circumferential plane for models 10_15_G_NW_1, 10_20_G_NW_1 and 10_25_G_NW_1 at height 0m

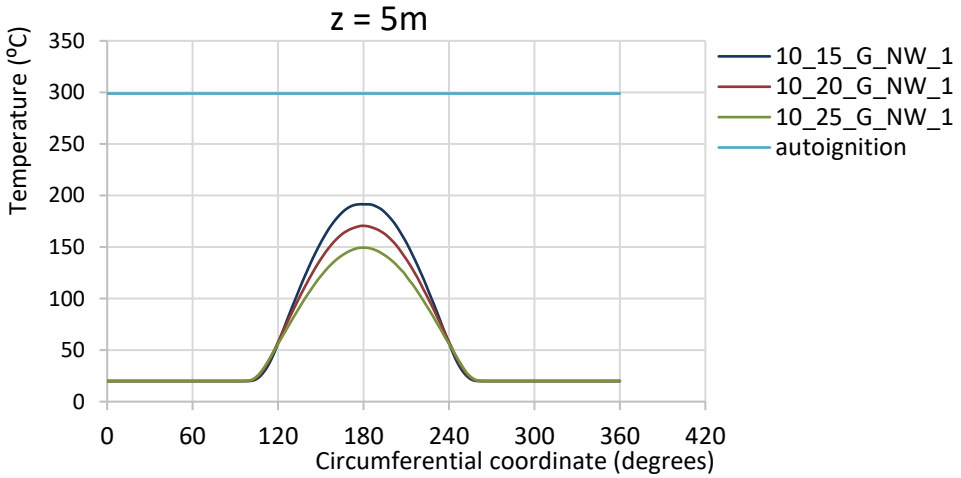

Figure A-32 Temperature distribution along the circumferential plane for models 10_15_G_NW_1, 10_20_G_NW_1 and 10_25_G_NW_1 at height 5m

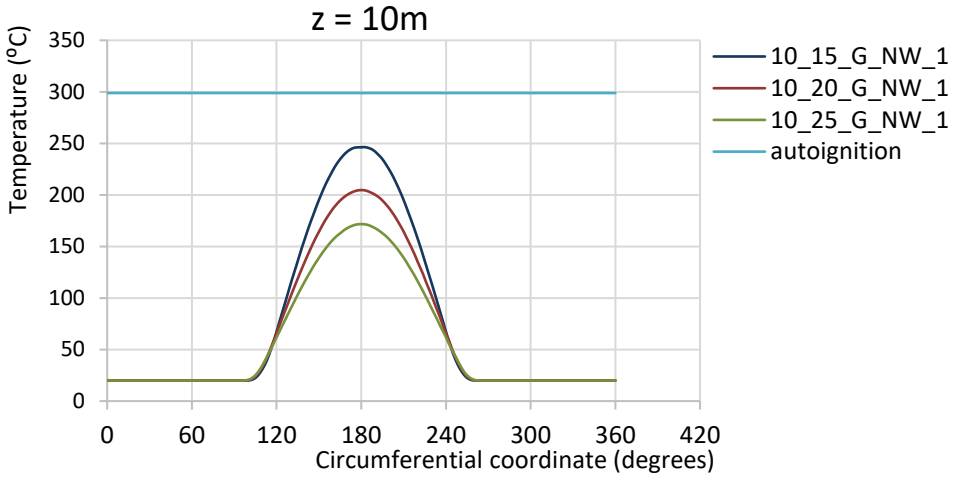

Figure A-33 Temperature distribution along the circumferential plane for models 10_15_G_NW_1, 10_20_G_NW_1 and 10_25_G_NW_1 at height 10m

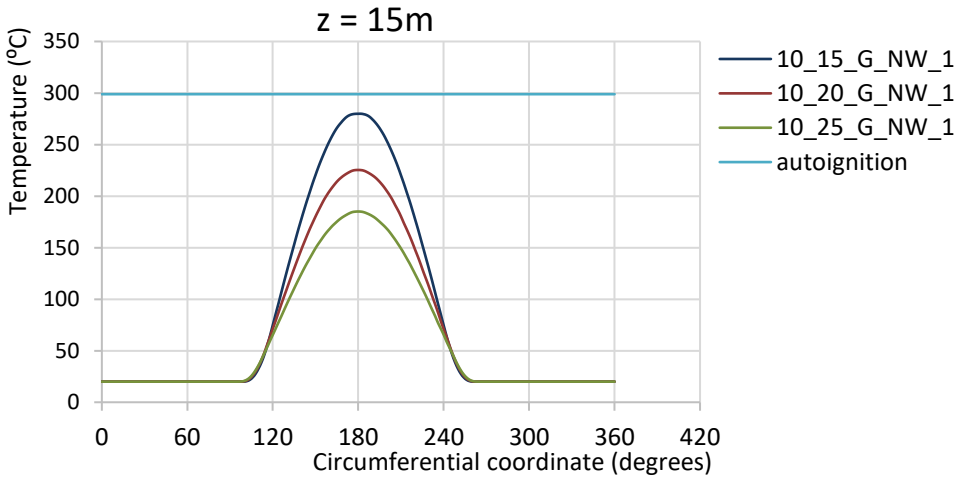

Figure A-34 Temperature distribution along the circumferential plane for models 10_15_G_NW_1, 10_20_G_NW_1 and 10_25_G_NW_1 at height 15m

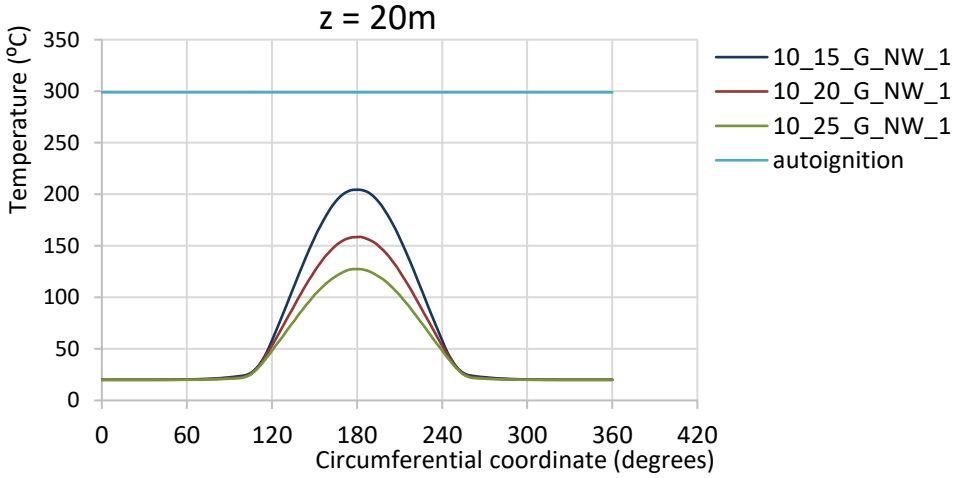

Figure A-35 Temperature distribution along the circumferential plane for models 10_15_G_NW_1, 10_20_G_NW_1 and 10_25_G_NW_1 at height 20m

The following figure (A.36) shows the comparison of temperature distribution between the three models, 10_15_G_NW_1, 10_20_G_NW_1 and 10_25_G_NW_1 along the vertical plane. The temperature distribution is captured at the meridian that develops the highest temperatures. The autoignition temperature curve is also shown.

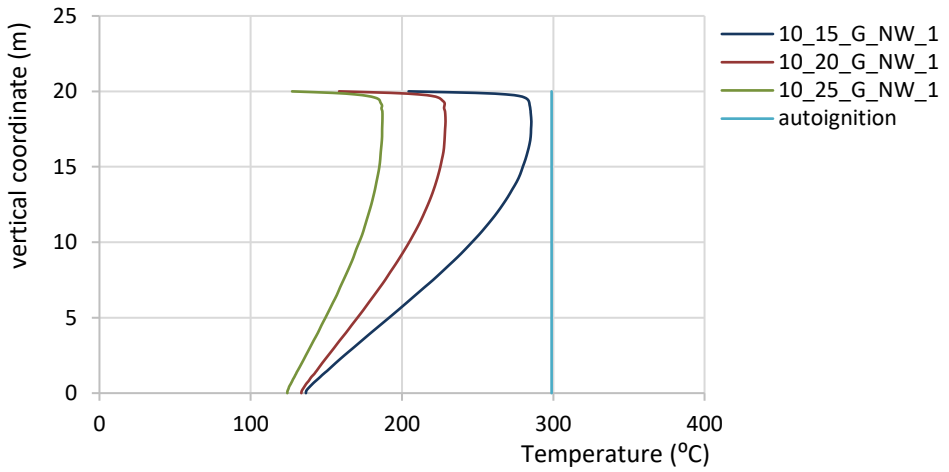

Figure A-36 Temperature distribution along the vertical plane for models 10_15_G_NW_1, 10_20_G_NW_1 and 10_25_G_NW_1

The following figures (A.37, A.38, A.39) present the temperature distribution of the models 15_15_E_NW_1, 15_20_E_NW_1 and 15_25_E_NW_1 respectively, along the circumferential plane for every 5m high, that is 0m, 5m, 10m, 15m and 20m. The autoignition temperature of Ethanol is also captured.

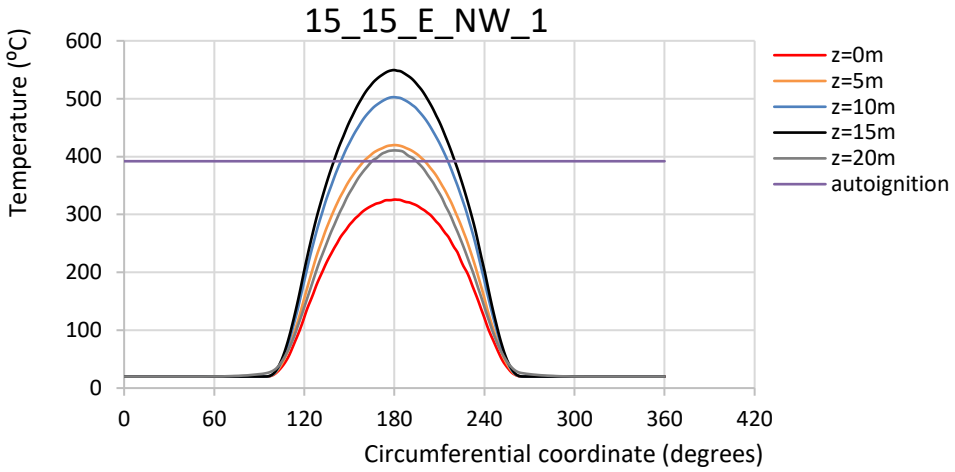

Figure A-37 Temperature distribution along the circumferential plane for model 15_15_E_NW_1

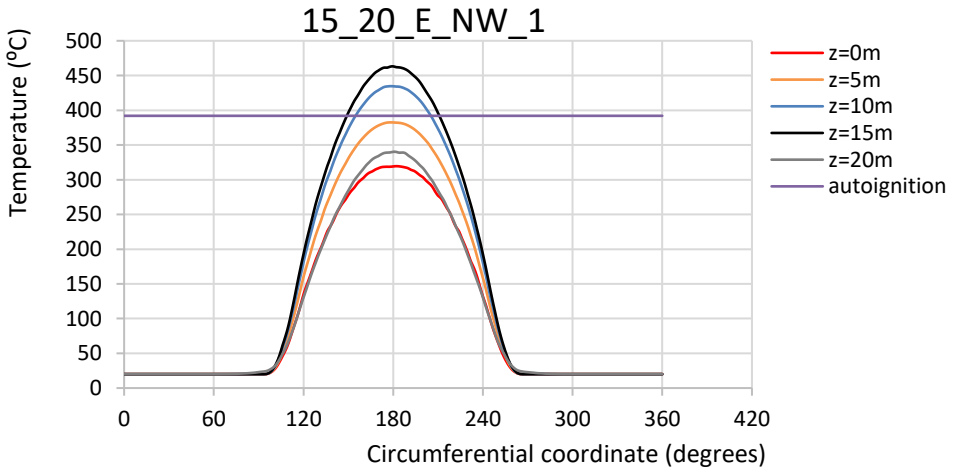

Figure A-38 Temperature distribution along the circumferential plane for model 15_20_E_NW_1

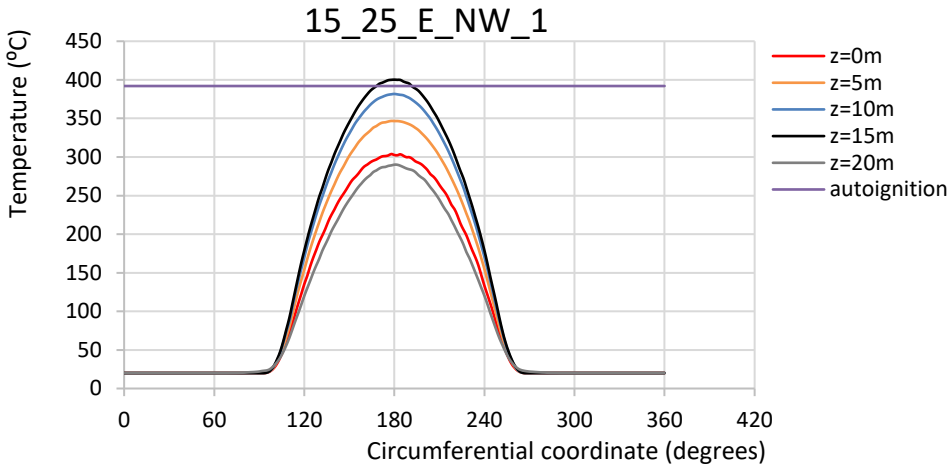

Figure A-39 Temperature distribution along the circumferential plane for model 15_25_E_NW_1

The following figures (A.40 – A.44) show the comparison of temperature distribution between the three models, 15_15_E_NW_1, 15_20_E_NW_1 and 15_25_E_NW_1 along the circumferential plane at height 0m, 5m, 10m, 15m and 20m. The autoignition temperature of Ethanol is also captured.

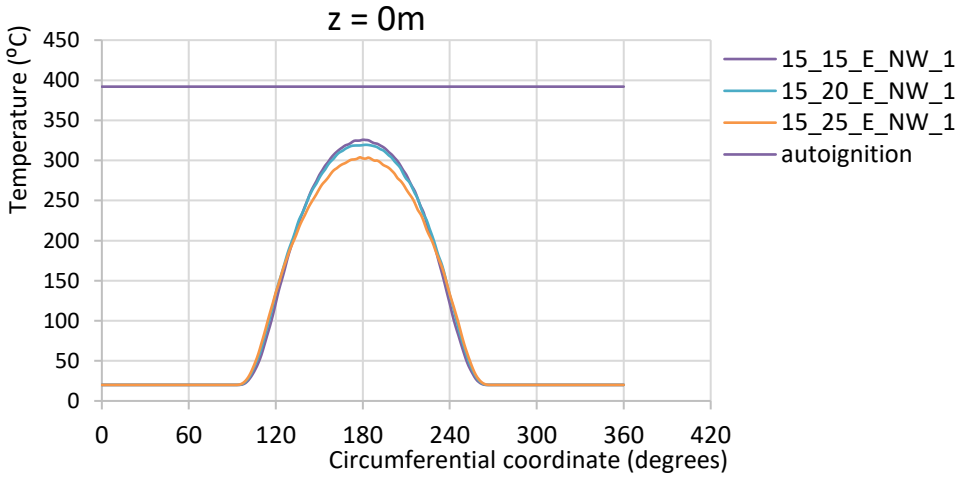

Figure A-40 Temperature distribution along the circumferential plane for models 15_15_E_NW_1, 15_20_E_NW_1 and 15_25_E_NW_1 at height 0m

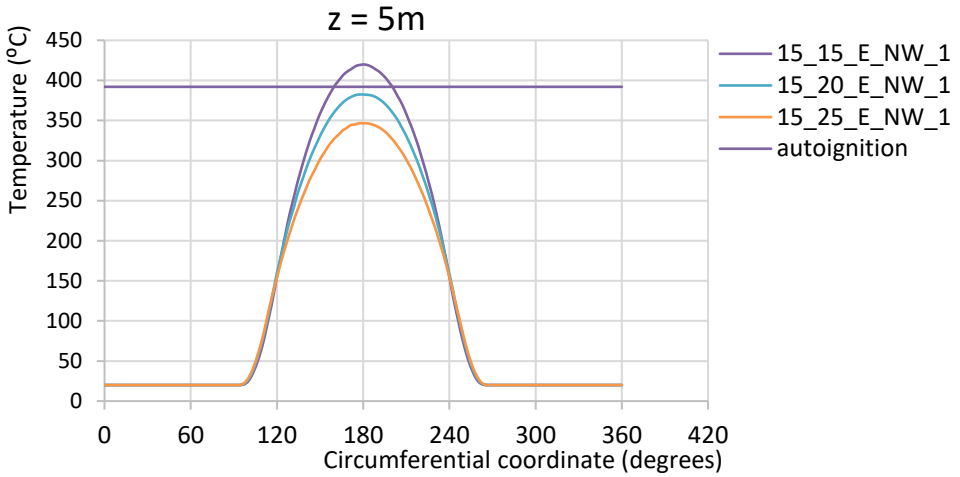

Figure A-41 Temperature distribution along the circumferential plane for models 15_15_E_NW_1, 15_20_E_NW_1 and 15_25_E_NW_1 at height 5m

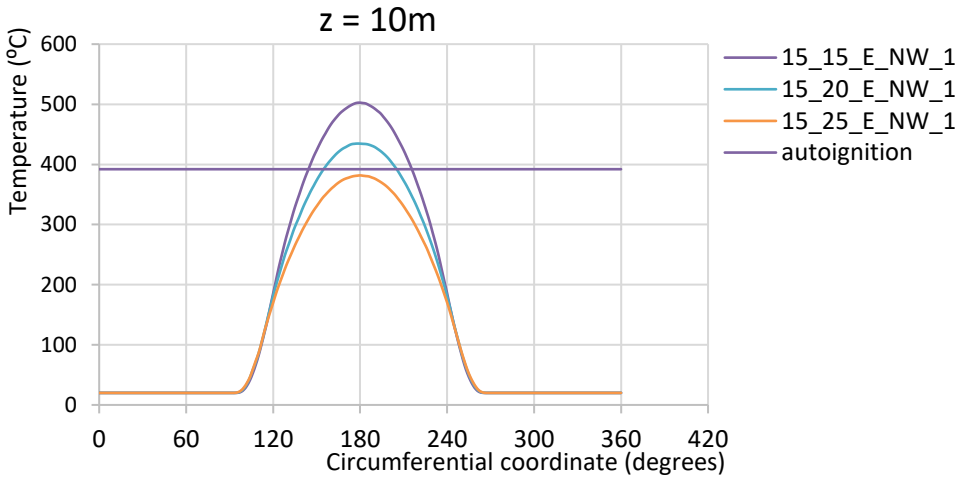

Figure A-42 Temperature distribution along the circumferential plane for models 15_15_E_NW_1, 15_20_E_NW_1 and 15_25_E_NW_1 at height 10m

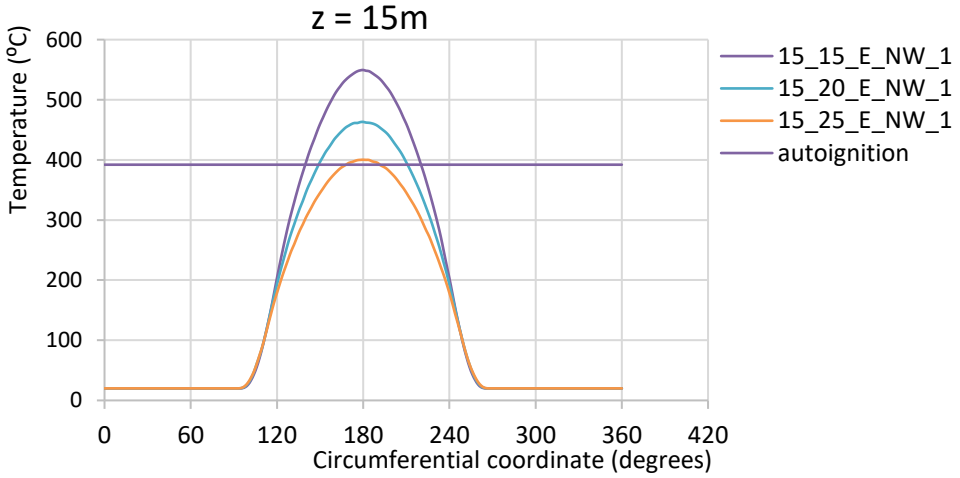

Figure A-43 Temperature distribution along the circumferential plane for models 15_15_E_NW_1, 15_20_E_NW_1 and 15_25_E_NW_1 at height 15m

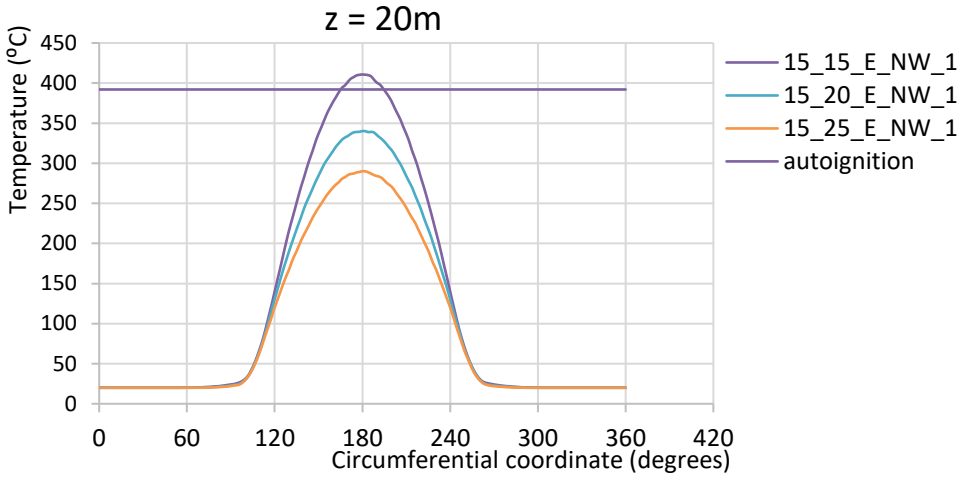

Figure A-44 Temperature distribution along the circumferential plane for models 15_15_E_NW_1, 15_20_E_NW_1 and 15_25_E_NW_1 at height 20m

The following figure (A.45) shows the comparison of temperature distribution between the three models, 15_15_E_NW_1, 15_20_E_NW_1 and 15_25_E_NW_1 along the vertical plane. The temperature distribution is captured at the meridian that develops the highest temperatures. The autoignition temperature curve is also shown.

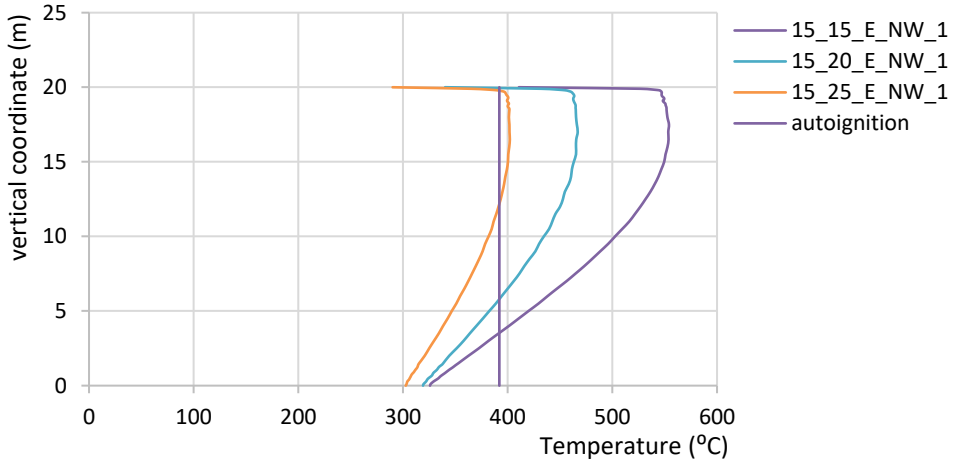

Figure A-45 Temperature distribution along the vertical plane for models 15_15_E_NW_1, 15_20_E_NW_1 and 15_25_E_NW_1

The following figures (A.46, A.47, A.48) present the temperature distribution of the models 15_15_G_NW_1, 15_20_G_NW_1 and 15_25_G_NW_1 respectively, along the circumferential plane for every 5m high, that is 0m, 5m, 10m, 15m and 20m. The autoignition temperature of Gasoline is also captured.

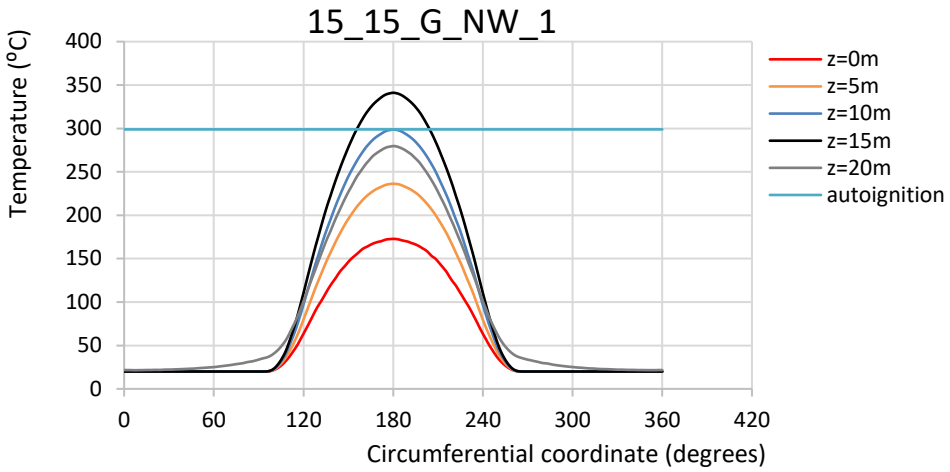

Figure A-46 Temperature distribution along the circumferential plane for model 15_15_G_NW_1

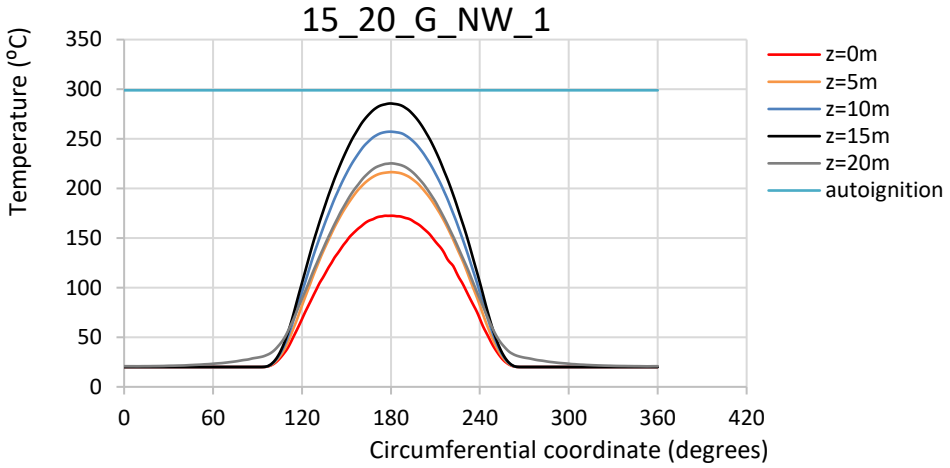

Figure A-47 Temperature distribution along the circumferential plane for model 15_20_G_NW_1

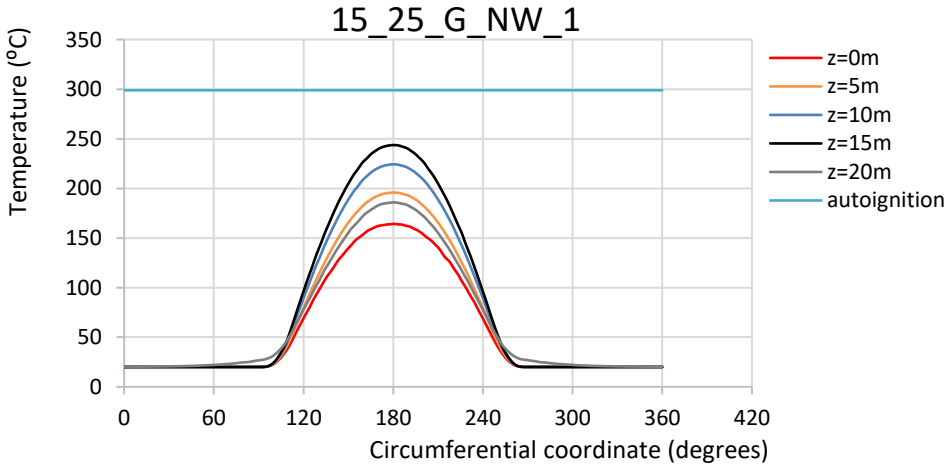

Figure A-48 Temperature distribution along the circumferential plane for model 15_25_G_NW_1

The following figures (A.49 - A.53) show the comparison of temperature distribution between the three models, 15_15_G_NW_1, 15_20_G_NW_1 and 15_25_G_NW_1 along the

circumferential plane at height 0m, 5m, 10m, 15m and 20m. The autoignition temperature of Gasoline is also captured.

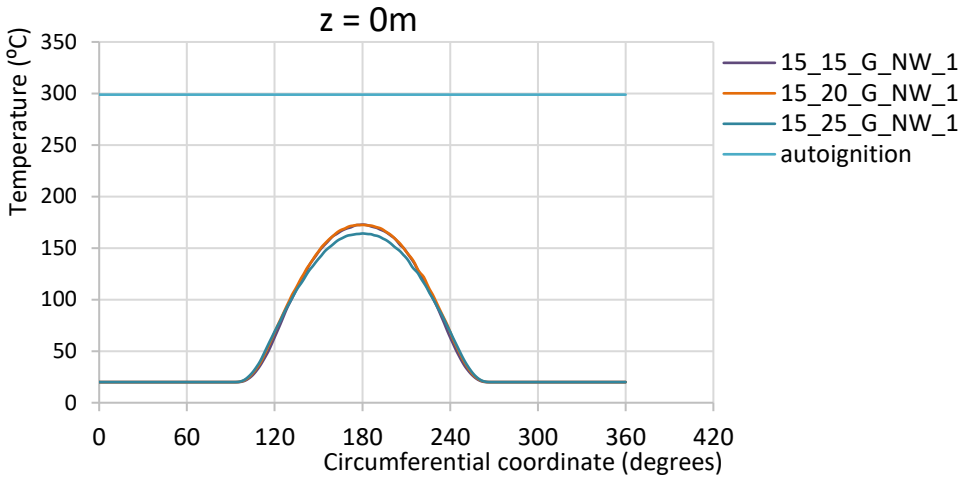

Figure A-49 Temperature distribution along the circumferential plane for models 15_15_G_NW_1, 15_20_G_NW_1 and 15_25_G_NW_1 at height 0m

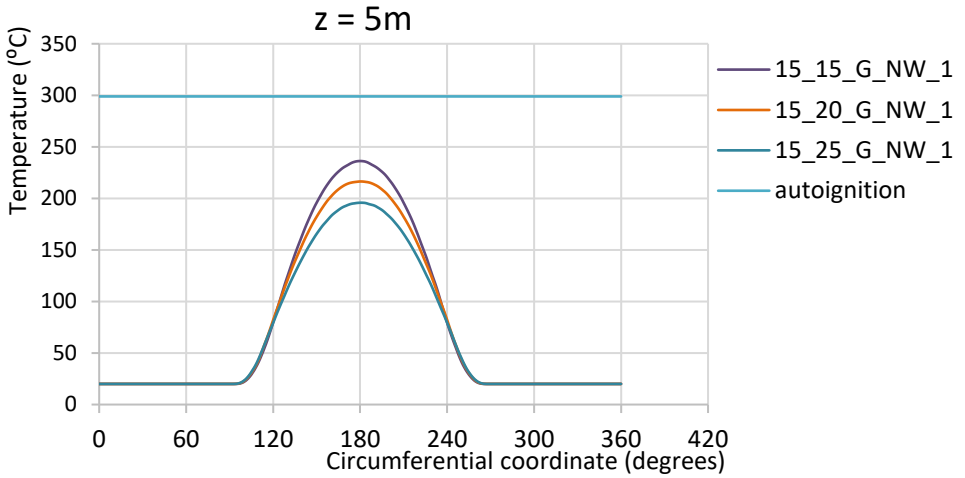

Figure A-50 Temperature distribution along the circumferential plane for models 15_15_G_NW_1, 15_20_G_NW_1 and 15_25_G_NW_1 at height 5m

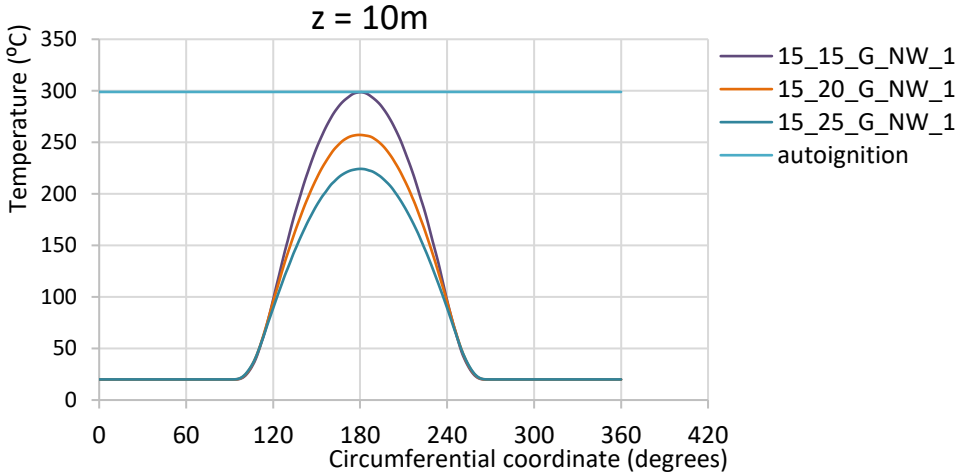

Figure A-51 Temperature distribution along the circumferential plane for models 15_15_G_NW_1, 15_20_G_NW_1 and 15_25_G_NW_1 at height 10m

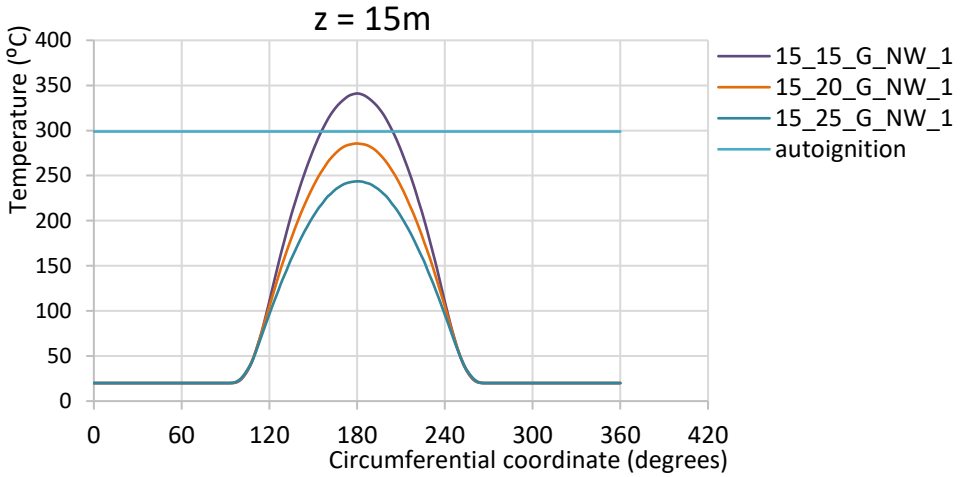

Figure A-52 Temperature distribution along the circumferential plane for models 15_15_G_NW_1, 15_20_G_NW_1 and 15_25_G_NW_1 at height 15m

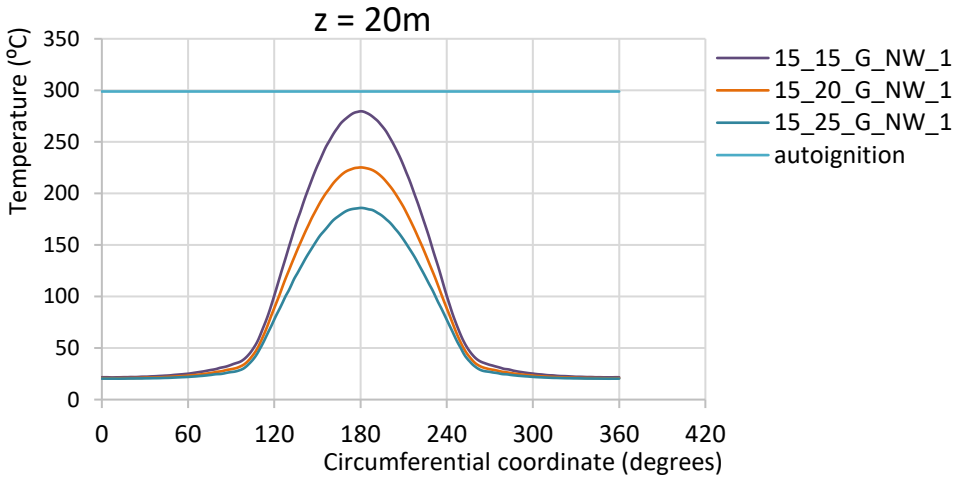

Figure A-53 Temperature distribution along the circumferential plane for models 15_15_G_NW_1, 15_20_G_NW_1 and 15_25_G_NW_1 at height 20m

The following figure (A.54) shows the comparison of temperature distribution between the three models, 15_15_G_NW_1, 15_20_G_NW_1 and 15_25_G_NW_1 along the vertical plane. The temperature distribution is captured at the meridian that develops the highest temperatures. The autoignition temperature curve is also shown.

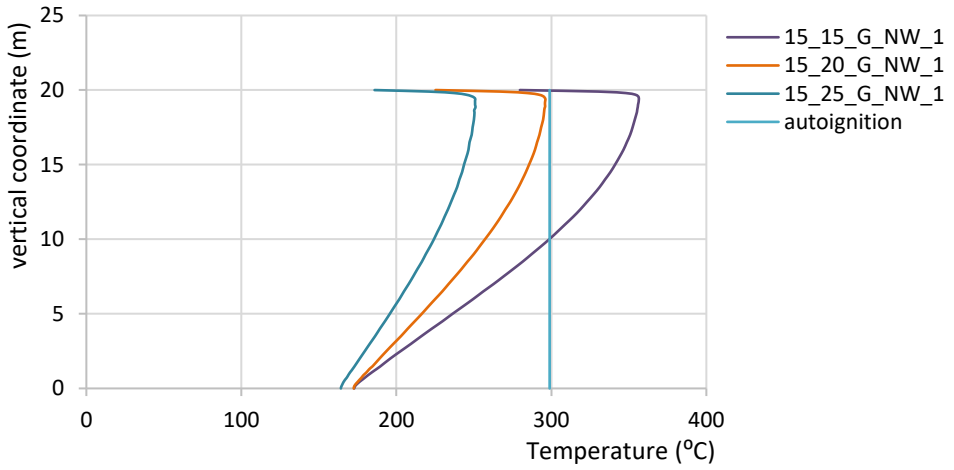

Figure A-54 Temperature distribution along the vertical plane for models 15_15_G_NW_1, 15_20_G_NW_1 and 15_25_G_NW_1

Ελληνική Περίληψη

Τα περιστατικά πυρκαγιάς στις δεξαμενές πραγματοποιούνται κυρίως σε διυλιστήρια πετρελαίου, τερματικά πετρελαίου ή δεξαμενές αποθήκευσης και μπορεί να αποδειχθούν καταστροφικές. Τα τελευταία χρόνια, οι μηχανολογικές εταιρείες (American Petroleum Institute, National Fire Protection Association κλπ) έχουν δημοσιεύσει αυστηρές τεχνικές οδηγίες και πρότυπα για την κατασκευή, την επιλογή υλικών, το σχεδιασμό και την ασφαλή διαχείριση δεξαμενών αποθήκευσης. Παρ 'όλα αυτά, τα περιστατικά πυρκαγιάς δεξαμενών αυξάνονται τις τελευταίες δεκαετίες. Ο μεγαλύτερος κίνδυνος για μια δεξαμενή αποθήκευσης καύσιμου υλικού είναι οι εκρήξεις που έχουν σαν αποτέλεσμα την εκδήλωση και τη διάδοση της φωτιάς. Όπως έχει παρατηρηθεί οι εκρήξεις σε μια πυρκαγιά είναι ο βασικός λόγος που μια δεξαμενή καταρρέει. Ταυτόχρονα το θερμικό φορτίο που αναπτύσσεται ενδέχεται να προκαλέσει βλάβες σε μια δεξαμενή με καταστροφικές γι’ αυτή συνέπειες.

Όταν μια δεξαμενή αποθήκευσης καύσιμου υλικού όπως η βενζίνη καίγεται, είναι αναμενόμενο ότι εξαιτίας των υψηλών θερμοκρασιών που αναπτύσσονται αυτή θα καταρρεύσει. Ταυτόχρονα όμως αποτελεί θερμικό φορτίο για τις γειτονικές δεξαμενές. Η θερμότητα μεταφέρεται κυρίως μέσω της ακτινοβολίας στις διπλανές δεξαμενές οι οποίες φορτίζονται θερμικά. Η ανάπτυξη των θερμοκρασιών στα τοιχώματα της διπλανής δεξαμενής ή αλλιώς της δεξαμενής στόχου αναμένεται να μην είναι ομοιόμορφη ούτε κατά την περίμετρο αλλά ούτε και καθ’ ύψος. Η διαφορά θερμοκρασίας που παρατηρείται μπορεί να οδηγήσει στην κατάρρευση της δεξαμενής ακόμα και στη διάδοση της φωτιάς στις γειτονικές δεξαμενές.

Το πρόβλημα που αντιμετωπίζεται σε αυτή τη διατριβή είναι η θερμική απόκριση των χαλύβδινων κυλινδρικών δεξαμενών αποθήκευσης υδρογονανθράκων σταθερής οροφής που θερμαίνονται κατά τη διάρκεια των πυρκαγιών της πισίνας. Οι βασικοί στόχοι της παρούσας διπλωματικής εργασίας είναι αρχικά ο προσδιορισμός των παραμέτρων που περιγράφουν τις δεξαμενές καύσης και στη συνέχεια ο υπολογισμός των γεωμετριών χαρακτηριστικών των φλογών. Προσομοιώνεται η φλόγα για τη δεξαμενή που καίγεται και στη συνέχεια προσδιορίζεται το θερμοκρασιακό πεδίο που αναπτύσσεται στη δεξαμενή στόχο, οι παράγοντες που επηρεάζουν περισσότερο τη θερμοκρασιακή κατανομή και τέλος ελέγχεται αν και κατά πόσο υπερβαίνεται η θερμοκρασία αυτοανάφλεξης. Ο έλεγχος αυτός προτείνεται από τον κανονισμό NFPA 30/2012 για τον προσδιορισμό των ελάχιστών αποστάσεων ασφαλείας μεταξύ δύο δεξαμενών.

Για την επίτευξη όσων προαναφέρθηκαν ακολουθείται μια συγκεκριμένη μεθοδολογία. Αρχικά, προσομοιώνεται η φλόγα με όσο το δυνατό μεγαλύτερη ακρίβεια σύμφωνα με την βιβλιογραφία. Οι μαθηματικές εξισώσεις που περιγράφουν το ύψος της, την κλίση της, τη διάμετρο λόγω ανέμου και την εκπεμπόμενη ενέργεια, εξαρτώνται από τη διάμετρο της φλεγόμενης δεξαμενής, το καύσιμο υλικό και τις επικρατούσες συνθήκες ανέμου. Προκειμένου να επιβεβαιωθεί ο τρόπος με τον οποίο γίνεται η εισαγωγή του προβλήματος της μετάδοσης της θερμότητας στις αναλύσεις, προσομοιώνονται πειράματα μετάδοσης θερμότητας από τη βιβλιογραφία τα οποία δίνουν πολύ ικανοποιητικά αποτελέσματα.

Κατασκευάζονται αριθμητικά μοντέλα που περιλαμβάνουν τόσο τις δεξαμενές καύσης όσο και τη θερμαινόμενη δεξαμενή. Το πρόβλημα επιλύεται αριθμητικά χρησιμοποιώντας τη μέθοδο των πεπερασμένων στοιχείων. Ο κώδικας πεπερασμένων στοιχείων MSC Marc, ο οποίος βελτιστοποιείται για μη γραμμικά προβλήματα, χρησιμοποιείται για την προσομοίωση.

Τα τρισδιάστατα μοντέλα αναπτύσσονται μέσω στοιχείων κελύφους τεσσάρων κόμβων. Η διακριτοποίηση είναι πιο πυκνή στη βάση και στην οροφή της περιμετρικής επιφάνειας της δεξαμενής. Η επιβολή της θερμοκρασίας γίνεται στους κόμβους, η μετάδοση της θερμοκρασίας μέσω ακτινοβολίας εισάγεται μέσω της ανοιχτής κοιλότητας (open cavity) ενώ η συναγωγή μέσω επιφανειακής συνθήκης (face film, 25W/m2/K). Τα μοντέλα επιλύονται με χρονικά μεταβαλλόμενη θερμική ανάλυση (Thermal Transient Analysis).

Η συμπεριφορά της θερμαινόμενης δεξαμενής εξετάζεται για πολλαπλά σενάρια πυρκαγιάς. Πρώτον, εξετάζεται η περίπτωση μιας μοναδικής δεξαμενής καύσης. Στα υπόλοιπα σενάρια, η φωτιά εξαπλώνεται σε γειτονικές δεξαμενές. Έτσι, σε αυτά τα σενάρια η εξεταζόμενη δεξαμενή θερμαίνεται από πολλαπλές πηγές (δεξαμενές καύσης). Παραμετρικές αριθμητικές αναλύσεις διεξάγονται για να μελετήσουν την επίδραση ενός συνδυασμού διαφόρων παραμέτρων: διάμετρος της δεξαμενής καύσης, τύπος αποθηκευμένου καυσίμου (βενζίνη ή αιθανόλη), επίπτωση αιολικής ενέργειας, απόσταση διαχωρισμού μεταξύ των δεξαμενών και αριθμός εμπλεκόμενων δεξαμενών καύσης. Επιπλέον, η μελέτη στοχεύει να προτείνει ένα δείκτη για την αξιολόγηση του κινδύνου αυτοανάφλεξης του καυσίμου στη θερμαινόμενη δεξαμενή. Επίσης εξετάζεται εάν οι αποστάσεις ασφαλείας που συνιστώνται στους ισχύοντες κανονισμούς (NFPA30: 2012) είναι ασφαλείς ή όχι. Οι ιδιότητες υλικών του χάλυβα σε υψηλές θερμοκρασίες είναι σύμφωνα με το EN 1993-1-2.

Διαπιστώθηκε ότι η κατανομή θερμοκρασίας στα τοιχώματα της δεξαμενής στόχου δεν είναι ομοιόμορφη ούτε κατά την περιφέρεια αλλά ούτε και καθ' ύψος. Η άνοδος της θερμοκρασίας πραγματοποιείται στην πλευρά της δεξαμενής που βρίσκεται ακριβώς απέναντι, που "βλέπει" δηλαδή, την πηγή της θερμότητας, ενώ η αντίθετη πλευρά δεν επηρεάζεται από τη φωτιά. Ο τρόπος με τον οποίο κατανέμεται η θερμοκρασία γίνεται πιο περίπλοκος καθώς προστίθενται περισσότερες δεξαμενές καύσης. Το ποσοστό επιρροής της περιμέτρου όταν έχουμε μία φλεγόμενη δεξαμενή είναι περίπου το 1/3 και αυξάνεται καθώς αυξάνονται οι φλεγόμενες δεξαμενές, με αποτέλεσμα να φτάνει περίπου στο 90% όταν έχουμε τέσσερις δεξαμενές να καίγονται.

Οι θερμοκρασίας που αναπτύσσονται στη δεξαμενή στόχο μειώνονται όσο η φλεγόμενη δεξαμενή απομακρύνεται από αυτή. Η μείωση αυτή είναι γραμμική και είναι ανεξάρτητη της διαμέτρου, του υλικού και των συνθηκών ανέμου που επικρατούν. Και στους δύο τύπους καυσίμων - Αιθανόλη και Βενζίνη - ο ρυθμός μείωσης της μέγιστης θερμοκρασίας, καθώς η απόσταση μεταξύ της φλεγόμενης δεξαμενής και της δεξαμενής στόχου αυξάνεται, επηρεάζεται περισσότερο από την παρουσία ανέμου απ΄ ότι από τη διάμετρο της δεξαμενής καύσης. Υπό συνθήκες ανέμου, σε μικρότερες διαμέτρους της φλεγόμενης δεξαμενής, ο ρυθμός μείωσης της θερμοκρασίας με την αύξηση της απόστασης των δεξαμενών δεν επηρεάζεται από το είδος του καυσίμου.

Σύμφωνα με τις συστάσεις του NFPA30: 2012, σχεδόν το 62,5% των περιπτώσεων που μελετώνται είναι στη μη ασφαλή πλευρά. Συμπεραίνεται ότι ο άνεμος είναι η πιο κρίσιμη παράμετρος που πρέπει να ληφθεί υπόψη για τον προσδιορισμό της απόστασης διαχωρισμού μεταξύ των δεξαμενών.

Όσον αφορά τον δείκτη επικινδυνότητας που ορίζεται στην παρούσα εργασία, τα αποτελέσματα των αναλύσεων δείχνουν ότι υπό συνθήκες ανέμου, και για τους δύο τύπους καυσίμων, σε μεγάλες διαμέτρους, ο κίνδυνος πυρκαγιάς μειώνεται γραμμικά. Σε μικρές διαμέτρους και για τους δύο τύπους καυσίμων, ο κίνδυνος πυρκαγιάς υποδηλώνει ταχεία μείωση σε μικρότερες αποστάσεις μεταξύ των δεξαμενών. Όταν η απόσταση μεταξύ της

φλεγόμενης δεξαμενής και της δεξαμενής στόχου αυξάνεται, ο κίνδυνος πυρκαγιάς καθίσταται μηδενικός. Τέλος, ο κίνδυνος αυτοανάφλεξης στη θερμαινόμενη δεξαμενή αυξάνεται καθώς αυξάνεται ο αριθμός των δεξαμενών καύσης και, επιπλέον, ο κίνδυνος στην περίπτωση της αιθανόλης είναι μεγαλύτερος στα μοντέλα βενζίνης υπό αμφότερες τις συνθήκες ανέμου.